

Polymers with spatial or topological constraints: theoretical and computational results

Cristian Micheletti

*SISSA, International School for Advanced Studies and
CNR-IOM Democritos and Italian Institute of technology (SISSA Unit)
via Bonomea 265, I-34136 Trieste, Italy*

Davide Marenduzzo

*SUPA, School of Physics and Astronomy, University of Edinburgh,
Mayfield Road, Edinburgh EH9 3JZ, Scotland*

Enzo Orlandini

Dipartimento di Fisica and Sezione INFN, Università di Padova, I-35131 Padova, Italy

Abstract

In this review we provide an organized summary of the theoretical and computational results which are available for polymers subject to spatial or topological constraints. Because of the interdisciplinary character of the topic, we provide an accessible, non-specialist introduction to the main topological concepts, polymer models, and theoretical/computational methods used to investigate dense and entangled polymer systems. The main body of our review deals with: (i) the effect that spatial confinement has on the equilibrium topological entanglement of one or more polymer chains and (ii) the metric and entropic properties of polymer chains with fixed topological state. These problems have important technological applications and implications for the life-sciences. Both aspects, especially the latter, are amply covered. A number of selected open problems are finally highlighted.

Keywords: Polymers, Knots, Confinement

Contents

1	Introduction	3
2	First part: basic knot theory and polymer models	4
3	Basic knot theory	5
3.1	Prime and composite knots	8
3.2	Knot handedness	9
3.3	Some knot families	12
3.4	Geometric techniques	13
3.5	Polynomial invariants	13
3.6	Open knots	17

4	Coarse-grained models of polymers in \mathbb{R}^3: from freely-jointed chains to semi-flexible self-avoiding ones.	18
4.1	Flexible and semi-flexible chains: the cylinder and rod-bead models	22
4.2	Polymer models on regular lattices: combinatorial arguments and rigorous results	23
5	Second Part: Self-entanglement of single polymer chains	25
6	Sampling at equilibrium by Monte Carlo methods	27
6.1	Advanced sampling techniques: multiple Markov chains or parallel tempering . .	30
6.2	Reweighting techniques	30
6.3	Knot simplifications	32
7	Knotting probability and knot complexity in ring polymers	34
8	Polymers under geometrical confinement.	36
8.1	Scaling arguments for confined polymers	38
8.1.1	Blob picture	39
8.1.2	Odijk regime	39
8.2	Rigorous results of lattice models of polymers in slabs and prisms	41
8.2.1	Walks and polygons in D -slabs	41
8.2.2	Walks and polygons in (D_1, D_2) -prisms	42
8.3	Sampling confined polymers at equilibrium	43
9	Knotting probability in confined geometries	47
9.1	Rigorous results for polygons in slabs and prisms	47
9.2	Numerical results for polygons in slabs and prisms	50
9.3	Knot spectrum in slabs and channels: an open problem.	53
9.4	Polymer rings confined in spheres and cubes.	55
10	DNA knotting inside viral capsids	57
11	Knotting of polymer rings undergoing adsorption transition	60
12	Knotting of polymers under tension	62
13	Third part: Mutual entanglement of several polymer chains	69
14	Mutual entanglement between polymer rings in solution: linked states	70
14.1	Linking statistics of two rings in unconstrained spaces	72
14.1.1	Some analytical and rigorous results	72
14.1.2	Numerical results on linking probability	74
14.2	Linking probability in confined geometries	76
14.2.1	Statistics of two-components links confined in a cube	76
14.2.2	Statistics of two-components links in D -slabs and (D_1, D_2) -prisms	77
14.3	Mutual entanglements for polymers in concentrated solution	77
15	Fourth part: properties of polymers with fixed topology	81

16	Equilibrium properties of topologically constrained polymers	82
16.1	Ring polymers in diluted solution: fixed knot type	82
16.1.1	Limiting entropy and entropic exponents of rings at fixed knot type	82
16.1.2	Metric properties of rings at fixed knot type.	86
16.2	Knotted rings in proximity of an impenetrable surface	88
16.3	Topological and volume exclusion interaction between pairs of rings	90
16.4	Topological constraints in concentrated solutions.	93
16.4.1	Out-of-equilibrium and entropic effects in chromosome territories	94
17	The size of knots	96
17.1	Knotted arc	96
17.2	Flat knots	98
17.2.1	Size of flat knots	100
17.3	The size of “real knots”	101
17.3.1	The size of globular knots	101
17.3.2	The size of adsorbed knots	102
18	Summary and perspectives	104
19	Acknowledgements	116
Appendix A	Distance between two segments	116
Appendix B	Local chain moves that preserve topology	116

1. Introduction

Linear polymers are examples of soft-matter systems consisting of a series of identical, or similar, covalently-bonded subunits (monomers). The fundamental physical properties of a polymer, such as its size and flexibility, strongly depend on its polymerization degree, that is the number of constituting monomers. Because of steric hindrance and electrostatic self-repulsion, short polymer chains can be aptly described as rigid molecules. On the other hand, when the number of monomers in a chain is sufficiently large, polymers are highly flexible and, in canonical equilibrium, explore a large number of conformations that are typically highly self-entangled.

For individual open polymer chains this entanglement is purely geometrical; in fact, a knot in the chain can be untied by a suitable reptation of the polymer in space. On the other hand, if a closure (cyclization) reaction occurs, or if the polymer termini are otherwise constrained, then the geometrical self-entanglement is trapped in the form of a knot (possibly a trivial knot, that is a ring), whose topology cannot be changed by any manipulation of the polymer except by cutting it.

Topological entanglement is a genuine characteristic of polymeric systems that, in some circumstances, may severely affect not only the physical properties of individual polymer chains, but also of polymer melts. For example, entanglement can be trapped during the crystallization of artificial polymers, and determine the properties of the resulting crystal, such as its degree of purity [1, 2, 3]. It is likely that the entanglement colocalizes with amorphous regions of the crystal.

Artificial knotted polymer rings can be, nowadays, easily synthesized in laboratory but their most ubiquitous and pervasive manifestation is found in biopolymers such as DNA and RNA. These biomolecules can be sufficiently long that they become entangled *in vivo* [4], thus providing an ideal playground to study the occurrence of knots and their biological implications. For example, knots and other entanglements in DNA are known to severely affect the efficiency of fundamental genetic events such as replication and transcription [5, 6, 7, 8]. The biological necessity to maintain a control on the degree of entanglement of these biomolecules *in vivo* is highlighted by the fascinating fact that there exist specific cellular machineries, such as topoisomerase enzymes, which are capable of simplifying the topological complexity of the DNA entanglement by favouring the selective cross-passage of pairs of DNA strands [9, 4, 10, 11, 12].

As illustrated by the above-mentioned examples, topological entanglement is a ubiquitous aspect in polymer systems and has important ramifications either in technological contexts or for the understanding of complex physical and/or biological systems.

The objective of this review is to provide an overview of the salient advancements that have been made in the past decades in the theoretical and computational characterization of topological entanglement in polymeric systems. In this regard, it should be mentioned that most of the latest developments have been stimulated by the advent of single-molecule manipulation techniques that have redefined the “hot” open problems and applicative horizons of polymer entanglement. We mention, in particular, the perspectives opened by the possibility of confining one or more polymer chains in nano-pores, nano-channels or through surface adsorption as well as that of mechanically manipulating individual polymeric filaments.

The topics covered by the present review may broadly be collected into four main sections which cover respectively: (i) the fundamental notions of entanglement and polymer models, the state-of-the-art characterization of (ii) self-entanglement of individual polymers and (iii) several polymer chains in “topological equilibrium” and finally (iv) the behaviour of one or more fluctuating polymers of fixed topology. For each section, we provide not only an up-to-date account of available results, but also a full overview of the main methodological (theoretical and computational) tools that can be profitably used to attack the state-of-the-art problems. Finally, we provide a perspective for future research by highlighting the key open questions.

2. First part: basic knot theory and polymer models

The first part of the review consists of sections 3– 4 and aims at providing the reader with an overview of:

- the main topological concepts,
- the polymer models that are most-commonly studied theoretically or computationally,
- the methods and algorithms used to characterize the degree of polymer entanglement.

In the literature there are several models of polymer chains in solution and we will review some of them by pointing out advantages and drawbacks. A common, essential feature of these models is that they neglect the chemical details of the monomers as much as possible and describe the polymer in terms of a discrete (coarse-grained) chain made by the repetition, in a string-like fashion, of the elementary monomeric subunits. Ideally, viable models ought to be simple enough to be theoretically tractable and yet sufficiently detailed to capture the key characteristics of the

macromolecule in equilibrium such as its connectivity, its local rigidity and its flexibility at large scales.

At the simplest level of model complexity one has the so called *ideal chains* where only the chain connectivity and local stiffness are considered. In these models, the polymer chain is typically embedded in the continuum three-dimensional space, and self-avoidance is not accounted for. This leaves the chain free to attain configurations that would be incompatible with steric hindrance, such as those where distinct chain nodes or bonds are overlapping. The minimalistic character of these models make them amenable to extensive analytical characterization and to straightforward numerical simulations, see Section 4.

More realistic descriptions of the polymer do take into account the excluded-volume constraint in the chain, These constraints introduce long-range (along the chemical sequence) correlations in the system which make analytical progress very difficult. As a consequence, these models are almost exclusively characterised by means of computationally-intensive numerical simulations. The scope of the latter is often extended by reducing the conformational degrees of freedom of the model polymer, for example by embedding the chain on a regular lattice.

In Section 3 we finally provide a concise summary of the key concepts needed to define and characterize the topological entanglement of a closed chain (and discuss to what extent it can be extended to open linear chains) which is at the heart of the modern branch of topology known as the *knot theory*. Interested readers can find a more systematic and in-depth coverage of the concepts and results introduced below, in one of the several books that have been published on the subject, see e.g. refs. [13, 14, 15, 16, 17, 18]

3. Basic knot theory

An operational definition of a knotted curve can be given by resorting to our common experience of taking a piece of rope, tying a knot in it and finally gluing the two ends together. The knotted rope can be geometrically manipulated in three-dimensional space (\mathbb{R}^3) in countless ways but, unless we use scissors and glue to cut and rejoin the rope, it is impossible to turn it into a plain, unknotted ring. The above example builds on our intuitive notion that a rope has an approximately uniform thickness that forbids the rope self-crossing during the manipulations.

Since all the configurations obtained by deforming the rope preserve the initial knot type, it appears natural to define a knot as the class of equivalence of configurations obtained by these manipulations in the three-dimensional embedding space.

Mathematically it is appealing to define a knot in a similar fashion, that is as the set of continuous simple closed curves (i.e. S^1) that are related by continuous deformations in \mathbb{R}^3 (isotopy). However, in contrast with our practical example, a curve in S^1 has no thickness so that, based on the above definition, any knot would be found equivalent to the unknot. This is readily seen by considering the continuous deformation resulting from pulling the curve tighter and tighter until the knot reduces to a point and hence disappears (see Figure 1).

This difficulty can be overcome by basing the knot equivalence on the notion of *ambient isotopy*. An ambient isotopy is a geometrical manipulation of the curve (isotopy) through the space in which the curve is embedded (ambient). In other words, instead of deforming the knots alone, one deforms the whole space in which they sit. These deformations preserve the orientation of the curve and do not allow the occurrence of instances such as the one depicted in Figure 1 in which the knot has been shrunk down to a point.

This restriction is sufficient to rule out the occurrence of singularities, such as the one shown in Figure 1, as the result of a continuous deformation of a curve.

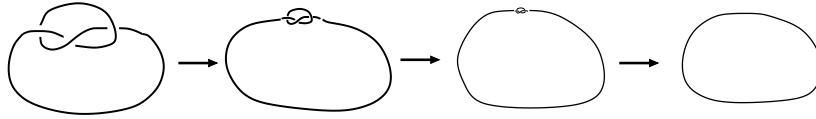


Figure 1: Knot elimination by continuous deformation on a knotted loop.

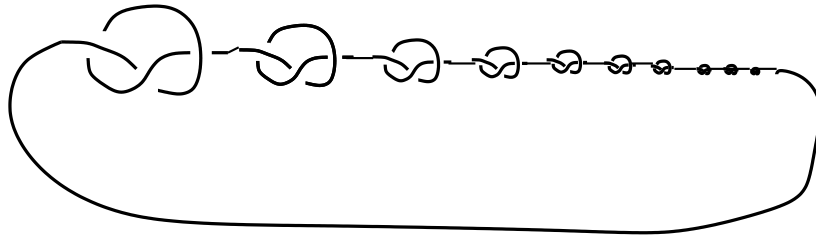


Figure 2: A wild knot.

Yet, it appears necessary to introduce restrictions also on the types of admissible curves in order to disallow the occurrence of “pathological” cases such as the one depicted in Figure 2 and known as *wild knots*. These cases, that are very far from the intuitive, physical notions of a proper knot, can be ruled out by requiring the curves to be differentiable. This severe constraint is impractical in the discrete polymer models used in standard numerical studies. In this situation the constraint is relaxed by defining a knot as a simple, closed curve that is ambient isotopic to a piecewise-linear (or polygonal) curve in \mathbb{R}^3 (*tame knot*) [17]. This definition eliminates wild knotting because polygonal curves are necessarily composed of a finite number of bonds or edges. Within the space of polygonal curves, two configurations are topologically equivalent (or ambient isotopic) if one can be obtained from the other by a finite sequence of *triangular moves* (see Figure 3).

Detecting knot equivalences is at the heart of knot theory. For instance, proving that it is impossible to deform one knot into another is equivalent to proving that the two knots lie in different equivalence classes. On the other hand proving that a knot is not trivial i.e. that no ambient isotopy can move it into a perfectly planar ring is equivalent to showing that it does not

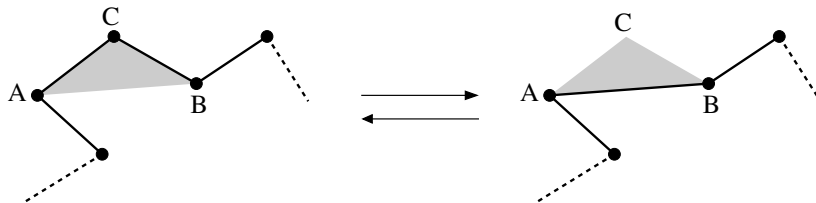


Figure 3: Triangular moves: the removal or addition of the vertex C is allowed if the interior of the non-degenerate triangle with vertices ABC does not intersect any chain segment. We stress that the number of vertices and the length of the polygonal curve will increase or decrease after each triangular move.

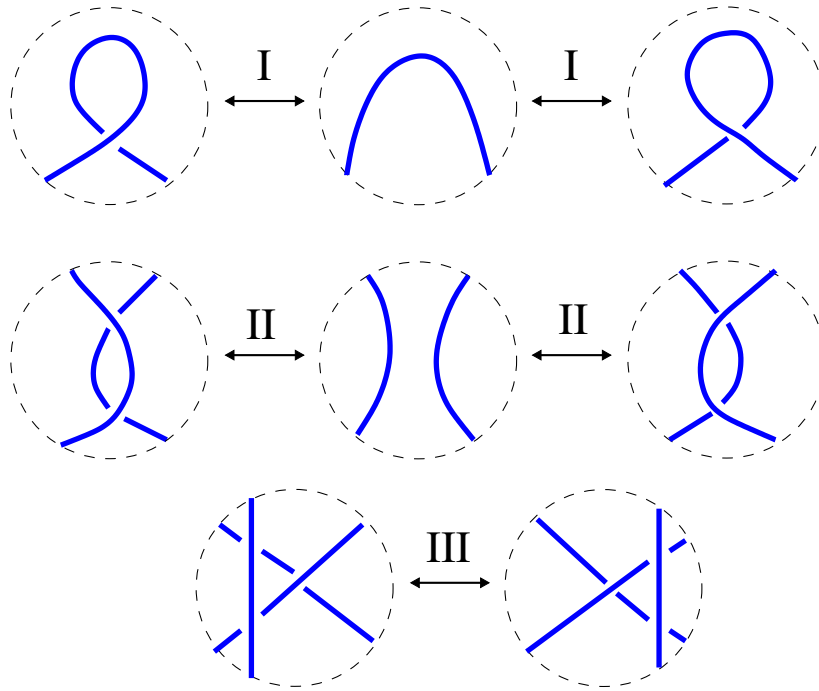


Figure 4: Reidemeister moves.

belong to the equivalence class of the unknot.

Another way of detecting the knot type of a closed polygonal curve with a definite arrangement (embedding) in $3d$ space consists of looking at its planar representation, i.e. its *knot diagram*. Knot diagrams are planar projections of the three-dimensional curve embedding whose only singularities are transverse double points at which the *underpass-overpass* information is given by interrupting one of the branches of the projected curves. In this mapping a movement of an embedding in \mathbb{R}^3 corresponds to a change in its planar projection. For this description there is a well established theorem stating that two knots are equivalent if and only if (any of) their projections can be made identical by a sequence of three possible *Reidemeister moves* [19] and planer isotopies (see Figure 4). Each knot diagram is characterized by a set of transversely crossings whose number depends on the particular projection direction and on the specific geometric realization of the knot type. By using Reidemeister moves one can, in principle, minimise the number of crossings compatible with the topology of that knot type. This gives rise to a minimal knot diagram representation of that knot type having the smallest possible number of crossings n_{cr}^{min} (*crossing number*).

As a matter of fact, if we neglect chiral enantiomers (see Section 3.2 below for a proper definition), the value of n_{cr}^{min} provides the most used criterion for classifying knots in groups of increasing topological complexity. An unknotted curve is, in fact, associated to $n_{cr}^{min} = 0$. At the next level of complexity one has the trefoil knot, which has $n_{cr}^{min} = 3$ etc., as shown in Figure 5. As n_{cr}^{min} increases one finds topologically different knots having the same number of minimal crossings which are conventionally distinguished by a different numerical subscript appended

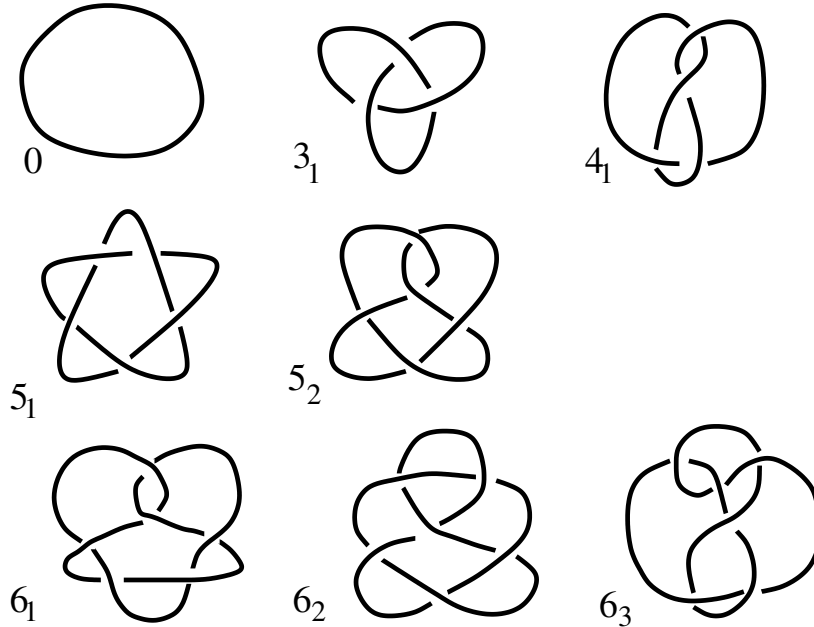


Figure 5: Prime knots up to crossing number 6.

to n_{cr}^{min} . The simplest example is offered by the pair of 5-crossing knots, 5_1 and 5_2 sketched in Figure 5.

3.1. Prime and composite knots

As common experience teaches us, a non-trivial knot τ in a rope cannot be untied by introducing a second non-trivial knot τ' in different portion of the same rope (that is a portion that does not interfere with the first knot), no matter how one manipulates the doubly-knotted rope (with closed or otherwise constrained ends). The notion that anti-knots do not exist can be actually proved rigorously by using geometrical techniques (see Section 3.4 below). A further result is that the resulting knot, $\tau\#\tau'$, belongs to a knot type that is different from both τ and τ' and is called the *connected sum* or the *composite knot* of the two original knots. The two knots in the sum are called *factors* of $\tau\#\tau'$.

The notion of composite knots is very important as it leads to the concept of a *prime* knot i.e. of a non-trivial knot that cannot be decomposed into a non-trivial connected sum. In other words, if a prime knot τ is equivalent to the connected sum $\tau'\#\tau''$ this implies that either τ' or τ'' are unknots.

The basic facts about connected sums are that: (i) the operation is commutative (i.e. $\tau\#\tau' = \tau'\#\tau$) and (ii) that each non-trivial knot has a unique and finite factorization into prime knots.

For this reason standard knot tables, see for example the knot table in [18], lists only prime knots (some of which can have two types of handedness, see next section). The simplest prime knots, those with $n_{cr}^{min} \leq 6$ are shown in Figure 5 while the simplest composite knots, which are clearly generated by the connecting two trefoil knots are given in Figure 6.

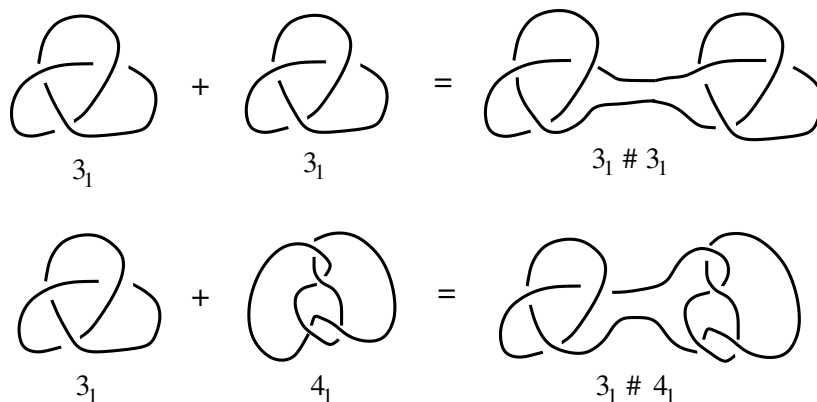


Figure 6: Connected sum of simple knots. The composite knot in the upper panel is known as the granny knot and is obtained by connecting two trefoils with the same handedness.

An important fact is that the number of prime knots existing at a given value of n_{cr}^{min} grows exponentially with n_{cr}^{min} [20, 21, 22]. This rapid growth is reflected in the fact that presently available exhaustive tables of prime knots (minimal representations) exist only for knots with up to ~ 16 crossings [23]. For special knot families, such as the alternating knots described later on, there exists tables of up to 22 crossings [24].

3.2. Knot handedness

An important notion in knot theory is *chirality*, or *handedness*. Suppose we look at a knot in a mirror. Is the mirror image equivalent to the original one or not? As an example let us consider the trefoil knot and its mirror image in Figure 7. The “right handed” knot of (panel *b*) cannot be continuously deformed into the “left-handed” version shown in panel *a*. For this reason, the trefoil knot is said to be *topologically chiral*. The homotopy inequivalence of the two chiral versions of the trefoil was first proved in 1914 by M. Dehn. By contrast if a knot can be continuously deformed into its mirror image we say that the knot is *topologically achiral*, or simply achiral (see for example the 4_1 knot in Figure 8).

Achiral knots are relatively rare. Indeed among the first 35 prime knots in the knot table less than a 1/4 are achiral ($0, 4_1, 6_3, 8_3, 8_9, 8_{12}, 8_{17}, 8_{18}$); all 49 9-crossings knots are chiral and only 13 of a total of 165 10-crossings knots are achiral. The knot nomenclature introduced before is clearly incapable of distinguishing enantiomers, as they have the same minimal crossing number. For prime knots with 7 or less crossings, the enantiomers can be distinguished by computing the balance of left- and right-handed crossings in the *minimal diagram*. To do so, it is first required to assign an orientation to the knot diagram¹. The handedness of each crossing is assigned by the right-hand rule applied to the oriented over- and under-passing segments as shown in Figure 9.

The overall chirality is then established by assigning a “+1” value to right-handed crossings and “-1” to the others and then taking the algebraic summation of the crossing signs. A right- and left-handed trefoil would therefore be associated to signed crossing numbers equal to +3 and

¹We mention that there exist knots that, by using an appropriate ambient isotopy, can be transformed into themselves but with the reversed directionality. These knots are termed invertible and the simplest one is given by 8_{17}

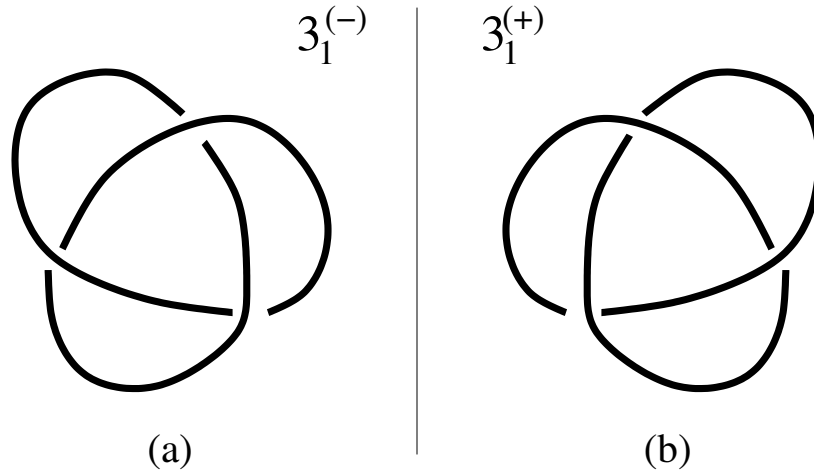


Figure 7: The trefoil knot and its mirror image. The trefoil knot in panel (a) is left-handed and the one in panel (b) is right-handed

-3, respectively. The resulting +/- sign of the summation can be appended to the knot name to distinguish the two types of enantiomers. For example the right- and left-handed enantiomers of the trefoil are denoted respectively by $3_1(+)$ and $3_1(-)$.

We stress that the above rule is formulated for the minimal diagram representation of prime knots with less than 8 minimal crossings and alternating knots (see next subsection) but can fail for an arbitrary diagram of these knots. In general, the rule will fail even for minimal diagram representations of prime knots, as pointed out by A. Perko [25]. Bearing in mind these important limitations, the chirality of connected sum of different prime knots can be suggested by the sign of the summed crossings in the minimal diagram. For example the composite knots $3_1(+)\#3_1(+)$ and $3_1(-)\#3_1(-)$ are two enantiomers of the granny knot while the knot $3_1(+)\#3_1(-)$ is achiral and is called the *square knot*.

The concept of signed crossings can be also used to discuss the minimal topological changes that can be applied to a given knot to turn it into an unknot. Within a minimal knot diagram representation it is easy to realize that one can convert a knot into the unknot by reversing one or more crossings in the knot diagram. For example the trefoil knot in its simplest form has only three crossings, and by changing in one of these crossing the under-passing strand into the overpassing one and vice-versa, we obtain the unknot. In general, for a given knot diagram it is always possible to find a set of crossings that can be switched over to obtain the unknot. On the other hand, for each knot diagram there can be several possible choices of crossings that can lead to the unknot. Moreover the number of crossing changes required might depend on the diagram. It is then natural to define the *unknotting number* as the minimum (taken over all possible knot diagrams) number of crossing reversals needed to turn a given knot into the unknot [18, 17].

There is no simple relation of the unknotting number to the minimal number of crossings of a knot. For example, the trefoil and figure eight knots both have unknotting number 1. Of the two five-crossing knots, 5_2 has unknotting number 1 and 5_1 has unknotting number 2. The granny knot has unknotting number 2 (essentially because each trefoil has to be unknotted). It turns out that if a knot has unknotting number 1 then it is automatically prime [26], but the converse is not

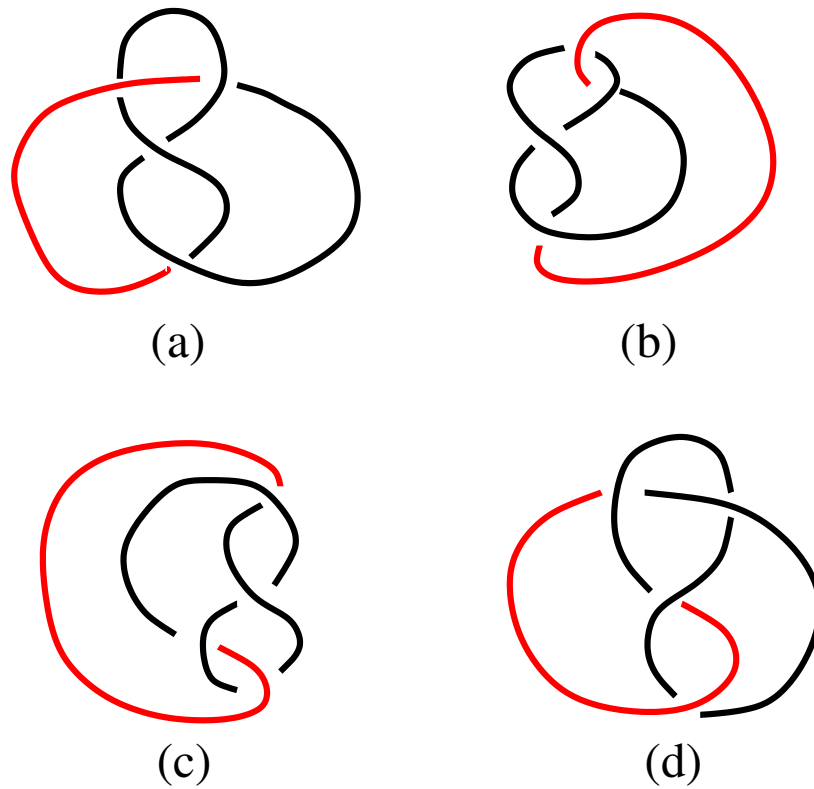


Figure 8: Achiral knots: How to pass from the 4_1 (a) to its mirror image (d) by smooth deformation. (b) Rearrange the red part of the curve. (c) Rotate the knot by 180° .



Figure 9: The sign convention for signed crossings. The arc labelling is for the computation of the Alexander polynomial.

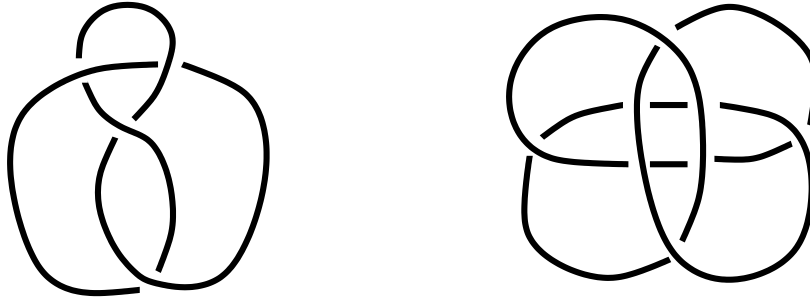


Figure 10: A minimal (alternating) knot diagram for 4_1 (left) and a diagram of the same knot that is not alternating.

true.

A natural generalization of the above scheme is the definition of the minimum number of crossing changes required to convert one given knot into another one. This number provides a distance in the space of knots. General topological considerations can be used to provide upper and lower bounds for knot distances which, in fact, are known exactly only for a limited subsets of knot pairs [27]. A recent practical application of this distance in knot space has been described in ref. [4, 28] in connection with the topoisomerase action on circular DNA.

3.3. Some knot families

As anticipated, prime knots can be partitioned in families according to salient topological indicators, such as the minimal number of crossings. An important one is the *alternating knots*, that is knots admitting a minimal diagrammatic representation where under and over crossings alternate along the path. Note that not all diagrams of an alternating knot need to possess the alternating properties described above, as illustrated in Figure 10. Interestingly, most of the simplest types of knots, that is those with sufficiently small crossing number, are alternating. In fact, all prime knots with crossing number smaller than 8 are alternating, with the simplest non-alternating instance being the 8_{19} knot.

With the exception of the unknot no other knot can be drawn on the surface of a sphere without self-intersections. Notably, there is a class of knots that, nevertheless, can be drawn as a simple closed curve on the surface of a standardly embedded (i.e. unknotted) torus. This is the family of *torus knots*.

As an example we show in Figure 11 the trefoil as a (2,3)-torus knot: the knot is shown to wind around the torus for $p = 2$ times longitudinally and $q = 3$ times meridionally (a meridian being a circle bounding the disc inside the torus). The p and q numbers can be positive or negative depending on the orientation of the winding directions and fully classify the (p, q) -torus knot. Basic properties of such knots are:

- p and q must be relatively prime;²
- a (p, q) -torus knot is topologically equivalent to a (q, p) -torus knot;
- if p or q is 1 or -1 the curve is unknotted;

²if p and q are not relatively prime one obtains links (see subsection 14 for definition).

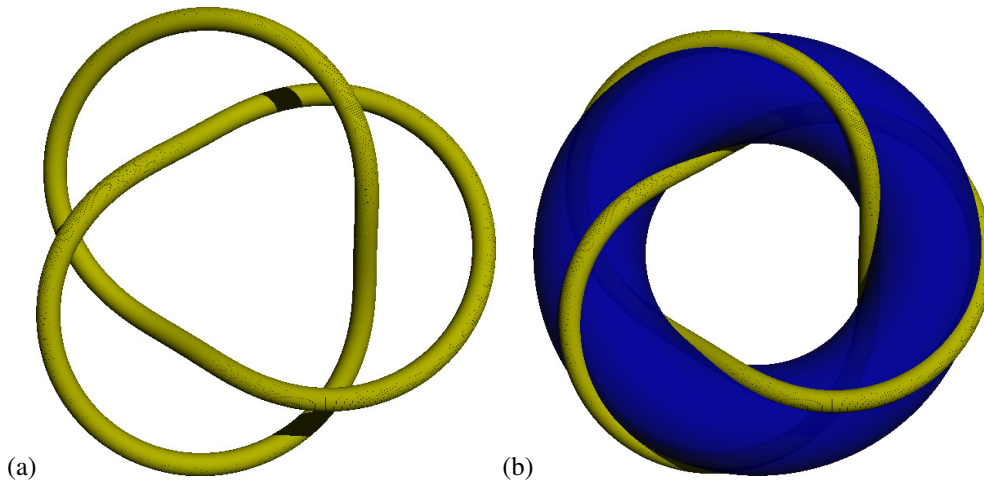


Figure 11: The trefoil knot (a) drawn on the surface of a torus as a $(3,2)$ torus knot (b).

- the mirror image of a (p, q) torus knot is a $(p, -q)$ torus. In other words all the non-trivial torus knots are chiral.

A number of exact results have been proven for torus knots. Two noteworthy ones regard the minimal crossing number and the unknotting number. For torus knots (p, q) , the former is given by $\min\{p(q-1), q(p-1)\}$ [29] while the unknotting number is given by the simple formula $((p-1)(q-1))/2$ [30].

3.4. Geometric techniques

One can also use geometrical quantities to characterize knots. The boundary of a punctured sphere is necessarily the unknot. If, on the other hand, we puncture a higher genus surface (e.g. a torus) the boundary curve can be knotted. In fact there is a well established theorem saying that every knot is the boundary of an orientable surface. The proof consists of an explicit construction first derived by Seifert and the orientable surface is called a *Seifert surface* of the knot (see Figure 12 for a sketch of the Seifert surface of the trefoil). A knot can have many Seifert surfaces. The lowest genus (orientable) Seifert surface of a knot defines the *genus* of that knot. For instance the trefoil and figure eight knots both have genus 1 since they can each be the boundary curve of a punctured torus. It is not difficult to prove that genus adds under the connected sum operation so the granny knot has genus 2. As a by-product one has the important result that a knot cannot be untied by connecting it to another non-trivial knot. In other words anti-knots cannot exist.

It is important to distinguish between the genus g of a knot (related to be the boundary of a genus- g surface) and its possibility of lying on a standardly embedded surface of genus G . For example the figure-eight knot has genus 1 but it cannot be placed on a unknotted torus (surface with $G = 1$); it can lie however on a standardly embedded surface with $G = 2$.

3.5. Polynomial invariants

One of the fundamental open problems in knot theory is to devise general schemes for establishing whether two given knots are equivalent or not. The use of sophisticated “motion

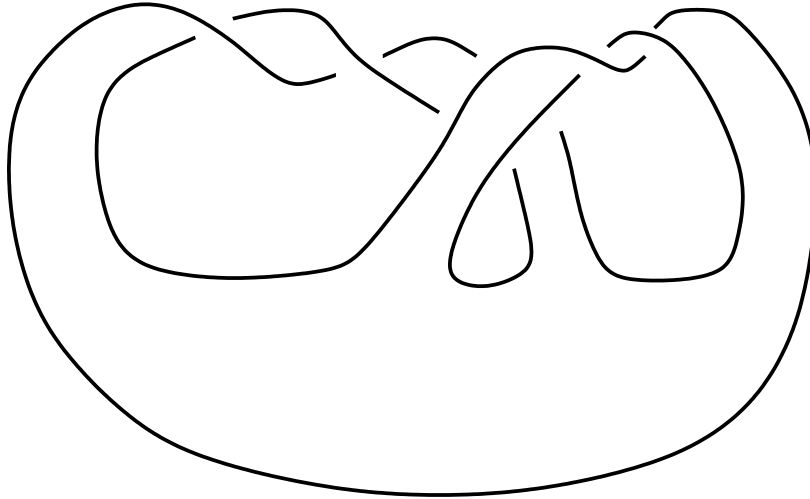


Figure 12: The surface obtained from a disk by attaching two twisted bands is an orientable surface whose boundary is the trefoil knot.

planning” computational algorithms have proved useful in past years to aid the geometrical simplification of knots to a minimal, or otherwise unique [31], conformation which can then be straightforwardly used to establish topological equivalence. However, the geometrical embedding of even an unknotted closed curve in \mathbb{R}^3 can, in fact, be so entangled that the simplification to a planar loop is impractical. This may indeed be impossible for unknotted polygonal curves deformed by moves preserving the length of their edges [32].

A powerful strategy, alternative to the geometrical simplification, consists of associating to each knot type an *invariant* quantity whose value is unaffected by topology-preserving geometrical manipulations of the curves.

In this way if the value of the invariant differs for two different embeddings (or diagrams), then the two embeddings have different knot types. Some invariants that have been obtained by studying the three-dimensional manifold left after the knot is removed from space, are *the knot group*, the *topology of branched and unbranched covering spaces* and the properties of *Seifert surfaces* [18, 16].

Nevertheless, these very precise invariants are not very useful in applied numerical contexts, where it is typically necessary to identify the knot type of thousands or millions of rings. For such purposes it is customary to resort to invariants which are computed combinatorially from knot diagrams and put in the algebraic form as polynomials. Perhaps the best known knot polynomial invariant is the *Alexander polynomial*. The latter is defined in terms of a single variable t and is computed starting from a given diagram according to the following general algorithm:

- I. Attach an orientation to the diagram and establish the sign of each crossing using the right-hand rule, as in Figure 9.
- II. Assign a progressive numbering index to the n arcs of the diagrams and (separately) to the n crossings.
- III. Define an $(n \times n)$ matrix M . The elements of the x th row of M are calculated by considering the x^{th} crossing in the diagram and the three arcs, i , j and k taking part to the crossing. For

definiteness we shall assume that the i^{th} arc passes over arcs j and k . All elements of the x^{th} row of M are set to zero except for $M(x, i)$, $M(x, j)$, $M(x, k)$. These three entries are calculated as follows:

- (A) if the crossing x is positive then $M(x, i) = 1 - t$, $M(x, j) = -1$ and $M(x, k) = t$.
- (B) if the crossing is negative then set $M(x, i) = 1 - t$, $M(x, j) = t$ and $M(x, k) = -1$.

Iterating the procedure for all crossings the matrix is completely defined.

Deleting any one of these columns and any one row yields a $(n - 1) \times (n - 1)$ matrix. This is the *Alexander matrix* associated to a given diagram. The determinant of the Alexander matrix (which is therefore a minor of M) is the desired Alexander polynomial, $\Delta(t)$ [18].

The calculation of the Alexander polynomial for the five-crossing prime knot 5_2 is illustrated in Figure 13.

Strictly speaking, the Alexander polynomial is not uniquely defined for a given knot type. This is evident because the size of the matrix, M , and hence the determinant, depend of the number of crossings and hence on the details of a given diagrammatic representation. It turns out that the Alexander polynomials of two different diagrammatic representations of the same knot type can differ only by a multiple of $\pm t^m$, $m \in \mathbb{Z}$. This ambiguity is immaterial if one computes $\Delta(-1)$, which is indeed a topological invariant. This ambiguity, which is immaterial if one computes the topological invariant $\Delta(-1)$, is however present if the value of the polynomial is calculated for other values of t . By factoring out and removing the $\pm t^m$ contribution one obtains a polynomial that is independent on the chosen projection of the knot.

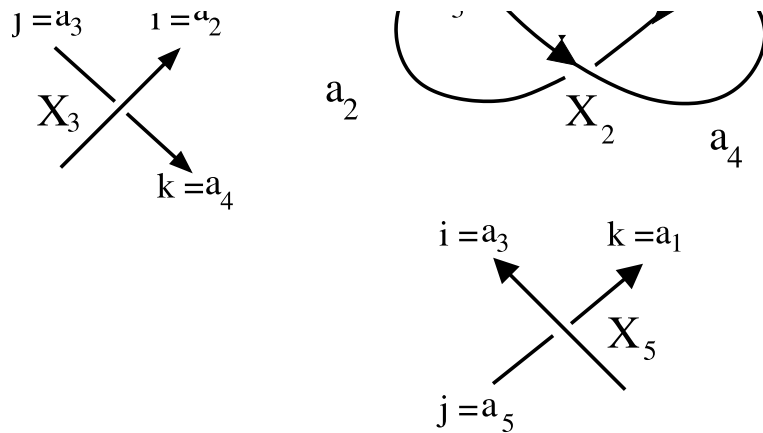
This gives the so called *irreducible* Alexander polynomial. For example in the typical case of $t = 2$ the algorithm returns the number $\pm 2^m \Delta(-2)$, $m \in \mathbb{Z}$. To deal with this ambiguity one can find the largest value of $k \in \mathbb{Z}$ such that the product $\pm 2^m \Delta(-2) 2^{-k}$ is an odd integer. With a slight abuse of notation, it is customary to use the notation $\Delta(t)$ also for the irreducible Alexander polynomial.

The Alexander polynomial satisfies a number of properties including:

- I. $\Delta_\tau(t^{-1})$ and $\Delta_\tau(t)$ can differ only by factors of $\pm t^{\pm m}$;
- II. $\Delta_\tau(1) = -1$;
- III. $\Delta_{\tau\#\tau'}(t)$ is equivalent to $\Delta_\tau(t)\Delta_{\tau'}(t)$. For example, since the Alexander polynomials of 3_1 and 4_1 are respectively $\Delta_{3_1}(t) = t^2 - t + 1$ and $\Delta_{4_1}(t) = t^2 - 3t + 1$, we have for the granny knot $\Delta_{3_1\#3_1}(t) = (t^2 - t + 1)^2$ and $\Delta_{3_1\#4_1}(t) = (t^2 - t + 1)(t^2 - 3t + 1)$.

The first property can be used to check the correctness of a calculated polynomial. For example, no correct calculation can return the polynomial $\Delta_\tau(t) = t^3 + t^2 - 1$, because $\Delta_\tau(t^{-1}) = t^{-3} + t^{-2} - 1$ is not in the form $\pm t^p (t^3 + t^2 - 1)$ and property 1 is not satisfied.

The Alexander polynomial is relatively easy to implement on a computer and it is often used in detecting the knot type of a large number of configurations obtained by stochastic sampling, for example. There are however some shortcomings in using the Alexander polynomial as a knot detector. First, and most importantly, the Alexander polynomial cannot distinguish between knots and their mirror images. Second, there are several pairs of knot types having the same Alexander polynomial. For instance, the (irreducible) Alexander polynomial of knot 8_{20} is $\Delta(t) = (t^2 - t + 1)^2$, which is identical to the polynomial of the granny knot $3_1\#3_1$ while 8_{21} has the same Alexander polynomial as $3_1\#4_1$. The ambiguity can be even more dramatic in the sense that non-trivial knots can have the same Alexander determinant of the unknot. The simplest of such knots are the Kinoshita-Terasaka Knot and its mutant, the Conway knot, which have minimal crossing number equal to $n_{cr}^{\text{min}} = 11$.



$$\begin{bmatrix}
 1-t & 0 & 0 & t & -1 \\
 t & -1 & 0 & 1-t & 0 \\
 0 & 1-t & t & -1 & 0 \\
 0 & t & -1 & 0 & 1-t \\
 -1 & 0 & 1-t & 0 & t
 \end{bmatrix}
 \longrightarrow
 \begin{array}{c}
 1 \cdot \\
 t \\
 0 \\
 0
 \end{array}$$

$$\longrightarrow 2t^3 - 3t^2 + 2t \longrightarrow 2t$$

Figure 13: Computation of the Alexander polynomial for knot 5_2 . The top panel shows the knot diagram with a given orientation: X_i denotes the i^{th} crossing (found as one goes around the diagram along the given orientation) whereas a_i the arc between two consecutive undercrossings. Each crossing of the diagram is then drawn separately and coded according to the arcs involved taken with their orientation. From these $n = 5$ coded crossings it possible to calculate the elements of the matrix 5×5 according to the algorithm described in the text. By deleting the last column and row one obtains the 4×4 Alexander matrix associated to the starting oriented knot diagram. The determinant of this matrix gives the Alexander polynomial. Note that in this example a term t can be factorized out of the diagram.

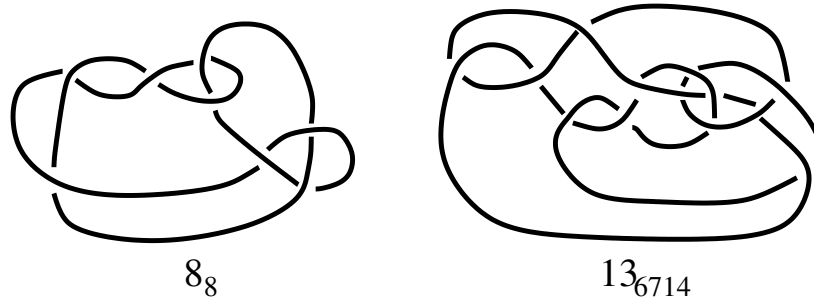


Figure 14: Two different knot types having the same HOMFLY polynomial.

Other polynomials are known which are better discriminants of knots. For example the Jones polynomial, the HOMFLY polynomial (see [16] for a simple introduction) and the Vassiliev invariants are known to be sensitive to knot chirality and to distinguish a large class of knots that cannot be distinguished by the Alexander polynomial. However, also for these polynomials there are known examples of topologically inequivalent knots having the same polynomials. For example the two knots in Figure 14 have the same HOMFLY polynomial. Even the proof that at least one of the known invariants is a perfect detector of chirality or non-triviality is an open issue and there may exist non-trivial knots for which all the known polynomials are trivial.³ An additional drawback of these more sophisticated knot polynomials is that their computational cost increases dramatically with the number of crossings in the diagram. For this reason, if one is interested in performing a detailed investigation of the knot complexity in random loops, a strong reduction of n_{cr} is recommended before computing these invariants. The reduction of n_{cr} for a given embedding is, in general, a highly non-trivial task to perform. Stochastic algorithms have been recently introduced to tackle this problem and some of them are reviewed in Section 6.3.

3.6. Open knots

In various contexts, the notion of knottedness is loosely transferred to open curves. Strictly speaking this is inappropriate because a piece of curve is topologically equivalent to a linear segment, no matter how many knots have been tied in. Indeed, an appropriate set of manipulations of the open curve can lead to the untying of the knots. It is, nevertheless, a common experience that these operations can be lengthy and complicated and ultimately the characteristics of the curve in terms of its spatial arrangement or fluctuation dynamics are very much affected by its degree of entanglement.

To characterize the latter a “virtual closure” of the open chain is often introduced so that the usual topological indicators of knottedness can be used to specify the degree of self-entanglement. Several closure procedures are possible. The simplest one is the end-to-end closure obtained by bridging the two ends with one segment. The amount of spurious entanglement introduced by this closure depends on the proximity of the chain ends. If their spatial separation is small

³There is in fact a perfect algebraic knot and link detector—two links are equivalent if and only if there is an isomorphism of the fundamental group of the link complement that matches up all (longitude, meridian) pairs—this is called the peripheral structure of the link, and follows from a result of Waldhausen [33]. The problem is that this invariant is not computable in any known way, so is not very useful in computations.

compared to the chain radius of gyration then the entanglement added by the end connector is typically negligible. The opposite is true when the connector length is large.

To deal with the latter case it is preferable to prolong the chain ends “at infinity” so that they can be connected by an arc not intersecting the original chain. If the knots are localised in a small portion of the chain, then the detected topological state will not depend significantly on the specific closure procedure. Other situations, for example when the chain attains a globular shape with one or both ends tucked inside, the result will depend on the closure scheme. These ambiguities have motivated the introduction of a probabilistic concept of knottedness for an open curve. In this situation, closure at infinity along all possible directions of prolongation of the chain ends are considered and a probability profile for the detected topological states is considered in place of a single topological identifier [34]. In several cases of practical interest these different schemes yield consistent results. One notable example of this consensus is provided by knotted proteins which constitute about 1% of the set of presently-known protein structures [35]. A very high consistency exists among the different methods of closure regarding the knotted/unknotted state of individual protein chains and also regarding the occurring types of knots [36, 37, 38, 39, 40, 41, 42, 35].

Clearly, the cases of minimal ambiguity for the knotted state of an open curve are associated to situations where knots are localised in a small portion of the chain. Indeed a closely-related problem is the determination of the length of a knot (in either a closed or open chain) [43]. This problem, which has been recently tackled in ref. [44] by comparing existing and new closure schemes, will be addressed in Section 17 of this review.

4. Coarse-grained models of polymers in \mathbb{R}^3 : from freely-jointed chains to semi-flexible self-avoiding ones.

In this section we shall introduce a number of standard polymer models whose geometrical and topological properties in a variety of physical conditions will be extensively discussed in the rest of this review. The models will be described in the “open chain” formulation as it is understood that the chain closure can be introduced by simply enforcing the coincidence of the first and last monomer of the chain, to obtain polymer rings.

Arguably, the simplest discrete polymer model is represented by the *freely-jointed chain*. The model consists of a succession of equally-long segments, usually termed bonds, that can take any arbitrary relative orientation. This model essentially captures the chain connectivity property while other salient aspects associated to the energy cost of introducing local bends in the chain, or disallowing self-avoidance, are not considered.

The oversimplified nature of the model brings the advantage of allowing for a straightforward analytical or numerical characterization and is a natural first step for characterizing the behaviour of more realistic polymer models.

To illustrate this point, and for the purposes of introducing the notation that will be used hereafter, we consider a freely-jointed chain configuration, Γ , with nodes at positions $\{\vec{r}_0, \vec{r}_1, \dots, \vec{r}_N\}$. All bonds joining consecutive nodes, $\vec{b}_i \equiv \vec{r}_i - \vec{r}_{i-1}$, have the same length, b , as illustrated in Figure 15a.

The mean square end-to-end distance has a linear dependence on the chain length:

$$\langle R_{ee}^2 \rangle = \left\langle \sum_{i,j=1}^N \vec{b}_i \cdot \vec{b}_j \right\rangle = \sum_{i,j=1}^N \langle \vec{b}_i \cdot \vec{b}_j \rangle = \sum_{i=1}^N \langle \vec{b}_i \cdot \vec{b}_i \rangle = Nb^2 \quad (1)$$

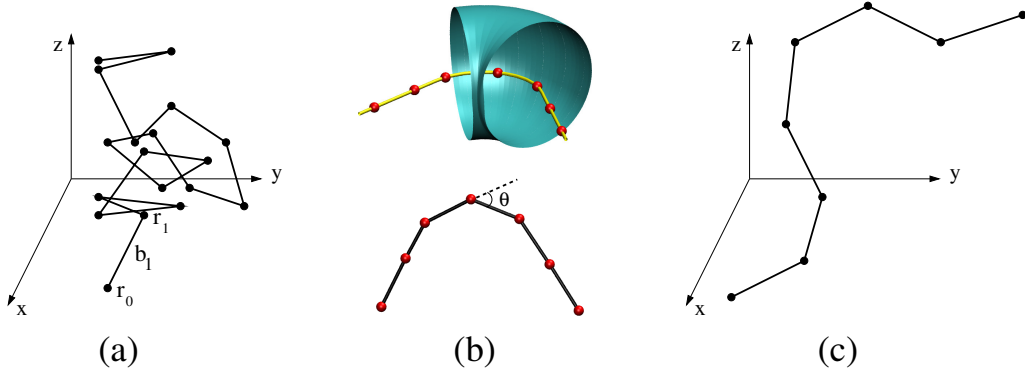


Figure 15: (a) Possible configuration of a freely-jointed chain. (b) The yellow curve indicates the centerline of a continuous polymer with uniform thickness (tube). A portion of the tube hull is shown explicitly to illustrate that the polymer thickness cannot excessively have small local radii of curvature without self-intersecting. When the polymer is discretized (red beads), the curvature constraint reflects in a maximum allowed value for the angle, θ , formed by consecutive bonds, as shown in the bottom panel. (c) Configuration of a discrete chain where the angle of two consecutive bonds is not allowed to exceed 45° .

where the statistical independence of the orientation of different bonds was used. Besides the end-to-end distance, a commonly employed measure of the typical spatial size of the chain is given by the radius of gyration, R_g :

$$\langle R_g^2 \rangle = \left\langle \frac{1}{N+1} \sum_{i=0}^N |\vec{r}_i - \vec{r}_{CM}|^2 \right\rangle = \frac{1}{2} \left(\frac{1}{N+1} \right)^2 \left\langle \sum_{i,j=0}^N |\vec{r}_i - \vec{r}_j|^2 \right\rangle. \quad (2)$$

where \vec{r}_{CM} denotes the location of the chain center of mass, $\vec{r}_{CM} \equiv \sum_{i=0}^N \vec{r}_i / (N+1)$. In the limit $N \gg 1$ one has that the average end-to-end distance and the radius of gyration are tied by a simple linear relationship, namely $\langle R_g^2 \rangle = N^2 b = \langle R_{ee}^2 \rangle / 6$ which highlights that also R_g^2 depends linearly on N [45].

As anticipated, the model is highly simplified and needs to be suitably generalised before it can be used to describe key physical aspects of a free polymer in solution. Arguably, the simplest physical effect that can be introduced in the model to make contact with the phenomenology of flexible chains is to consider the correlations in the directionality of consecutive bonds.

These correlations arise, for example, when accounting for the polymer bending rigidity. By analogy with the case of an ideal elastic rod slightly perturbed from the straight configuration, the bending energy of a chain configuration, Γ , can be approximated by the following energy function:

$$E_{bend}(\Gamma) = K_c \sum_i \left(1 - \frac{\vec{b}_i \cdot \vec{b}_{i+1}}{b^2} \right) \quad (3)$$

where K_c is the chain bending rigidity. Freely-jointed chains endowed with a bending rigidity term as above are termed *Kratky-Porod chains*.

Because of the simple form of the energy function of eq. 3 (which does not account for chain self-avoidance), it is possible to compute analytically several properties of Kratky-Porod chains in thermal equilibrium. Specifically, we shall assume that the statistical weight of a chain configuration, Γ , is given by the canonical Boltzmann weight:

$$\frac{e^{-E_{bend}(\Gamma)/K_B T}}{\sum_{\Gamma'} e^{-E_{bend}(\Gamma')/K_B T}} \quad (4)$$

where K_B is the Boltzmann constant, T is the temperature and the correct normalization of the statistical weight is ensured by the denominator where the summation stands for the integrated contribution over all possible chain configuration.

The effects that the local bending energy has on the correlation of the bonds directionality in the chain can be ascertained by calculating the average (equilibrium value) of the scalar product of two chain bonds at a separation l along the chain. This quantity is straightforwardly calculating starting from $l = 1$ and iterating to larger values of l obtaining [45]:

$$\langle \vec{b}_i \cdot \vec{b}_{i+l} \rangle = b^2 e^{-l/l_p} \quad (5)$$

where $\langle \rangle$ denotes the equilibrium average where configurations are weighted with the canonical weight of eq. 4 and the quantity l_p , termed the persistence length, is given by

$$l_p = -b / \log \left[\coth \left(\frac{K_c}{K_B T} \right) - \frac{K_B T}{K_c} \right]. \quad (6)$$

The above expression clarifies that the bending rigidity introduces an exponentially decaying correlation in the orientation of bonds along the chain, as readily perceived by the comparative inspection of panels (a) and (c) in Figure 15.

Notice that, in the limit $K_c \gg K_B T$, that is when the average value of the bending angle between consecutive bonds is small, the expression of the persistence length simplifies to: $l_p = b \frac{K_c}{K_B T}$, which is the well-known simple relationship tying the persistence length and the bending rigidity in the continuum limit of the Krakty-Porod chain (which leads to the so-called *worm-like chain*) [46].

A further physical effect that introduces correlations in the bonds orientations is the steric hindrance associated with a finite thickness of the chain. When accounting for this effect, the model chain should be viewed as the centerline of a discrete thick polymer with cross-sectional radius equal to Δ . At a global level, the finite thickness of the chain introduces correlations in portions of the chain that can be even far apart along the “polymer sequence”. In addition, this self-avoidance has an impact at a local level as the chain cannot attain local radii of curvature smaller than Δ [47], see Figure 15b . This implies that the angle θ formed by two consecutive bonds must satisfy the following constraint:

$$\cos \theta \geq 1 - \frac{b^2}{2\Delta^2}. \quad (7)$$

which, propagated along the chain, introduces an exponentially-decaying correlation of the chain orientation that is entirely analogous to the one in eq. (5):

$$\frac{\vec{b}_{n+1} \cdot \vec{b}_1}{b^2} = \left[1 - \frac{b^2}{4\Delta^2} \right]^n. \quad (8)$$

This correlation, which is readily perceived by the comparative inspection of panels (a) and (c) in Figure 15 and the decay length can be viewed as a thickness-related persistence length given by [48]:

$$l_p = -\frac{b}{\ln\left(1 - \frac{b^2}{4\Delta^2}\right)}. \quad (9)$$

We stress that the above expression merely captures the *local* effects of the finite thickness of the chain.

We conclude this discussion by considering how the interplay of the chain contour length (that is the total chain length obtained by summing the length of all its bonds), $L_c = Nb$, and of the persistence length, l_p , controls the physical behaviour of the system.

To do so we shall consider a Kratky-Porod model of given contour length, $L_c = Nb$, and given persistence length, l_p . The discretization step, b , is assumed to be much smaller than the persistence length (and therefore K_c is suitably adjusted so to reproduce the given persistence length). In this situation, the mean square end-to-end distance is given by [45]

$$\langle R_{ee}^2 \rangle = \left\langle \sum_{i,j} \vec{b}_i \cdot \vec{b}_j \right\rangle = b^2 \sum_{i,j} \exp\left[\frac{-|i-j|b}{l_p}\right] \quad (10)$$

$$\approx 2l_p L_c \left[1 - \frac{l_p}{L_c} \left(1 - e^{-\frac{L_c}{l_p}} \right) \right] \quad (11)$$

From this expression it is readily seen that when the contour length is much smaller than l_p , the polymer can be viewed as a stiff chain. In fact, the mean square end-to-end distance is approximately

$$\langle R_{ee}^2 \rangle \approx L_c^2 \left[1 - \frac{L_c}{3l_p} + O\left(\frac{L_c^2}{l_p^2}\right) \right] \quad (12)$$

which, for $L_c \gg l_p$ reduces to the rigid rod value, $\langle R_{ee}^2 \rangle \approx L_c^2$. For future reference it is worth calculating separately the contributions to eq. (12) along the direction approximating the straight rod, $\langle R_{ee}^{\parallel 2} \rangle$ and in the plane perpendicular to it, $\langle R_{ee}^{\perp 2} \rangle$. The first term, $\langle R_{ee}^{\parallel 2} \rangle$, is readily obtained by noting that the average directionality of the chain is biased by the first bond, \vec{b}_1 , so that

$$\langle \vec{R}_{ee}^{\parallel} \rangle = \frac{1}{b} \sum_l \langle \vec{b}_l \cdot \vec{b}_1 \rangle = b \sum_l \exp\left(\frac{-l}{l_p}\right) = \frac{1 - \exp\left(\frac{-L_c}{l_p}\right)}{1 - \exp\left(\frac{-b}{l_p}\right)}. \quad (13)$$

From expressions (13) and (12) and using $\langle R_{ee}^{\perp 2} \rangle = \langle R_{ee}^2 \rangle - \langle R_{ee}^{\parallel 2} \rangle$ one has, to leading order in L_c/l_p and b/L_c :

$$\langle R_{ee}^{\perp 2} \rangle = \frac{2}{3} \frac{L_c^3}{l_p}. \quad (14)$$

When $L_c \approx l_p$ the chain is said to be semi-flexible, in that appreciable deviations from the straight configurations are possible in thermal equilibrium. Instead, in the limit $L_c \gg l_p$, one has

$$\langle R_{ee}^2 \rangle \approx 2l_p L_c \quad (15)$$

By comparison with eq. (1), the latter identity can be used to say that the equilibrium size of the chain is equivalent to that of a freely-jointed chain with same contour length, but where the statistically independent segments have effective length equal to twice the persistence length, $l_K = 2l_p$. The equivalent length, l_k , is termed the *Kuhn length*.

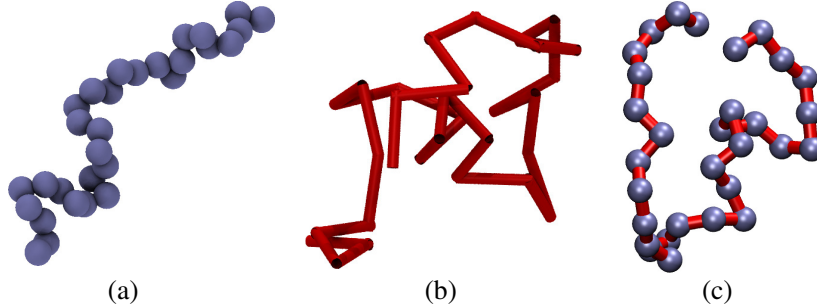


Figure 16: Possible configurations of: (a) a chain of beads, (b) a chain of cylinders, (c) a chain of beads and cylinders.

4.1. Flexible and semi-flexible chains: the cylinder and rod-bead models

It is important to stress that in the rigid and semi-flexible regimes the non-local self-avoidance effects in unconstrained chains can be largely neglected, as steric clashes will not be likely to occur because of the limited contour length of the chain.

This is not true when L_c largely exceeds l_p , which is the condition in the flexible polymer regime. When self-avoidance is taken into account, the end-to-end distance, R_{ee} or, equivalently, the radius of gyration, does not have a linear dependence on the contour length anymore, rather it obeys the more general formula

$$\langle R_{ee}^2 \rangle \propto N^{2\nu} b^2 \quad (16)$$

where the self-avoiding exponent ν is about 0.588 [49], and is often approximated by its mean-field estimate $3/5$ [45, 50]).

The above discussion has been mostly focused on considerations of the relative magnitude of the persistence and contour length. For modelling purposes a key element to consider is also the relative magnitude of the polymer thickness, Δ , and the persistence length, l_p .

For several biopolymers, such as polysaccharides, proteins and single-stranded DNA, the persistence length is comparable with the thickness. In such contexts, it is natural to model the polymers as chains of spherical beads of radius Δ , as shown in Figure 16a. The so called *bead model* can be endowed with a bending rigidity which, together with constraints on the minimum attainable local radius of curvature imposed by the self-avoidance (see eq. 7), determines the chain persistence length [51, 52].

Notice that when the persistence length largely exceeds the chain thickness, then the bonds at a small arclength separation would tend to be collinear. This observation suggests the possibility of modifying the model so as to reduce the number of effective degrees of freedom in the system. An effective way to do this is to describe the chain as a sequence of cylinders with thickness Δ and axis length, l , equal to a fraction of the persistence length (and yet much larger than Δ). A possible configuration of a flexible chain of cylinders is shown in Figure 16b.

Again, the correct persistence length would be reproduced by the introduction of a suitable bending rigidity between consecutive cylinders [53]. The excluded volume interaction is simply enforced by disallowing pairs of non-consecutive cylinders from overlapping. This is done by calculating the distance of minimum approach of the centerlines of the two cylinders and requiring to be larger than 2Δ , see Appendix A. Note that the presence of a non-zero thickness, or excluded volume, renders an exact calculation of the tangent-tangent correlations impossible.

Excluded volume interactions cause the tangent-tangent correlation to acquire appreciable deviations from the exponential decay above a certain arclength separation which depends on the interplay of l , Δ and $K_c l/k_B T$ (for more details see e.g. the comparison between the discretized Kratky-Porod model which disregards steric effects and molecular dynamics simulations above the θ point in [54] which holds for the bead-and-spring polymer model defined above).

The *cylinder model* (with flexible joints) has been largely adopted to model a variety of molecules and especially double-stranded DNA (dsDNA). In fact, the dsDNA persistence length is equal to 50 nm while the bare DNA diameter has the much smaller value of 2.5 nm (larger effective diameters are reported depending on the concentration/type of counterions in solution [53, 51, 52]).

A model that interpolates between the beads model and the cylinder model may be described by a sequence of equally-long cylinders of thickness Δ_1 ; at the joints of the cylinders a sphere of radius Δ_2 is introduced, see Figure 16c. By varying Δ_1 and Δ_2 at fixed cylinder length, it is possible to explore the interplay of various excluded volume terms on the conformational statistics of the polymer rings of interest. In the limiting case of unit length cylinders with $\Delta_1 = 0$ and Δ_2 finite, it is obtained the *rod-bead model* [55] which has been often used to study the effect of self-avoidance on the knotting probability of polymer rings (see Section 7)

We conclude by observing that, when the polymers are subjected to spatial confinement, one needs to take into account further length-scales in the problem, namely the typical width of the confining geometry. In this case, the viability of cylinder models depends on the possibility of identifying a cylinder length that is not only much larger than Δ , but also appreciably smaller than the width of the confining region.

4.2. Polymer models on regular lattices: combinatorial arguments and rigorous results

The above mentioned models allow for a description of polymeric chains through a limited number of continuous degrees of freedom. Albeit greatly simplified, the models are sufficiently complicated that the characterization of their properties (especially when subject to confinement) requires the use of advanced stochastic sampling techniques such as those described in the next sections.

Occasionally, one deliberately resorts to over-simplified polymer models to achieve an exhaustive enumeration of the configuration space rather than sampling it with stochastic techniques. Almost invariably, these approaches entail the embedding of the model polymer chain on a discrete lattice, for example the cubic lattice.

In the simplest case, the polymer is modeled as a walk which joins nearest neighbours on the lattice. The self-avoidance is introduced by preventing the chain from multiply-occupying any lattice edge or node, as shown in Figure 17. A bending rigidity can also be introduced by giving an energy penalty for non-collinear consecutive segments of the walk. Other variants of this model are possible by allowing the walk to bridge not only nearest neighbours but also, for example, second-nearest neighbours. In this case chains are endowed with a larger configuration freedom though the bond lengths can fluctuate from configuration to configuration [56].

Denoting by c_N the number of distinct (up to translation) self-avoiding walks with N segments, hereafter referred to as edges or bonds, on 3D lattice, one can use simple counting arguments to compute by hand the values of c_N for small N values: $c_1 = 6$, $c_2 = 30$, $c_3 = 150$, $c_4 = 4 \times c_3 - 24 = 726$ etc. Clearly, as N increases the manual computation of hand c_N is unfeasible so that it is necessary to resort to efficient numerical techniques for the exhaustive generation, and hence enumeration, of *all* possible different walks or rings on a lattice up to a certain number of segments.

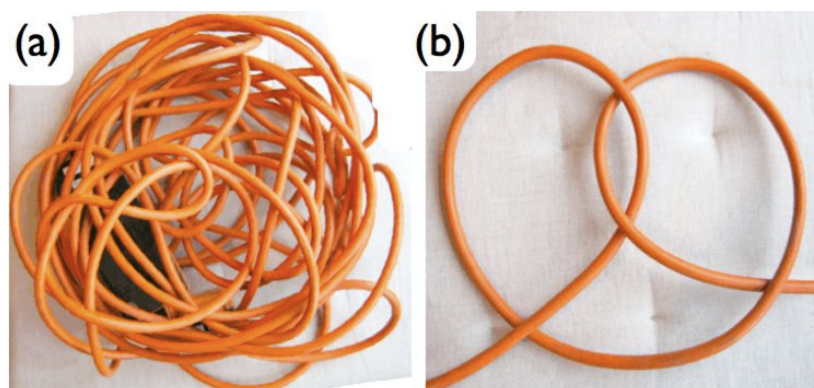


Figure 18: (a) A 10m extension lead taken from the cupboard where it was stored. When the cable ends are attached to the power socket and to the Hoover cable its entanglement is trapped in the form of a knot that can be of considerable complexity. The knot cannot be removed unless one of the cable ends is released and suitably passed through the tangle. By spreading out the cable in (a) so to simplify the geometry of the trapped knot, we recognise the 4_1 knot, see panel b. In our experience the knot complexity in the extension cord increases as it is repeatedly used and stored away (that is before our spouses force us to get up from the couch and engage the endless battle against the cable configuration entropy!).

5. Second Part: Self-entanglement of single polymer chains

In the second part of this review, spanning from sections 6 to 12, we summarize the state-of-the-art of the characterization of the types and abundance of knots formed by polymers which circularize either in unrestricted environments or under spatial confinement.

The interest in characterizing the probability that polymers, fluctuating in equilibrium, form a knot upon circularization has grown in parallel with the availability of experimental techniques capable of detecting the knotted/unknotted state of circular polymers.

Common experience suggests that long ropes that are shaken or shuffled, tend to become highly self-entangled. When their ends are joined, the chances that the resulting arc loop is knotted are quite high, just think of your garden hose or extension cord after it has been repeatedly used and stored away, see Figure 18.

This observation leads to the question: what is the degree of knotting of flexible polymers fluctuating in thermal equilibrium? A first answer to this was already proposed in the early sixties by Frisch, Wasserman [61] and Delbruck [62] (FWD) who conjectured that infinitely-long rings are almost certainly knotted (their knotting probability tends to 1 when their length goes to infinity). About twenty years later this conjecture was turned into a rigorous theorem for different models of polymer rings [63, 64]. The key concepts underpinning the proof are given in Section 7.

Since the FWD conjecture several efforts have been spent on the precise characterization of how the knotting probability depends on the length of the ring polymer. More recently, the interest has shifted towards characterizing how the knot spectrum (that is the knot type and relative abundance/frequency) depends on the polymer length. Most of these investigations have been carried out by numerical means. The computational cost of such studies is significant and arises from two separate factors. On one hand, the sampling of a statistically-significant ensemble of independent polymer ring configurations can be very demanding, especially for confined rings.

On the other hand, the precise assignment of the knotted state of each sampled configuration can be computationally intensive too as it entails the combinatorial calculation of global topological invariants, which rapidly grows as a function of the ring length (or degree of confinement).

Both these challenges are discussed in detail in the following sections. Particular attention is paid to the description of efficient stochastic techniques which have proved to be useful in sampling polymer ring conformations in a variety of physical situations (see Section 6). Specifically, we first discuss and illustrate the efficient sampling of unconstrained, flexible and self-avoiding ring polymers. These results are used to illustrate the viability of simplified polymers models in reproducing the experimental knot spectrum, found via gel electrophoresis techniques, for specific biomolecules, particularly DNA [65, 53].

Next, attention is turned to the case of polymer rings subject to a variety of external physical constrains. On one hand, this problem is motivated by the advent of novel experiments based on micro- and nano-fluidic devices, or on micromanipulation tools such as AFM [66, 67] and optical tweezers [68]. These techniques allow an unprecedented quantitative characterization of the detailed behaviour of long polymers in confined conditions [69, 70, 71, 72, 73]. This may be achieved by inserting these molecules in narrow channels [69, 74], by adsorbing them onto smooth surfaces [75], or by subjecting them to tensile stress [76]. A detailed understanding of the statical and dynamical properties of macromolecules in confined environment is crucial also for designing novel applicative avenues for nano-confinement, such as the use of nanochannels to pre-stretch and stabilize DNA molecules prior to their threading through a nanopore [77] or to make a binding site along a long coiled DNA molecule accessible to external probes [78]. On the other hand, as noted previously, genomic materials are also subject to spatial confinement *in vivo*, and their entanglement properties are crucial to the correct functioning of DNA replication, transcription etc.

The interest in polymer and knot adsorption is also motivated by the fact that this is rather easy to realise in the lab. For instance, when a polymer is rooted at the surface, by modulating (e.g. by means of temperature) the effective attractive potential between the polymer and the surface, it is possible to trigger an adsorption transition from an extended regime (with high configuration entropy) to an adsorbed one when it is mostly localised in proximity of the surface [50, 79]. This phenomenon may provide a way to visualise the impact of quasi-2D confinement on topology. For a polymer embedded exactly in a 2D plane or a sphere it is impossible to form knots – how is this regime reached in practice as a function of temperature? This question may now be answered experimentally.

The interest in the behaviour under stretching is further sparked by the recent use of modern micromanipulation techniques [80, 81, 68] to characterize the mechanical response of entangled polymers [2]. Remarkably, it is nowadays possible even to tie a knot in a piece of DNA or actin fiber [82] and then monitor its reptation dynamics along the stretched filament [83].

The experimental difficulties in establishing the knotting probability for ring polymers subject to geometrical/spatial constraints is paralleled by the challenges found in theoretical characterizations of analogous properties for simplified models. The difficulty arises from the competition of several length scales, e.g. the polymer contour length, the size of the confining geometry, and the polymer persistence length (a measure of its flexibility). We shall present the key theoretical concepts that have been introduced to tackle this problem such as the de Gennes blob picture and the Odijk deflection theory [84] which are valid, respectively, for weak and strong confinement. We shall also report on the state-of-the-art computational techniques used to reduce the impact on the sampling efficiency of the long relaxation times in dense polymer phases. Finally, for lattice models, it is possible to extend some of the rigorous results found in the unconstrained

situation to the confined case – these results are reviewed in Section 8.2.

Specifically, here we discuss 3D confinement, adsorption and stretching in Sections 9, 11, 12 respectively.

For the aspect of 3D confinement, we here address the following key questions:

- How does the knotting probability depend on the degree and the geometry of the confinement?
- Does the crossover between the De Gennes and the Odijk regimes correspond to a significant change in the knotting probability?
- What is the knot spectrum of linear polymers that circularize under spatial confinement?

As a biological application, we will review the studies of the topological entanglement of viral DNA inside viral bacteriophage capsids[85, 86]. This is an extremely intriguing problem for a number of reasons. For instance, until very recently, it was not possible to account theoretically for the experimentally-observed viral knot spectrum using simplified DNA models. Furthermore, one may ask how it is possible that bacteriophages are still infective and can eject their DNA into their bacterial host, given the high level of entanglement of the DNA inside the capsid. As we shall see, computer simulations helped shed light on both these issues.

Finally, the three-dimensional confinement is complemented by the discussion of the adsorption of polymer rings onto a two-dimensional surface, and the behaviour of knots upon mechanical stretching [2, 87].

In Section 11 we discuss the adsorption of polymer rings onto a two-dimensional surface, and discuss the following issues:

- How does the knotting probability depend on the degree of adsorption?
- How are the universal properties of polymer adsorption affected by topology?
- The critical point governing the adsorption transition of linear polymers has been well characterised [88, 79]. Is this critical point governing also a topological transition separating a regime of high knotting probability from one in which knot formation is negligible?
- What do we know about the knot spectrum of adsorbed polymers?

We close this Section with a list of unsolved open problems. It is particularly long because there have been very few investigations on the topic to date.

Finally, in Section 12 we survey the few results which have been obtained on the knotting probability and entanglement complexity of polymer chains under stress at equilibrium. Most of them refer to lattice models and are based on combinatorial arguments valid in the thermodynamic limit and on numerical simulations.

6. Sampling at equilibrium by Monte Carlo methods

The analytic characterization of the behaviour of polymers subject to geometrical or topological constraints is a challenging task even for the simplest polymer models, such as freely-jointed chains [89].

Essential tools for making progress in such characterizations are stochastic computational techniques such as Monte Carlo approaches.

In the present context, a Monte Carlo scheme consists of a set of rules for the stochastic generation of a succession of polymer configurations so that the steady state probability of visiting any given conformation is given by its canonical weight.

In brief, the scheme can be formulated as follows. We denote by Γ_A the polymer configuration at a given Monte Carlo step, and by E_A its energy. At the next step a new polymer configuration Γ_B (with energy E_B) is selected with uniform probability in the polymer configuration space. A stochastic criterion is next used to decide whether, at the next Monte Carlo step, the system configuration is given by Γ_B or if the “old” one, Γ_A , must be retained. Virtually all employed selection criteria are chosen so to satisfy the detailed balance condition [90, 91]. In other words they ensure that the probability of accepting the change in configuration, $w_{A \rightarrow B}$, satisfies,

$$\frac{w_{A \rightarrow B}}{w_{B \rightarrow A}} = \frac{e^{-\beta E_B}}{e^{-\beta E_A}}, \quad (20)$$

where $w_{B \rightarrow A}$ is the probability with which one would accept a change of configuration from B to A and β is the inverse temperature: $\beta^{-1} = K_B T$. Eq. (20) can be satisfied by many choices of the w 's. The one most commonly adopted is known as the Metropolis criterion and states that the probability to accept the change from A to B , $w_{A \rightarrow B}$ is equal to 1 if $E_B < E_A$ otherwise, it is equal to $\exp^{-\beta(E_B - E_A)}$. In a definite MC simulation, this probabilistic acceptance of the move is implemented by picking a random number in the $[0,1]$ unit interval, r , and accepting the change to configuration B if $r < \exp^{-\beta(E_B - E_A)}$. Notice that the condition $r < \exp^{-\beta(E_B - E_A)}$ can be used even when $E_B < E_A$ as in this case the inequality will always be satisfied. Because at each Monte Carlo step, the probability of accepting the trial configuration depends only on the configuration at the previous step (and not on “older” ones), the MC evolution realizes a Markov chain [90, 92, 93]

Starting from an initial conformation, the repeated application of the acceptance/rejection scheme ensures that in the long run, polymer configurations Γ_i are picked with probability proportional to their canonical weight, $e^{-\beta E_i}$ [90, 92, 91].

In contexts of practical interest, the implementation of the Monte Carlo algorithm differs from the above general formulation in that the new conformation, Γ_B is not picked randomly from the conformational ensemble but is generated from Γ_A by applying some stochastic structural changes to it.

The choice of the set of stochastic deformations, commonly termed “moves”, severely impacts the performance of the Monte Carlo sampling. First, the moves must be compatible with the ergodicity requirement. By this it is meant that any two possible conformations might be connected by a finite number of deformation steps. If this is so, then clearly the succession of generated states viewed with a sufficiently large (but finite) time stride is equivalent to the most general formulation where any configuration can be proposed at each Monte Carlo step. In addition, the moves can strongly affect the autocorrelation time of the system. For a similar computational investment, two sets of moves can, in fact, be associated with very different breadths of visited phase space and hence number of statistically-independent configurations.

Customarily, the set of polymer moves usually consists of a combination of local and global deformations. Local deformations are those in which only a small number of consecutive monomers are displaced from their current positions. In polymer models where the chain length is not preserved (that is where the chain connectivity is enforced by a suitable potential [94]), the local moves are simply accomplished by displacing the monomers randomly within a cube or sphere of preassigned size and centered in the current position. In polymer models where the chain length is preserved (as in the freely-jointed or Kratky-Porod chain) the *local* displacement is obtained through a crankshaft move as illustrated (in a cubic lattice context [93]) in Figure 19a.

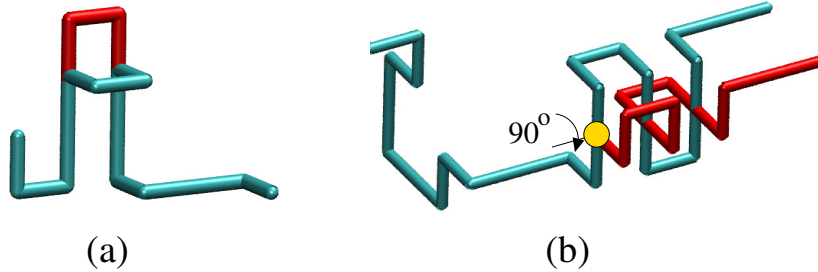


Figure 19: Example of (a) crankshaft and (b) pivot moves on a self-avoiding chain embedded in a cubic lattice. The portion of the chain that is modified after the (a) local and (b) global move is highlighted in red. For case (b) we have highlighted the bead, rotation axis and rotation angle around which the pivot move is performed.

These local deformations are associated with changes of the polymer self-energy that are sufficiently small that the deformed structures are accepted with good probability (say, about 50%). This does not necessarily imply a high efficiency of the scheme. In fact, the long time required before the cumulated local deformations can globally alter the structure, is reflected in large autocorrelation times that scale proportionally to $N^{2+2\nu} \sim N^{\geq 3}$ (N being the polymer length) [95].

The latter can be significantly reduced by introducing global moves where a sizeable fraction of the polymer chain is moved. In an open chain, a global deformation is obtained by a pivot move. The latter consists of picking randomly a polymer bead and a random unit vector through it (see appendix in [96] for a discussion of how to uniformly pick unit vectors in three-dimensions). The chain portion following (or equivalently preceding) the picked bead is next displaced by rotation through a random angle around the unit vector. In closed chains (rings) the global move is instead realized by operating a crankshaft move around an axis passing through two randomly-picked points of the chain. By analogy with the open chain case this move is also termed “two-point pivot” move. Similar procedures are performed also for lattice polymer models; the main difference here is that the rotations in \mathbb{R}^3 are replaced by symmetry operations of the underlying lattice [97, 98], as shown in Figure 19b.

Global moves are obviously more computationally demanding than local ones and the associated changes in polymer self-energy are usually large and unfavourable[99]. As intuitively expected, they in fact, often lead to violations of self-avoidance. Despite the fact that their acceptance probability is small the extent of their associated structural changes is so large that they can dramatically reduce the system autocorrelation time τ [97]. In particular, denoting by f the acceptance fraction of pivot moves, it is possible to show that $f \sim N^{-p}$ where $p \approx 0.11$ in $d = 3$ [97]. On the other hand after a time of order $1/f \sim N^p$ the global conformation of the polymer should have reached an “essentially” new state. Consequently the autocorrelation function [93] of global properties of the configuration, such as mean-squared radius of gyration, span along x , y , z directions, should have a decay time (autocorrelation time) of the order $1/f \sim N^p$. Local observables typically evolve a factor N more slowly than global one, i.e. with $\tau \propto N^{1+p}$; topological properties, however, are expected to be more slowly relaxing than global geometric properties. A vivid illustration of this latter aspect in the contexts of open polymers undergoing a collapse transition is shown in ref. [100].

Besides the above-mentioned local and global moves, a further type of move, termed rep-

tation, is adopted for polymer melts or confined polymers. The use of this move is suggested by the observation that the severe excluded volume constraints arising in dense polymer phases, force each chain to move by slithering through the surrounding polymer network [50]. Algorithmically, the reptation move consists of deleting the end bond from one of two chain extremities and adding it, with a random orientation, to the other. The autocorrelation time associated to this type of move scales like N^3 .

6.1. Advanced sampling techniques: multiple Markov chains or parallel tempering

The combination of the above mentioned local and global moves is, in general, not sufficient to adequately sample the relevant conformational space of polymers in dense solutions or in confined geometries. In these situations, which are the main object of the present review, even local moves are likely to incur in a high ejection rate as a consequence of the high polymer density.

For a given computational investment the breadth of visited conformational space can be enhanced by a generalised sampling scheme where several Monte Carlo evolutions are run in parallel. In this scheme, equivalently referred to as parallel tempering or more aptly as multiple Markov chains, each Monte Carlo evolution is associated to a different thermodynamic parameter which, for simplicity we shall here take as an effective temperature [101, 102]. In contexts of polymer confinement the parameter is more suitably chosen to be a confining isotropic pressure. We shall also assume that the copies are labelled and indexed so that the temperature systematically increases from the first copy to the last.

Each copy of the system is evolved independently under a standard Monte Carlo evolution for a preassigned number of steps. After this, two neighbouring (in the sense of consecutive indexing) system copies, are picked. We shall indicate with E_A [E_B] and β_A [β_B] the energy and inverse temperature of the copy A [B]. A swap of the configurations between the two copies is proposed. After the swap the energy of copy A , which is kept at temperature T_A , would be E_B while the energy of copy B would be E_A . The canonical weight of the system corresponding jointly to copies A and B is $\exp(-\beta_A E_A - \beta_B E_B)$ before the swap while it would be equal to $\exp(-\beta_A E_B - \beta_B E_A)$ after the swap. By considering the ratio of these two canonical weights it is possible to generalize the Metropolis criterion so to ensure that the proposed swap is accepted/rejected respecting the combination of canonical weights. By analogy with the single Monte Carlo evolution this condition is ensured if the swap is accepted with probability given by $\min(1, \exp(-\beta_A E_B - \beta_B E_A) / \exp(-\beta_A E_A - \beta_B E_B))$.

By adopting this generalised Monte Carlo scheme the exploration of phase space is greatly aided by the fact that different conformations are passed between copies of the system kept at different thermodynamic conditions [102]. Note that, although the lag time separating the swap can be chosen arbitrarily, the procedure becomes inefficient compared to the single Monte Carlo evolution if the lag time is set to be longer than the autocorrelation time of the individual Monte Carlo copies.

6.2. Reweighting techniques

It is important to observe that the scheme described above does not necessarily need be performed by assigning different temperatures to the various copies of the system. It is very often convenient to generalize the canonical weight of a configuration by introducing suitable conjugate variables in addition to energy and temperature.

In the specific context of confined polymers, one such choice is offered by volume and confining pressure, as discussed hereafter.

The simplest way by which one can generate an ensemble of conformations under spatial confinement is to introduce a significant energy penalty for configurations that do not respect the spatial constraint. If, for example, one wishes to study a chain confined in a spherical region one could add to the polymer potential energy a very large energy penalty for each of its beads or segments protruding from the spherical boundary. As explained later in section 8.2, when the system density is large, most of the Monte Carlo moves applied to a configuration that correctly lies within the allowed spherical region will likely cross the sphere boundary and hence be rejected. The Monte Carlo evolution under the spatial constraint will therefore be very inefficient.

A practical solution to this problem is to substitute the constraint of the “hard” boundary with a “soft” one resulting, for example, from the application of an isotropic confining pressure P . Accordingly, to the potential energy of a polymer configuration is added the quantity $P V$, where V is the volume of the smallest sphere that enclosed the configuration. The multiple Markov chain scheme can then be run with polymer copies kept at the same system temperature, but at different confining pressures. In this scheme, for a given computational investment, we will generate many more independent configurations with very different degree of confinement. Each of the system copies corresponds, in fact, to a constant-pressure ensemble and not to a constant-volume one as in the previously-described scheme. The data collected in the multiple-Markov chains evolving at different pressures can nevertheless be suitably processed to recover the equilibrium behaviour of the constant-volume ensemble. This method is known as thermodynamic reweighting [103] and its principal aim is to optimally combine the data of the various Markov chains so to compute the density of states as a function of the relevant physical variable(s).

For the case considered here the key variable is the confining volume, V . Let us focus on the set of independent configurations sampled by i^{th} Markov chain kept at pressure P_i . The histogram of how many configurations have been sampled for various finely-discretized values, V_0, V_1, \dots of the confining volume is computed. We shall indicate with $n_i(V_j)$ the number of hits in the j^{th} volume binning interval. When the total number of sampled configurations in the i^{th} Markov chain is N_i , the *expected* value of $n_i(V_j)$ is:

$$n_i(V_j) = N_i W(V_j) \frac{e^{-\beta P_i V_j}}{\sum_l W(V_l) e^{-\beta P_i V_l}} \quad (21)$$

where $W(V_j)$ is the desired weighted density of states of the system which accounts not only for the large number of configurations with volume V_j , but also for their canonical weight. The density of states, $W(V_j)$ can therefore be recovered, up to a multiplicative constant (which can be fixed by a suitable normalization procedure) by inversion of the above relationship. In principle, an infinitely-large number of configurations sampled at a given pressure could be used to recover the density of states $W(V_j)$ over the full range of allowed values of the enclosing volume. In practice, in a finite simulation, most of the configurations will cover a limited interval of volume values. The data collected in the various Markov chains running at different pressures will cover different volume ranges. If the ranges overlap appreciably, the information can be combined into single determination of $W(V_j)$. The optimal combination can be made using criteria which minimize the statistical uncertainty on the W profile [104, 103, 105].

The method presented above can be generalised so that it is possible to obtain the system density of states as a function of more than one parameter. In particular, for the purpose of discussing how spatial confinement affects the degree of knotting of polymers that circularise in equilibrium it becomes necessary to recover the density of states as a function of both the confining volume V and the knot type τ : $W(V, \tau)$. By doing so, the data collected in the various

Markov chains can be used to estimate the probability of occurrence of various knot types as a function of confinement. Finally we mention that, while the example considered here pertains to an isotropic three-dimensional confinement, it can be straightforwardly applied also when the chain is confined in, say, a slab of width D . In this cases, in place of the isotropic confining pressure, P , conjugate to the configuration volume, V , one introduces an anisotropic pressure which conjugates with the calliper size of the configuration measured in the direction perpendicular to the slab planes (see Section 9).

6.3. *Knot simplifications*

One of the challenges that are faced when sampling spatially-confined polymer rings, is that the configurations have a very high degree of geometrical entanglement. For example, configurations of freely-jointed rings of 100 segments confined in a sphere of radius equal to 3 times the segment length produce planar projections with about 150 crossings. The high degree of entanglement poses several difficulties. For example, the calculation of Alexander determinants for these projections is prone to round-off errors. In addition, if, say, an unknotted configuration is associated to a badly-entangled projection with hundreds of crossings, then even if its determinant is correctly calculated, it will not be generally possible to assign unambiguously its knotted state due to the fact that, e.g. the same Alexander determinants may be shared by many knots with less crossings than in the reference projection.

These difficulties can be greatly reduced by subjecting the generated configurations and their diagrammatic projections to topology-preserving simplification procedures. To illustrate this point suppose that the diagram of a certain closed curve has 11 crossings and that its (irreducible) Alexander polynomial is equal to the one of the unknot. The knot identity cannot be established on the basis of these informations alone because it could correspond either to the unknot or to the Conway or Kinoshita-Terasaka knot (see section 3.5), which has minimal crossing number equal to 11. However, if by a sequence of Reidemeister moves the diagram was simplified to the point that it consists of 10 or less crossings, then the previous ambiguity would be resolved in favour of the unknot.

For off-lattice chains, the topology-preserving simplification algorithms involve the displacement, deletion and insertions of nodes in the ring so to ultimately make the latter as smooth as possible and with as few bonds as possible. In its simplest formulation, the method consists of repeated attempted “rectifications” of the chain. At each rectification step, a chain bead is chosen at random and is tentatively displaced so to make it more collinear with its flanking beads. The new bead position is accepted only if no bond crossing occurs during the continuous chain deformation obtained by bridging the previous bead position with the tentative one. Otherwise, the previous position is retained, see Appendix B for details. Whenever a bead can be made exactly collinear with its flanking ones, then the bead can be eliminated from the chain, so that the flanking ones become joined by a single chain bond. The repeated application of these moves typically results in dramatic simplifications of the projected diagram [106, 37]. Notice, however, that in general, this “greedy” approach cannot be expected to reach the minimally-complex diagram; in fact, it is known that the geometrical complexity of particular tangles needs to be increased first, before allowing for a full simplification of the configuration.

The above algorithm is explicitly formulated for off-lattice chains and does not lead naturally to an algorithm for chains embedded in a lattice, for which other types of topology-preserving geometrical simplifications have been introduced [107]. For self-avoiding polygons on a cubic lattice a very effective scheme is provided by the so-called BFACF algorithm, an acronym with

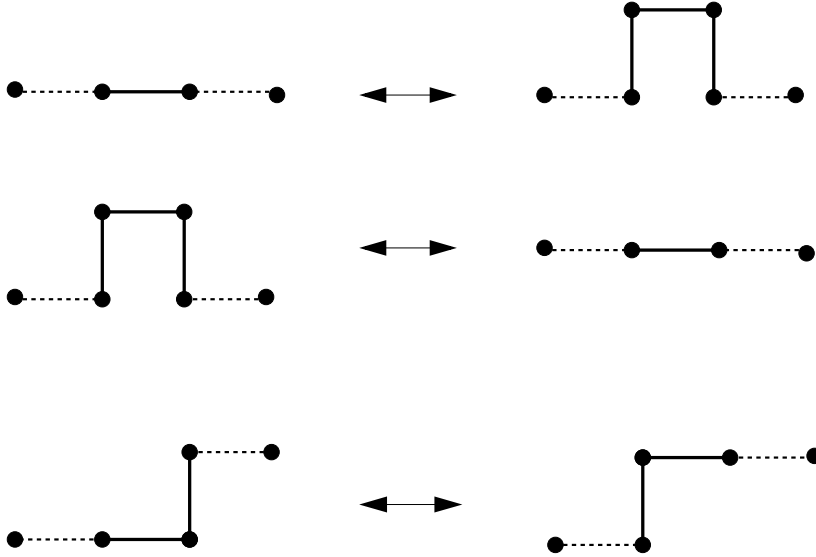


Figure 20: The BFACF moves.

the initials of the people who first introduced it to sample walks with fixed extremities [108, 109, 110].

The standard BFACF can be defined as follows: (i) pick an edge of the current polygon (say ω) at random with uniform probability. (ii) pick a unit vector e perpendicular to that edge (iii) move the chosen edge one lattice space along e and insert two more edges at its endpoints to keep the polygon connected. (iv) erase any double edges (spikes) that may result from this operation. It is easy to see that this procedure will result in one of the three moves illustrated in Figure 20 with possible changes in the length of the polygon $\Delta N \pm 2$ or $\Delta N = 0$. If the new configuration, ω' , does not violate the self-avoidance constraints (i.e. no steric clashes of chain beads) it then accepted with probability proportional to a weight $w(K^2)$ where $w(K^2) = 1$ if $\Delta N = 0, -2$ and $w(K^2) = K^2$ if $\Delta N = 2$. The parameter K is called *bond fugacity* and it is used to control the average length of the sampled polygons: for K approaching a critical value K_c the average length of the sampled polygons diverges while for $K \ll K_c$ the algorithm tends to sample polygons with the shortest length allowed. It is easy to check that this implementation of the BFACF algorithm is reversible.

Moreover, since neither BFACF move allows crossings of polygon bonds the succession of BFACF moves manifestly preserves the knot type of the original chain.

A more delicate question is whether by repeatedly applying BFACF moves to an initial configuration one can *in principle* generate all the possible polygon configurations with a certain knot type and polygon length. The question is equivalent to asking whether the ergodic classes of the Markov chain coincide with the knot types. A positive answer to this question was given in [111] using an argument based on Reidemeister moves. Since the BFACF is ergodic within each knot class it has been often used to investigate equilibrium properties of polygons with fixed knot type (see section 16.1). Moreover, if the bond fugacity K is slowly decreased (annealing procedure) the algorithm would bring (in principle) any given configuration to a minimal length that is compatible with its knot type. This would drastically reduce the number of crossings in the cor-

responding diagram allowing a sufficiently precise knot detection also for geometrically-intricate embeddings [107, 112].

When the structure cannot be further simplified geometrically it is still possible to manipulate the resulting projection removing further non-essential crossings. One practical way to do this is to associate the knot diagram with its Dowker code which essentially follows the numbered succession of over and underpasses in the projection.

Reidemeister moves can be performed very easily on the Dowker code by algebraically manipulating it [16]. Inspection of the Dowker code can further reveal the factorisability of a knot. After these simplifications, it could be the case that the simplified Dowker code of a diagram (or one of its factors) matches the tabulated Dowker code of a prime knot (there exist look-up tables of such codes for knots of up to 16 crossings). In such situations the knot identification is exact. In other cases such positive identification cannot be achieved. This might reflect either the fact that the knot is genuinely a very complicated one or that it has not been simplified sufficiently to allow for its identification.

7. Knotting probability and knot complexity in ring polymers

A fundamental question regarding the knottedness of discretised closed curves (polymer rings) in equilibrium is *what is the knotting probability as a function of the ring length?*

Systematic attempts to address this issue date back to the early 1960s when Frisch, Wasserman [61] and Delbruck [62] conjectured that *sufficiently long ring polymers would be knotted with probability one*. While the statement appears intuitive, it was not until 1988 that the validity of the Frisch-Wasserman-Delbruck (FWD) conjecture was proved true for self-avoiding polygons embedded in the cubic lattice [63, 64]. The difficulty of establishing the result rigorously is due to the fact that knottedness, being a topological attribute, is a global property of the chain and cannot be described in terms of local chain features which are much simpler to characterize and control.

Here we give a qualitative argument of the proof (see [113] or section 9 for more details) which is based on the ingenious idea of considering particular knot realizations having a localised geometrical representation. In particular, considerations are restricted to “tight knots”. A tight knot is the mathematical version of tying a knot in a piece of string, and pulling it as tight as possible. For a self-avoiding walk on the simple cubic lattice, each occupied vertex generates an excluded volume for itself, the dual 3-cell of the vertex. The key observation is that the tight knot occupies a compact region of space (3-ball) which, owing to the self-avoiding constraint, is inaccessible to the remainder of the chain. Consequently, one has that a tight knot tied with a small stretch of the chain cannot be “undone” by the remainder of the chain. Because anti-knots do not exist, it is clear that if the *local* inspection of the chain reveals the presence of a tight knot then the chain is necessarily knotted. Accordingly, the FWD conjecture would be proven if at least one tight knot is contained in sufficiently long rings.

The latter statement is proved resorting to the Kesten’s Pattern Theorem [114] for self-avoiding walks where the chosen pattern is the union of the curve portion taking part to the tight knot and the 3-ball. Based on the pattern theorem, and denoting by P_N the probability that an equilateral polygon with N bonds, or N -gon, is knotted, one has that the number of unknotted polygons decreases exponentially fast for large values of N :

$$P_N = 1 - \exp(-\alpha_0 N + o(N)), \quad (22)$$

where α_0 is a strictly positive quantity. The relationship in eq. (22) therefore proves the FWD conjecture for polygons in the cubic lattice.

Similar results have been obtained for off-lattice polygons with infinitely-thin bonds, such as Gaussian polygons [115] and equilateral random polygons i.e. freely-jointed rings [116]. Despite the fact that these non-self-avoiding polygons may thread several times through a knotted region, it is still possible to prove that tight local knots occur with high probability and that the topological 3-ball surrounding such knots is threaded through by the rest of the polygon with a vanishing probability. In this case the FWD conjecture is proven in the form

$$P_N > 1 - \exp(-AN^\epsilon) \quad (23)$$

where A and ϵ are strictly positive constants.

Extensions of these rigorous results to the case of off-lattice models with finite thickness are not available yet.

From the above account, it is clear that the arguments employed to prove the FWD conjecture are based on polygons with an arbitrarily large number of bonds, N . To present day, in fact, there are no exact (analytic) results for the probability of occurrence of knots in rings of a given finite length.

The latter question has been consequently addressed by numerical techniques such as exact enumeration or stochastic sampling methods. In particular, Monte Carlo approaches such as the ones described in Section 6, are commonly used to sample the equilibrium conformations of a ring with N bonds whose topology is, in turn, established by the knot identification routines described in Section 3. The knotting probability is next computed as a function of N and the value of α_0 is obtained from a best-fit procedure with the functional form given by eq. 22.

One of the earliest numerical attempts to characterise the knotting probability was carried out in ref. [117] in the context of polygons embedded on the body-centered cubic lattice. It was established that, although infinitely-long lattice polygons are certainly knotted, the constant α_0 in eq. (22) is typically so small that the occurrence of knots becomes detectable only for polygons with several hundred bonds.

The first attempt to estimate α_0 was done in [118] where a two-point pivot algorithm was used to generate polygons of up to $N = 1600$ bonds on the face-centered-cubic lattice. The study of their knotting probability (based on the non-triviality of the Alexander polynomial) led to estimate that α_0 was equal to $(7.6 \pm 0.9) \times 10^{-6}$. Interestingly, even at the largest chain lengths, $N = 1600$, almost all the knots found were of the simplest type, namely trefoils. An analogous calculation was later carried out for polygons with up to $N = 3000$ edges on the simple cubic lattice [119]. By using derivatives of the Jones polynomial to detect knotting, it was established that $\alpha_0 = (4.0 \pm 0.5) \times 10^{-6}$.

Both these findings were later confirmed by detailed and extensive simulations for polygons of up to $N = 4000$ edges on the simple cubic (SC), face centred cubic (FCC) and body centred cubic (BCC) lattices [120]. It was shown that, $\alpha_0 = (4.15 \pm 0.32) \times 10^{-6}$ (SC), $\alpha_0 = (5.91 \pm 0.32) \times 10^{-6}$ (FCC) and $\alpha_0 = (5.82 \pm 0.37) \times 10^{-6}$ (BCC). Note that these estimates indicate that α_0 is lattice dependent. If one interprets α_0 as the inverse of the characteristic polymer length, N_0 , required to have an appreciable fraction of knotted rings it turns out that, for each of these lattices, the value of N_0 is a little larger than 10^5 . This large value of N_0 is reflected in the computational difficulty of collecting a statistically-significant ensemble of knotted polygons through a simple stochastic sampling of the configuration space of (long) polygons. If one is interested in characterizing the properties of knotted polygons with a given topology then other

sampling strategies may prove much more efficient. For example, for polygons on the cubic lattice one could resort to the topology-preserving BFACF moves described in Section 6.3.

The knotting probability has been also investigated numerically for off-lattice models of rings such as the rod-bead model and the cylinder models described in Section 4.1.

For the rod-bead model the probability of being unknotted is still well represented by (22) but with α_0 increasing as the radius $\Delta_2 = r$ of the beads decreases, ranging from 3.7×10^{-3} for $r = 0.05$ [121] down to 1.25×10^{-6} for $r = 0.499$ [122, 106], which is rather similar to the value found for the lattice calculation.

The exponential decay of the unknotting probability of eq. 22 appears to hold also for off-lattice self-avoiding rings made by cylinders. This has been shown in ref. [123] where rings of up to $N = 150$ cylinders of unit length and different radii (see section 4.1) were considered. Interestingly, the study also showed that the characteristic length N_0 increases with radius of the cylinders which make up the ring; the dependence is approximately exponential for small cylinder radii. As expected, thinner rings of cylinders have a larger knotting probability at fixed number of cylinders.

The latter observation naturally prompts the consideration of the knotting probability for rings of cylinders with vanishingly small radius, that is freely-jointed rings. If the self-avoidance is neglected then sizeable occurrence of knots in relatively-small chains is expected [124, 125].

An early example of such study is given by ref. [126] who considered off-lattice ring polymers consisting of a N point masses tethered by harmonic bonds. The pointwise character of the masses implies that the ring polymer has no excluded volume. The ensemble of conformations explored in thermal equilibrium by ring of up to $N = 320$ beads was sampled by means of a Langevin dynamics simulations. For this model it was estimated that $\alpha_0 = (3.6 \pm 0.02) \times 10^{-3}$, which is a much larger value than for self-avoiding polygons in a lattice.

The exponential decay of the unknotting probability is confirmed also for Gaussian random polygons with α_0 being about 2.9×10^{-3} (i.e. $n_0 \simeq 340$) [127, 121].

8. Polymers under geometrical confinement.

The studies reported above considered the knotting probability of a single ring polymer that is unconstrained, i.e. not subject to spatial conformational restriction. The introduction of spatial restraints is expected to significantly increase the knotting probability, consistently with our common experience that the careless packaging of a long rope in a backpack will cause the rope to become highly entangled.

In this section we shall report on the increasing number of studies that in recent years have addressed the problem of knotting of chains confined in restricted geometries[85]. As an introduction the interplay between topological entanglement and geometrical confinement in ring polymers we shall first brief review the salient results obtained on the classical problem of how spatial confinement affects the physical properties of *open* chains.

Consider a polymer embedded in a convex subspace of \mathbb{R}^3 . For simplicity the subspace can be taken to correspond to a parallelepiped where, in principle, any of the edges can be infinitely long. The polymer is considered geometrically confined if the length of at least one of the parallelepiped edges is comparable or smaller than the typical equilibrium size (radius of gyration or end-to-end distance) of the chain in free, bulk, space. Let us consider three orthogonal edges for the parallelepiped and indicate with S_{\parallel} the linear subspace spanned by the unbound edge(s), and with S_{\perp} the co-space spanned by the bounded one(s). Denoting by D the typical length

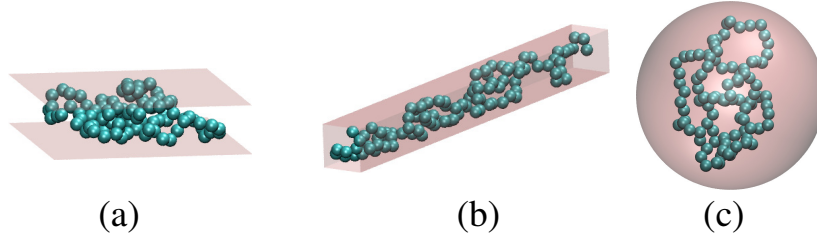


Figure 21: Examples of spatial confinement of a chain of beads. Cases (a), (b) and (c) correspond respectively to confinement in a slab, in a square channel (prism), and in a sphere.

scale associated to S_{\perp} , we can classify the possible geometrical confinements in the following tripartite scheme:

Slab-like confinement In this case the polymer is confined along a single direction, i.e., $\dim(S_{\perp}) = 1$ and $\dim(S_{\parallel}) = 2$. A simple geometry that describes this situation is the so-called *slab* (or *slit*) geometry where the chain is sandwiched between two parallel impenetrable walls set at a separation $D = L_z$ along the z axis, see Figure 21a.

In practical contexts, this type of polymer confinement can be achieved inside slab-like micro-channels with $D \sim 1\mu m$ and $D_{\parallel} \gg D (\sim 1cm)$ [128]. These devices can be realized for example by a soft lithography procedure [129] on polydimethylsiloxane (PDMS). Recently slab-like geometries at the nano-scales have been realized using electron beam lithography on silicon to define the patterns and wet-etched by inductive reactive ions (RIE). With this procedure nano-slabs with size $D \sim 33nm$ have been obtained [72]. Note that in experimental devices also S_{\parallel} is bounded but its typical length scales are much larger than the equilibrium polymer size and hence can be considered infinite for all practical purposes.

Tube-like confinement A tube-like confinement is realized when the polymer is bounded along two directions ($\dim(S_{\perp}) = 2$, $\dim(S_{\parallel}) = 1$), as in Figure 21b. The simplest realization one can think of is a tube-like geometry with cross section of diameter D .

Note that in biological systems this confinement is very common and occurs, for example, during the translocation of DNA through membrane or solid-state nano-pores [130]. In experiments micro- or nano-channels with rectangular cross-section are often employed. The size of the rectangle sides, D_1 and D_2 , usually ranges from 100 – 200nm [69] down to 35nm [70].

Full 3D confinement It is also possible to confine a polymer in a fully-bounded subspace of \mathbb{R}^3 such as a box or a sphere [131]. This problem has been studied theoretically from a variety of perspectives. For examples, scaling results are available for the free energy of compressed polymer chains with and without excluded volume, see e.g. section 19.4 of ref. [132]. Here we shall be particularly interested in the impact of the full-3D confinement on polymer entanglement. In this respect we note that, the confinement of flexible polymers in spheres or ellipsoids is particularly noteworthy since it has direct bearing on the packaging of DNA inside viral capsids.

The above cases represent prototypical examples of how the configuration space of a polymer chain can be limited by the introduction of a physical constraint, namely the impenetrability of the confining boundaries. It is important to note that polymer confinement can also be realised without resorting to such physical constraints. The simplest, and most important, example is offered by *surface confinement* where the polymer is constrained to fluctuate in proximity of an attracting surface (polymer adsorption) or around an interface between two immiscible fluids (polymer localization).

8.1. Scaling arguments for confined polymers

The equilibrium configurational properties of flexible self-avoiding polymers subject to spatial confinement are governed by the competition between two length scales: the average extension of the polymer in the bulk, R , and the characteristic transverse or calliper size of the bounded region D . Clearly, when D is large compared to R then both R_{\parallel} and R_{\perp} are equal to R . When D is smaller than R , then R_{\perp} will be equal to D , while the size of the squeezed-out polymer along the unbounded direction, R_{\parallel} , is expected to progressively grow for decreasing D . The dependence of R_{\parallel} on D can be established assuming the validity of the following scaling relationship [50]:

$$R_{\parallel} = R f\left(\frac{R}{D}\right), \quad (24)$$

where $f(x)$ is a dimensionless scaling function of the argument $x = R/D$.

For definiteness we shall first consider the case of a *slab confinement* ($\dim S_{\parallel} = 2$) of a self-avoiding polymer consisting of a large number, N , of monomers.

Consistent with the above observations, when $D \gg R$, or equivalently $x \rightarrow 0$, one must have $f(x \rightarrow 0) = 1$, so that $R_{\parallel} = R \sim N^{\nu}$, where $\nu \approx 3/5$ is the Flory value of the self-avoiding exponent in $d = 3$. In the extreme case $R \gg D$ the system essentially corresponds to a self-avoiding polymer in two-dimensions. For such situation, the characteristic polymer size in the slab plane is

$$R_{\parallel} \sim N^{\nu_{\parallel}} \quad (25)$$

with $\nu_{\parallel} = 3/4$ [79]. In the limit of large N , from the requirement of consistency between eqns. (24) and (25) it follows that: (i) for $x \gg 1$, $f(x)$ must grow like x^m and (ii) $m = \frac{\nu_{\parallel}}{\nu} - 1$.

In conclusion, for a slab-like confinement with $R \gg D$ one has:

$$R_{\parallel} \sim N^{\nu_{\parallel}} D^{-(\frac{\nu_{\parallel}}{\nu}-1)} \approx N^{3/4} D^{-1/4} \quad (26)$$

Since $3/4 > 3/5$ it is clear that the net effect of the confinement is to stretch the chain along the unconstrained directions. Notice that this is not true for ideal chains since in this case $\nu_{\parallel} = \nu = 1/2$, and therefore, the chain size in the unconstrained directions remains of the same order of the free case. This effect is illustrated in Fig. 22 for a freely-jointed chain confined in two slabs of different width. The figure shows the distribution of the lengths of the major and minor axis of the chain inertial ellipse projected in the slab plane. It is seen that the distribution hardly differs in the two cases of confinement. Notice that even in the unconstrained case, the distributions of the major and minor axis lengths are centred on rather different values, consistently with the known anisotropy of self-avoiding walks [133].

For self-avoiding chains the stretching effect is a genuine product of the competition between the excluded volume interaction and the geometrical confinement. It is worth to notice that

the law (26), obtained by a simple scaling argument, can be shown to be valid for arbitrary values of slab-width D and extended to soft confining walls. These results have been obtained by using variational arguments on the Edwards model of self-avoiding polymers [134]. The same technique, applied specifically to polymers in cylindrical pore, allows also to predict some more specific features of these confined systems such as the non-monotonic behaviour of the average extension as a function of the confining size D [135, 136] (see also Section 8.3)

The above argument can be transferred to the case of *tube-like confinement*. Here, when $R \gg D$ the chain proceeds almost straight along the axis of the tube, so that $\nu_{\parallel} = 1$. Therefore one has

$$R_{\parallel} \sim ND^{-2/3}. \quad (27)$$

As one would expect, a stronger confinement induces a more pronounced stretching effect on the polymer.

8.1.1. Blob picture

Considerable insight into the structural arrangement of confined flexible chains is provided by the *blob picture* which was first proposed by de Gennes to facilitate the understanding of concentrated polymer solutions and melts [50]. The key concepts used to formulate the blob picture are as follows:

- the confined chain is viewed as a string of “blobs”. Each blob consists of g monomers and has diameter B ;
- the chain portion in each blob does not experience the confining constraints and therefore behaves as an unconstrained self-avoiding chain. Thus one has $B \sim g^{\nu} b$ or, equivalently, $g \sim (Bb)^{\frac{1}{\nu}}$.
- The blobs can be viewed as the effective monomers of a chain subject to the imposed confining constraints. Accordingly, the average chain extension in the unconstrained direction(s), R_{\parallel} , would scale as $R_{\parallel} \sim (N/g)^{\nu_{\parallel}} D \sim N^{\nu_{\parallel}} D B^{-\frac{\nu_{\parallel}}{\nu}}$.

The latter expression can be consistent with the result given in the previous section, $R_{\parallel} \sim N^{\nu_{\parallel}} D^{-(\frac{\nu_{\parallel}}{\nu}-1)}$ only if $B = D$. This fact establishes an important structural property of confined self-avoiding chains. In fact, the latter appear organised as a succession of blobs with diameter equal to the characteristic size of the confining region.

8.1.2. Odijk regime

The considerations contained in the previous sections are limited to cases where the characteristic size of the confining region, D , is much larger than the chain persistence length. As a matter of fact, the blob picture was formulated for fully flexible polymers and for confinements where D is much larger than the monomer size, b .

When $D \ll l_p$ the physics of confinement is not dominated anymore by excluded-volume interactions but by the interplay of the geometrical confinement and the intrinsic polymer elasticity. In this regime of very strong confinement De Gennes’ blob theory is not valid any more and it must be replaced by the Odijk’s deflection theory [84, 137]. Hereafter we give a brief account of the theory of Odijk which was originally formulated for tube-like confinement.

The starting point is the observation that, in the limit of strong confinement back-folding is energetically unfavorable and the organization of the polymer in the geometry occurs by a

Freely-jointed chain of $N=200$ unit segments in a slab of width D

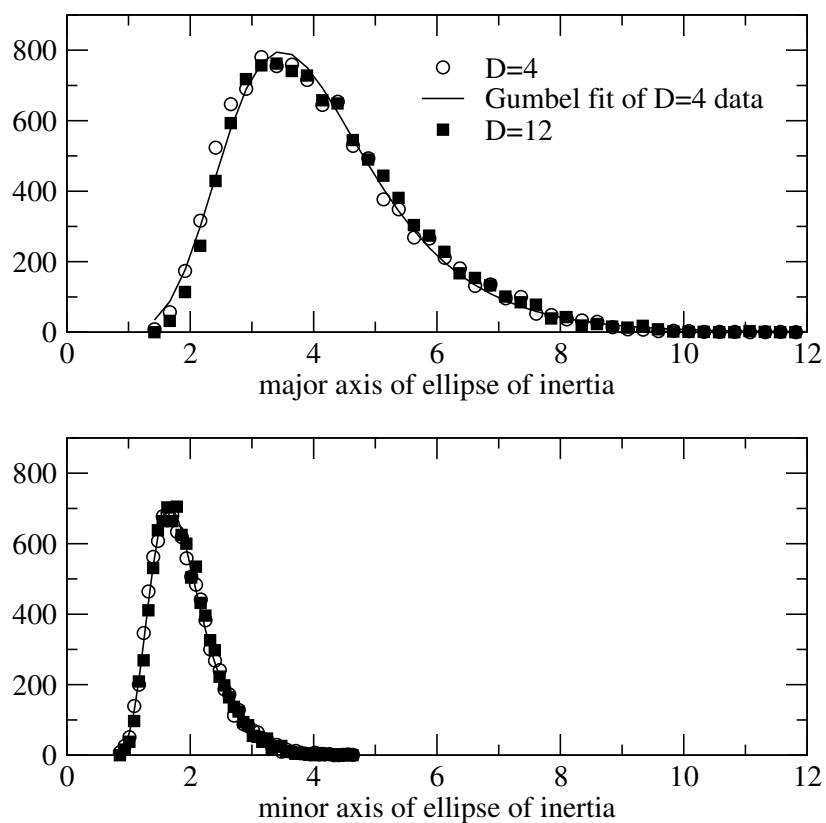


Figure 22: Slab confinement of a freely-jointed chain of $N = 200$ segments. A simple sampling technique was used to generate 10000 independent configurations of a FJC restricted in a slab of width $D = 12$ (about equal to twice the value of the unconstrained radius of gyration) and $D = 4$. The major and minor axis of the ellipse of inertia projected in the slab plane were calculated and their probability distributions are reported. No significant difference of the distributions for the two values of D is observed. The continuous line represents a fit of the $D = 4$ data using the Gumbel extremal statistics.

sequence of straight lines that deflect at the walls. Notably, recent theoretical work by Odijk has pointed out a previously-overlooked effect, namely the influence of the depletion attraction between the polymer and the confining walls[138]. This effective interaction is expected to introduce new additional regimes in the polymer behaviour because the localization at the confining walls makes the formation of backturns in the open chain probable.

To estimate the typical contour length separation of consecutive chain deflections, one considers first the statistics of an unrestricted (i.e. not confined) stiff Kratky-Porod chain. In particular let us consider a segment of the chain positioned in the middle of the tube and oriented parallel to the tube axis. Using the result from eq. (14) it is possible to estimate the contour length separation, λ , between this segment and the one that first hits boundary using the following equality [139]:

$$\langle R_{ee}^{\perp 2} \rangle \approx 2 \frac{\lambda^3}{3l_p} = \frac{D^2}{4}. \quad (28)$$

The distance between two deflection points along the chain is therefore

$$\lambda \simeq (D^2 l_p)^{1/3}. \quad (29)$$

Notice that, since $D \ll l_p$ then $\lambda \ll l_p$. This condition justifies the straight-line approximation for the chain between two deflection points. The typical deflection angle θ formed by the (straight) chain and the tube boundary is given by $\tan \theta = D/\lambda$. From this relationship it is easily obtained the size of the chain projected along the tube axis:

$$R_{\parallel} = L \cos \theta \simeq L \left[1 - (D/\lambda)^2 \right] = L \left[1 - \alpha_o \left(\frac{D}{l_p} \right)^{2/3} \right]. \quad (30)$$

The scaling (30) has been later generalized [140] for a prism whose cross-section is a rectangle with sides, D_1 and D_2 , both smaller than l_p :

$$R_{\parallel} = L \left[1 - \alpha_b \left[\left(\frac{D_1}{l_p} \right)^{2/3} + \left(\frac{D_2}{l_p} \right)^{2/3} \right] \right]. \quad (31)$$

Nowadays, the condition $D < l_p$ can be achieved experimentally by confining, e.g. ds-DNA molecules ($l_p \sim 50nm$) into nanochannels having typical sizes $D \sim 35nm$ [70, 73, 141]. This setup, combined with advanced imaging techniques, has made it possible to test the validity of the strong-confinement scaling relationships given by eqns. (30) and (31).

8.2. Rigorous results of lattice models of polymers in slabs and prisms

We next report on the rigorous results that have been established for the configuration entropy of confined self-avoiding walks and polygons in a lattice.

8.2.1. Walks and polygons in D-slabs

In the cubic lattice a slab of width D is defined by the subset of vertices

$$S_D = \{ \vec{r} \in \mathbb{Z}^3 | 0 \leq r_z \leq D \} \quad (32)$$

The boundaries of S_D are the planes

$$\{ \vec{r} \in \mathbb{Z}^3 | r_z = 0 \} \quad \text{and} \quad \{ \vec{r} \in \mathbb{Z}^3 | r_z = D \}. \quad (33)$$

A walk or polygon C is contained in S_D if every vertex $C_i \in S_D$. The system has translational invariance along the unrestricted x and y directions. In the light of this consideration it appears appropriate to remove the translational symmetry by regarding two walks or two polygons confined to a D -slab as distinct if they can not be superimposed by a suitable translation in the x or y directions.

We start by considering the case of open self-avoiding walks (SAW) in a D -slab. Let us denote by $c_N(D)$ the number of different such walks made of N bonds. It can be shown that the limit

$$\lim_{N \rightarrow \infty} \frac{1}{N} \log c_N(D) = \kappa(D) \quad (34)$$

exists for all slab widths, D . The limit $\kappa(D)$ defines the limiting entropy of SAWs confined in a D -slab. Moreover $\kappa(D)$ is a strictly increasing function of D [142]: $\kappa(D) < \kappa(D+1) < \kappa$ where κ is the limiting entropy of SAWs in free space (see section 4.2). In addition

$$\lim_{D \rightarrow \infty} \kappa(D) = \kappa. \quad (35)$$

The limit (34) implies $c_N(D) = e^{\kappa(D)N + o(N)}$ and from the property $\kappa(D+1) < \kappa(D)$ we have the interesting result that SAWs confined in a D slab are *exponentially* few compared to SAWs confined in a $D+1$ slab.

Analogous considerations can be made for polygons in a D -slab. Denoting by $p_N(D)$ the number of polygons in a D -slab we have [143, 93]

$$\lim_{N \rightarrow \infty} \frac{1}{N} \log p_N(D) = \kappa_p(D) = \kappa(D). \quad (36)$$

Equation (36) not only proves the existence of the limiting entropy for polygons in a D -slab but it generalizes the equality between this entropy and the one of self-avoiding walks in free space (see Section 4.2), to the case of walks under slab-like confinement. In other words, at least on a lattice, for closed and linear chain in slab-like geometries the configuration entropy per edge is the same.

8.2.2. Walks and polygons in (D_1, D_2) -prisms

Since the equivalence between the configuration entropy of rings and open chains holds both in free space and in slab-like geometries, it would appear plausible that a similar property holds also for polygons and walks confined within prisms. Remarkably, this is not the case. To see this, consider the case of a (D_1, D_2) prism whose cross-section is a rectangle with sides of length D_1 and D_2 . Similarly to D -slab we define a (D_1, D_2) -prism of average size $D = \sqrt{D_1 D_2}$ as the subset of vertices

$$S_{D_1, D_2} = \{\vec{r} \in \mathbb{Z}^3 | 0 \leq r_y \leq D_1 \quad \text{and} \quad 0 \leq r_z \leq D_2\} \quad (37)$$

The boundaries of S_{D_1, D_2} are the planes

$$\begin{aligned} \{\vec{r} \in \mathbb{Z}^3 | r_y = 0\} & \quad \text{and} \quad \{\vec{r} \in \mathbb{Z}^3 | r_y = D_1\} \\ \{\vec{r} \in \mathbb{Z}^3 | r_z = 0\} & \quad \text{and} \quad \{\vec{r} \in \mathbb{Z}^3 | r_z = D_2\} \end{aligned} \quad (38)$$

For self-avoiding walks confined in a (D_1, D_2) -prism a result similar to (34) holds [144]

$$\lim_{N \rightarrow \infty} \frac{1}{N} \log c_N(D_1, D_2) = \kappa(D_1, D_2) \quad \forall (D_1, D_2) \quad (39)$$

Also for polygons, in a (D_1, D_2) -prism the limiting entropy is well-defined

$$\lim_{N \rightarrow \infty} \frac{1}{N} \log p_N(D_1, D_2) = \kappa_p(D_1, D_2) \quad \forall (D_1, D_2), \quad (40)$$

but now the following inequality between the limiting entropies of SAWs and polygons holds [144]:

$$\kappa_p(D_1, D_2) < \kappa(D_1, D_2). \quad (41)$$

The non-trivial inequality of eq. (41) can be obtained by applying the Kesten’s pattern theorem as follows: for a given (D_1, D_2) prism, one can find a Kesten pattern which “fills” the entire prism and that can occur in a walk but not in a polygon. On the other hand, by Kesten’s pattern theorem, one knows that configurations not containing such pattern (in this case polygons) are exponentially rare and this gives the strict inequality between the connective constants. The above result has notable implications. In fact, it implies that polygons in a (D_1, D_2) -prism are *exponentially few* if compared to their self-avoiding walk counterparts. Hence, unlike the slab-like confinement, tube-like confinement provides a more dramatic reduction of configuration space for ring polymers than for linear ones. This is a first example of how interplay between polymer topology and geometrical confinement may lead to unexpected and notable phenomena.

8.3. Sampling confined polymers at equilibrium

An efficient sampling of configurations of open or closed chains fitting into a given convex region of \mathbb{R}^3 is, in general, a challenging task. The simplest possible approach would be to rely on unbiased sampling techniques, such as those described in section 6, to collect a large set of unrestricted polymer configurations. The sampled conformations could next be processed *a posteriori* to retain only those satisfying the given constraint. The combination of unbiased sampling followed by this *rejection scheme* has two important advantages:

- the ergodicity of the sampling is satisfied whenever the unbiased Markov chain is ergodic,
- for a given realization in free space the rejection technique can be easily applied to any desired geometries, making this method quite flexible and useful if one looks for a comparison between different types of confinement.

The major disadvantage of the method is that, although the unbiased algorithm can explore in principle the whole configuration space, in practice very few sampled configurations will satisfy the geometrical constraint, particular when $D < R$. Indeed, the rigorous results given in Section 8.2 indicate that number of SAWs and self-avoiding polygons (SAP) in a slab or prism with typical size D are *exponentially rare* compared to larger confinement size. Consequently, the computational time required to generate the same number of independent SAWs/SAPs grows exponentially as D decreases.

As an example let us consider the problem of sampling self-avoiding walks in the cubic lattice confined within slabs and prisms. We know from Section 6 that a very efficient method to sample SAWs in free space is based on pivot moves [93]. After collecting a large number, e.g. about $\sim 10^6$, of uncorrelated configurations and computing their metric properties the rejection technique is used to partition the configurations in subsets according to a given geometrical constraint. Estimates of the canonical averages are then performed on these subsets and plotted as a function of the typical size D of the confinement.

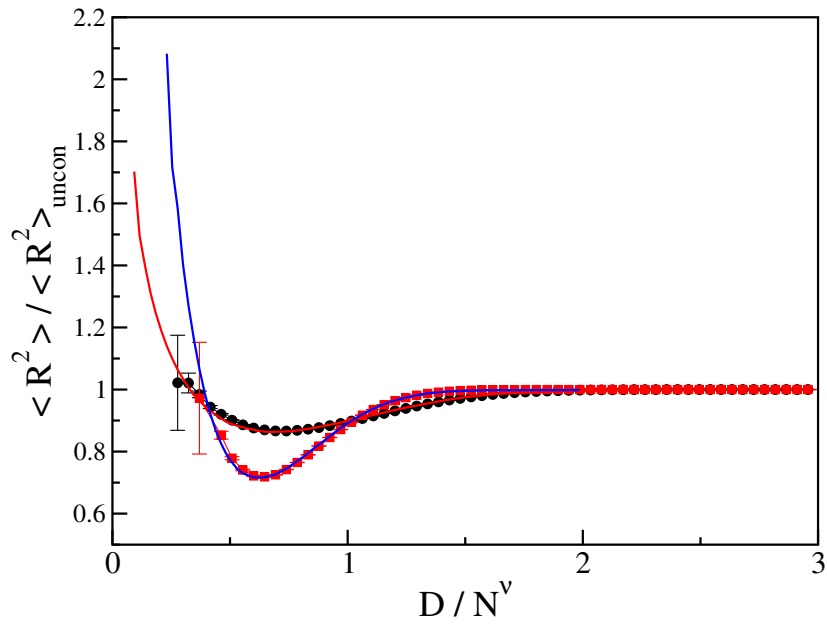


Figure 23: Numerical data, from both simple- and advanced-sampling techniques, illustrating the dependence of the mean square radius of gyration of a self-avoiding walk as a function of the size of the confining slab and prism. Data refer to self-avoiding walks of $N = 600$ bonds on the cubic lattice confined in to a D -slab (circles) and into a (D_1, D_2) -prism (squares) of average size $D = \sqrt{D_1 D_2}$. The mean squared radius of gyration $\langle R^2 \rangle$ was scaled by its value in free space, $\langle R^2 \rangle_{uncon}$ while the typical confinement size, D was scaled by N^ν , with $\nu = 0.588$. The symbols refer to the data obtained by rejection techniques while the continuous lines refer to the importance sampling plus reweighting techniques.

In Figure 23 we show the mean squared radius of gyration for self-avoiding walks on the cubic lattice confined into a D -slab (black circles) and into a (D_1, D_2) -prism (or rectangular channel) of average size $D = \sqrt{D_1 D_2}$ (red squares). The length D has been scaled by the mean extension N^ν ($\nu \approx 0.588$) of SAW's in free space while $\langle R^2 \rangle$ has been scaled by the corresponding average square size of the walks in free space. Note that when $D > R$ the extension is independent on the confinement, as intuitively expected. On the other hand for $D < N^\nu$ the configurations start to experience the confinement and the overall extension decreases down to a minimum value, suggesting an overall mild compactification of the SAWs [135, 145, 134, 136, 146]. This average compactification is the result of the interplay of several factors. For example it was pointed out by ten Brinke and co-workers [135, 145] that upon progressive confinement in a slab, the average (anisotropic) polymer conformations first aligns the major axes of the gyration matrix parallel to the plan, next it experiences a reduction in size along all directions and finally it spreads out along the unconstrained components. An analogous picture has been shown to hold for confinement in a channel [136].

The results in Fig. 23 indicate that the highest reduction of the chain overall size depends on the dimensionality of the confinement, being more pronounced in the case of prisms. Consistently with the picture reported above, when D is further decreased the SAWs start to stretch along the unrestricted subspace S_{\parallel} and the overall mean square size, $\langle R^2 \rangle$ increases rapidly. Note that for progressively smaller values of D the error bars increase in size due to the poor efficiency of the unbiased sampling based on the rejection technique.

This degradation of the efficiency of the method, for increasing confinement, can be quantified by plotting the acceptance ratio of configurations, with $N = 600$ bonds, that fit into a subspace of average size D as a function of the scaled variable $x = D/N^\nu$ (see Figure 24) Notice that at $x = 0.5$ only 5% of the sampled configurations fit into the chosen subspace.

A possible way to overcome the sampling problem for small D would be to modify the Monte Carlo scheme so that it preferentially samples configurations with the desired geometry. This goal, which clearly alleviates, or entirely eliminates, the inefficiency of the rejection scheme, can be achieved by e.g. mimicking the confining action of the boundaries of S_{\perp} through a repulsive potential $U(C)$ that is zero if the configuration C is in the interior of S_{\perp} and becomes strongly repulsive for configurations with R_{\perp} close to the size D of S_{\perp} . One can then perform a standard importance sampling – Monte Carlo – technique based on the generalised canonical weight $w = \exp(U(C))$.

In practice, at each Monte Carlo step the current configuration is stochastically modified by using the moves of the unbiased method. The usual Metropolis scheme is subsequently employed to reject or accept the newly generated conformations based on their statistical weight, w . In the simplest approach, the potential is set to infinity outside the boundaries and the attempted move is rejected whenever $R_{\perp}(C) > D$. This approach is often used in lattice contexts. Its major weakness is that a rejection of a proposed configuration that does not satisfy the boundary condition could trap the Markov chain into sub-regions of the conformational space and the ergodicity of the algorithm in free space is no longer guaranteed.

Although a softening of the repulsive confining potential can facilitate sampling, the method is prone to quasi-ergodicity problems. In fact, as anticipated in Section 6.2, for entropic reasons, most of the sampled configurations will attain the maximum allowed value of $R_{\perp}(C) = D$ and any stochastic modification is likely to produce a new configuration that violates the geometry constraint leading to a rejection with high probability.

A very effective way to circumvent the above mentioned problems is to use the multiple-Markov-chain scheme in combination with thermodynamic reweighting techniques, as outlined

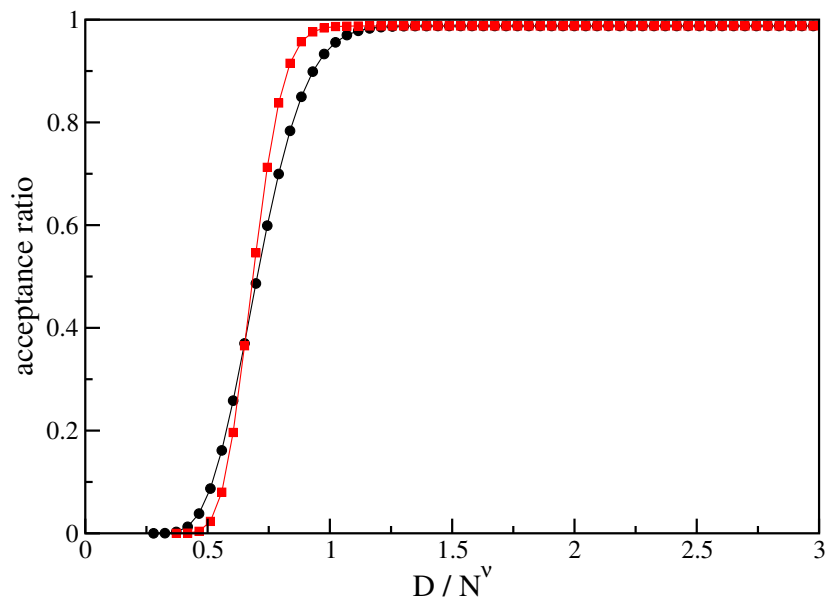


Figure 24: Acceptance ratio of configurations of a self-avoiding walk that fits into a D -slab (circles) and into a (D_1, D_2) -prism of average size $D = \sqrt{D_1 D_2}$ (squares). Data refer to walks of $N = 600$ bonds. The typical confinement size, D , was scaled with D/N^ν where $\nu = 0.588$. Data have been obtained by sampling 10^6 configurations and using the rejection technique.

in sections 6.1 and 6.2. To briefly recall the main points of the strategy, we mention that various copies of the system are evolved at different confining pressures. A suitable generalization of the Metropolis criterion is used to accept/reject swaps of configurations at different temperatures. The data collected at the various pressures are next optimally combined to recover the desired equilibrium information for different degree of confinement.

To understand why the method has major advantages over importance sampling, first focus on a particular copy of the system kept at a given pressure. Configurations sampled at this pressure will, in turn, have a certain typical degree of confinement (the higher the pressure, the stronger the confinement). Whenever the system copy is involved in a successful swap, the configuration of the Markov chain will be dramatically different from the previous one. The stochastic evolution of the copy will then restart from a new point in configuration space [147].

It is interesting to follow the evolution from another perspective, where a specific chain configuration (rather than a specific system copy) evolves under the action of standard Monte Carlo moves (crankshaft etc.) plus the swaps. When the latter are accepted the evolving configuration will be subjected to the action of a different pressure. When it eventually returns to its initial pressure it will have evolved at other smaller and/or larger pressures which expectedly will have left major changes to the configuration.

The set of pressures used in the multiple Markov chain scheme should be chosen such that the volume distribution of “neighbouring” copies have a substantial overlap. If this condition is not met then swaps or neighbouring copied would be accepted only rarely. This powerful method has become now a standard procedure in stochastic sampling mechanics and it is in particular used in strongly interacting systems.

Finally, as explained in Section 6.2, the data coming from the set of runs at different pressures are finally reweighted so as to recover the key thermodynamic information, such as $c_N(s_z)$ and in particular of $\sum_{s_z=0}^D c_N(s_z) \equiv c_N(D)$.

In Figure 23 we compare the mean squared radius of gyration of SAWs with $N = 600$, confined in slabs and prisms, obtained by the rejection technique (symbols) and with the importance sampling method (solid lines). Note that for all the values of D for which the rejection technique is still efficient the agreement between the two methods is manifestly good. On the other hand, for sufficiently small values of D , while the rejection estimates stops being reliable, the importance sampling data are still good enough to confirm the monotonic increasing of $\langle R^2 \rangle$ after the minimum.

9. Knotting probability in confined geometries

9.1. Rigorous results for polygons in slabs and prisms

The results reported in the previous section aptly illustrate the dramatic reduction on the configuration entropy of open and closed chains as a result of spatial confinement. Because the closed chains can differ in topology, it is natural to pose the following series of questions: (i) how is the balance between the populations of different types of knots affected by the introduction of the confining boundaries? (ii) Is it possible to have knots in rings confined in slabs of prisms when D is much smaller than the typical size of the unconstrained polymer chain, i.e. when $D \ll N$? (iii) Does the Frisch-Wassermann-Delbruck conjecture, originally formulated for unconstrained polygons, hold also for polygons in confined geometries?

We shall postpone to subsequent sections the answer to question (i), which up to now has been tackled exclusively by computational means, and focus on questions (ii) and (iii) which can

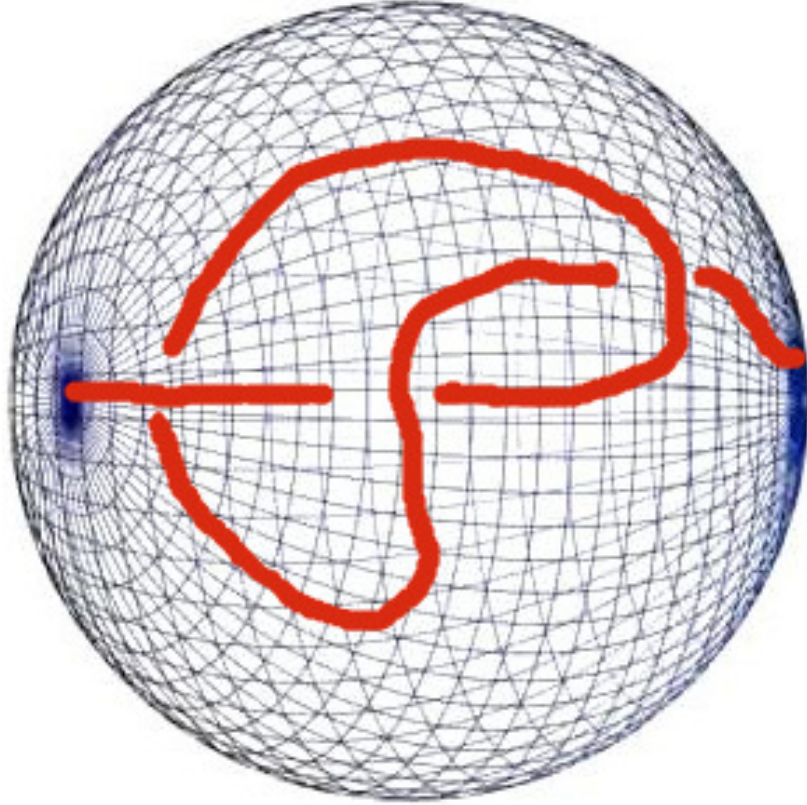


Figure 25: A knotted ball pair.

be addressed in rigorous terms for lattice polygons in a D -slab or a (D_1, D_2) -prism. We shall provide a brief, non-technical account of the results obtained originally in refs [148, 149].

As in the unconstrained case, to prove the FWD in D -slabs and (D_1, D_2) -prism it is sufficient to show that most sufficiently-long ($N \gg 1$) polygons contain at least a knot which is tied so tightly as to prevent the remaining part of the polygon to thread through the knotted region thus potentially unknotting the polygon. The proof is described by three main properties of knotted curves.

The first property is that there exist no *antiknots* that is tangles that once connected (through the connect sum) to a given knot will untie it. More precisely for any knot type K there does not exist a knot type K' such as the connected sum $K\#K'$ is the unknot. This properties can be proved by using the additivity of the genus under connected sum, see Section 3.

Secondly, one has the notion of a knotted arc (see [63] for a technical definition). One can capture the important part of a knot such as the trefoil and tie it so tightly on the lattice that the rest of the walk cannot pass through the neighbourhood of this subwalk and untie the knot. As mentioned in the introductory part of the review, the subwalk and its associated dual 3-cells (i.e. the Wigner-Seitz cells of the vertices of the subwalk) form a knotted ball-pair [63], see Figure 25.

exponentially rare (as a function of chain length) compared to the total number of polygons in a (D_1, D_2) -prism.

The three properties can be used to prove the FWD conjecture for polygons in D -slabs and (D_1, D_2) -prisms. To do so it is necessary to identify a Kesten's pattern T that is a tight trefoil arc. In this way the ball pair corresponding to T and its associated 3-ball neighbourhood is the knot 3_1 . A pattern T fulfilling these requirements and fitting into all D -slabs with $D \geq 1$ and all (D_1, D_2) prisms with $D_1 \geq 1$ and $D_2 \geq 4$ is provided by the example in Figure 26. Focussing on D -slabs, if we now call $p_N(\bar{3}_1, D)$ the number of N -edges polygons which *do not* contain a trefoil as part of the knot decomposition, we have the following set of inequalities

$$p_N^0(D) \leq p_N(\bar{3}_1, D) \leq p_N(\bar{T}, D). \quad (44)$$

By using now the pattern theorem (42) we obtain

$$\lim_{N \rightarrow \infty} \frac{1}{N} \log p_N^0(D) \equiv \kappa^0(D) < \kappa(D) \quad \forall D \geq 1. \quad (45)$$

Denoting by

$$P_N(D) = 1 - \frac{p_N^0(D)}{p_N(D)} \quad (46)$$

the probability that a polygon with N edges in a D -slab is knotted, one has that the limit (45) implies the following equality:

$$P_N(D) = 1 - e^{(\kappa(D) - \kappa^0(D))N + o(N)} = 1 - e^{\alpha_0(D)N + o(N)} \quad \forall D \geq 1 \quad (47)$$

where $\alpha_0(D) > 0$.

The above equality proves the validity of the FWD conjecture for lattice (cubic) polygons in a D -slab, i.e. that *in a D -slab in \mathbb{Z}^3 all polygons are knotted except for a subset that decreases exponentially fast with the polygon length, N* . Note that

$$\lim_{D \rightarrow \infty} \alpha_0(D) = \alpha_0. \quad (48)$$

Similarly, for polygons in a (D_1, D_2) -prism we have

$$P_N(D_1, D_2) = 1 - e^{(\kappa_p(D_1, D_2) - \kappa_p^0(D_1, D_2))N + o(N)} = 1 - e^{\alpha_0(D_1, D_2)N + o(N)}, \quad (49)$$

$\forall D_1 \geq 3, D_2 \geq 2$. Note that in (49) we cannot replace the free energy for polygons $\kappa_p(D_1, D_2)$ with the corresponding one for walks since $\kappa_p(D_1, D_2) < \kappa(D_1, D_2)$. Embeddings of graphs in lattices can also be knotted [150] and there are extensions of these results to knotted graphs [149].

9.2. Numerical results for polygons in slabs and prisms

The rigorous results described above concern the asymptotic behaviour of confined polygons. Quantitative estimates of the knotting probability or the knot spectrum at modest values of N , can be obtained, at present, exclusively through stochastic sampling techniques, such as Monte Carlo methods. The computational approach can be used to estimate parameters such as $\alpha_0(D)$. Although the probability that a polygon of length N approaches unity exponentially rapidly with increasing N (see eqs. (47) and (49)), the values of $\alpha_0(D)$ can be so small that to estimate them reliably it is necessary to sample extensively the configuration space of confined rings of several

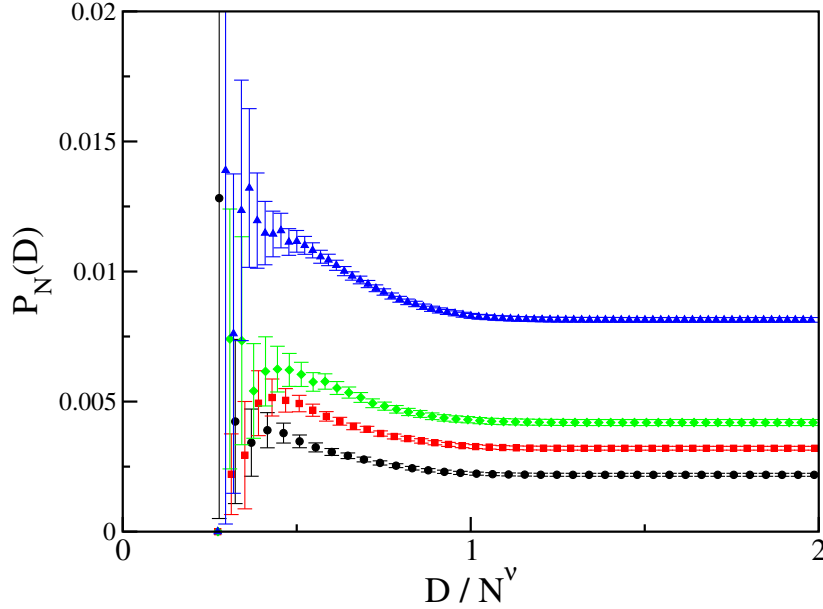


Figure 27: Knotting probability vs D/N^v for polygons of $N = 600, 800, 1000, 2000$ edges (bottom to top) on the cubic lattice confined inside a D -slab. The data are obtained by rejection technique.

hundred edges, and this can be computationally very challenging and demanding (see sections 6 and 8.3).

One of the first attempts to study the knotting probability for lattice polygons confined in D -slabs and (D_1, D_2) prisms was made in [148]. In this study a simple, unbiased sampling method based on two-point pivot moves with rejection techniques was used to select polygons respecting the confinement constraint. The study focused on the knotting probability of the confined rings (regardless of the knot type) by computing the value of the Alexander polynomial $\Delta(t)$ at $t = -1$ (see Section 3).

We have repeated, with present-day computational resources, the calculation of [148] and the results for the knotting probability for polygons in a D -slab are shown in Figure 27. For each fixed value of N the knotting probability increases as D is reduced. This is in accord with the intuition that the increasing density of the progressively confined polygons ought to reflect in a higher knotting probability.

However, it also appears that for sufficiently small values of D the knotting probability reaches a maximum at a particular value of D , which will be denoted by $D^* = D^*(N)$, and then decreases as D is further decreased. Unfortunately in the region below D^* the rejection techniques become very inefficient and the error bars are so large that it is not possible to establish with certainty the decrease of the knotting probability as $D \rightarrow 1$. To confirm the non-monotonic behaviour of the knotting probability it is therefore necessary to improve the efficiency of the sampling scheme. In ref. [148] this was accomplished by introducing an ergodic 1-slab two-point pivot move in the Monte Carlo algorithm. It was accordingly established that for $D = 1$ the knotting probability is vanishingly small for every value of N .

Importance sampling and reweighting techniques can be profitably used to study knotting

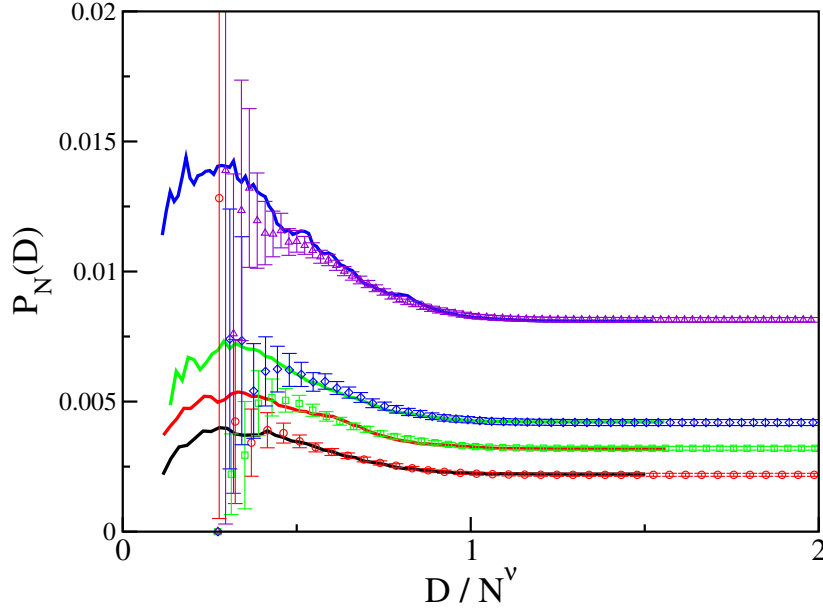


Figure 28: Knotting probability vs D/N^v for polygons of $N = 600, 800, 1000$ and 2000 bonds confined in to a slab. The symbols refer to the data of the previous Figure (i.e. obtained by rejection techniques) while the continuous lines refer to the importance sampling plus reweighting techniques.

probability throughout the interval $1 \leq D \leq D^*$ obtaining the results shown in Figure 28. In this figure it is possible to compare the performance of the rejection technique (symbols) with the ones (full curves) obtained by importance sampling. The differences of the sampling efficiency become very pronounced for $D < D^*$, where the importance sampling data start to decrease towards zero as expected from the $D = 1$ case.

The presence of a maximum in the knotting probability may reflect the competition between the higher probability for a polygon with smaller average extension to be knotted, and the difficulty of forming knots in confined geometries due to the polygon excluded-volume. If the polygon is squeezed along a certain direction to the width D , then it would spread out in the other directions leading to a decrease in the fraction of knotted conformation. According to this argument, the maximum of the knotting probability should correspond to a minimum in the average extension of the polygons, or a maximum of its density. This is indeed observed if one plots the mean squared radius of gyration as a function of D (see Figure 29).

At fixed value of D one can compute the knotting probability as a function of N and estimate the value of $\alpha_0(D)$ using (47) [148]. These estimates were performed for values of $D > D^*(N)$ and turned out to be consistent with a functional the form $\alpha_0(D) = \alpha_0 + \beta/D$, where β is a positive constant. This suggests the following scaling form for the unknotting probability

$$\frac{P_N^0(D)}{P_N^0} \simeq A e^{-N(\alpha_0(D) - \alpha_0)} = A e^{-N\beta/D} = f\left(\frac{N}{D}\right). \quad (50)$$

A similar analysis can also be performed for polygons in a (D_1, D_2) -prism. In the literature results are available for prisms of square cross-section, $D_1 = D_2$ [148]. Here we present results

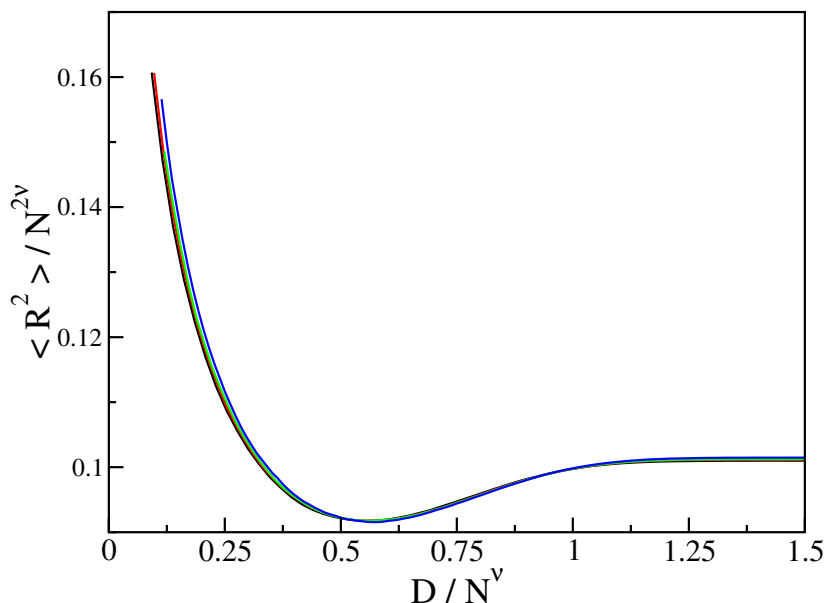


Figure 29: Mean squared radius of gyration, scaled by $N^{2\nu}$, as a function of D/N^ν . Data refer to polygons of $N = 600, 800, 1000$ and 2000 bonds confined inside a D -slab.

for a different ensemble where the rings are enclosed in prisms where the area of the rectangular cross-section is fixed to a given value, $D^2 \equiv D_1 D_2$, but the lengths of the individual sides, D_1 and D_2 , are not fixed. This is done because the fluctuating geometry allows for a more efficient exploration of the configuration space.

In Figure 30 it is shown the knotting probability for polygons in a (D_1, D_2) -prisms as a function of $D = \sqrt{D_1 D_2}$ and for different values of N . The behaviour is similar to the one found in the case of polygons in D -slabs. In particular, for fixed N , the probability increases as D decreases up to $D^*(N)$ (maximum) and then start to decrease for $D < D^*(N)$.

Note that in the limiting case $D_1 = D_2 = 1$ no knots can possibly be tied and the knotting probability must be equal to zero. The main difference with the slab case is reflected by the much higher values of the probabilities in the strongly confined regime (see Figure 31 left panel for a comparison between slabs and prisms for $N = 600$) and by the difficulty, even for importance sampling techniques, to sample the configuration space in where probability starts to decrease towards zero. This is to be expected because confining a polygon in a prism imposes more severe limitations to the polygon configuration space than a slab-confinement. Indeed, for a given polygon length, the minimum attainable radius of gyration is lower for the prism case than the slab one. Consistently, the knotting probabilities are higher for the prism confinement compared to the slab case, see Figure 31.

9.3. Knot spectrum in slabs and channels: an open problem.

All the results presented above concern the knotting probability of polygons confined in slabs and channels (of which prisms are a particular case). It would be very interesting to look at the knot spectrum (i.e. the relative frequency of occurrence of the different knot types) as a function

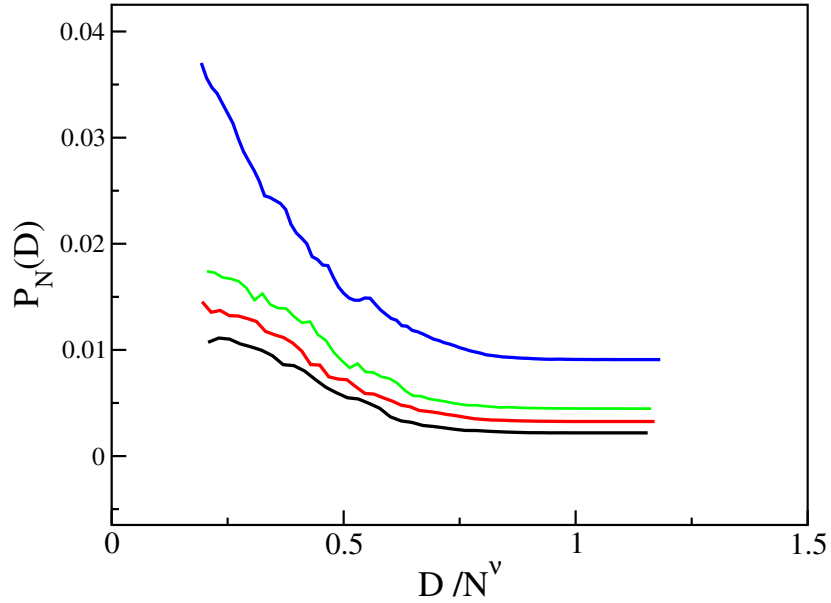


Figure 30: Knotting probability $P_N(D)$ vs D/N^v for polygons of $N = 600, 800, 1000$ and 2000 bonds (bottom to top) confined in to a (D_1, D_2) -prism of average size $D = \sqrt{D_1 D_2}$.

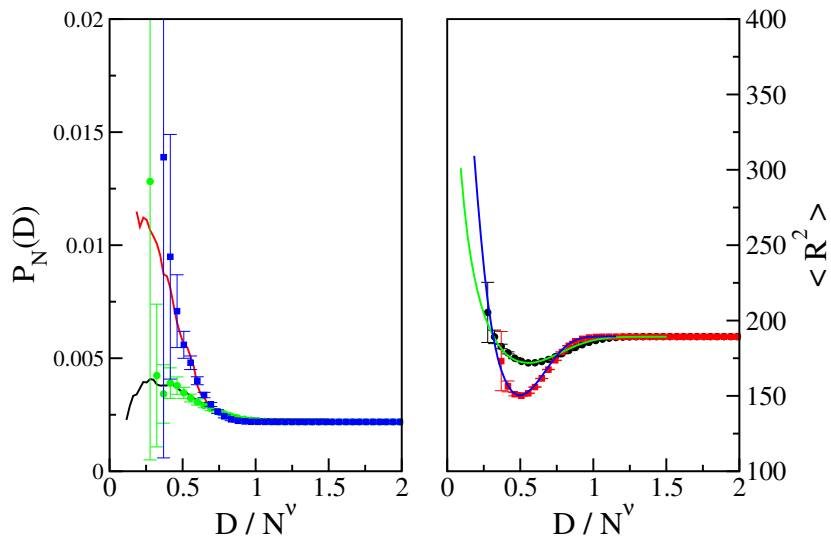


Figure 31: Knotting probability (left panel) and mean squared radius of gyration (right panel) vs D/N^v for polygons of $N = 600$ bonds confined inside a D -slab (circles) and (D_1, D_2) -prism (squares). The symbols refer to the data obtained by rejection techniques while the continuous lines refer to the importance sampling plus reweighting techniques.

of the parameters characterizing the confinement. As far as we know there are no results available in the literature on this argument.

9.4. Polymer rings confined in spheres and cubes.

Unlike the case of prisms and slabs, in a full three-dimensional confinement there is no unbound co-space, S_{\parallel} , available to the confined ring. We accordingly expect important differences in the knotting probability with respect to the slab and prism cases because upon the progressive reduction of the confinement calliper size, D , the polymer has no available co-space in which to expand. The result is a progressive compactification of the conformation either as N increases for fixed D or as D decreases at fixed N (except when the D is so small to be comparable with the size of the polymer monomeric units, e.g. a chain bead or a polygon edge). In both cases one should expect a monotonic increasing of the knotting probability unlike the cases of confinement in slabs and prisms where a maximum in probability is found for intermediate values of D .

One of the earliest systematic attempts to characterize the occurrence of knots in rings subject to spatial confinement was carried out by Michels and Wiegel in 1986 [126]. These authors used a simple-sampling scheme, based on stochastic molecular dynamics, to explore the conformational space of a polygon with N bonds, each of length b . The polygon had no excluded volume and was treated as a *phantom ring* in that bond crossings were allowed during the MD evolution. The rings were subjected to an isotropic spatial confinement by constraining them inside a sphere of radius R .

The simple sampling scheme allowed Michels and Wiegel to sample ring configurations constrained in a sphere with radius about 1/3 of the radius of gyration of the unconstrained polymer. From the analysis of data of chains of up to $N \approx 200$ segments they concluded that the unknotting probability could be expressed by a scaling formula:

$$P_N^0(R) = g\left(\frac{N^\alpha b^3}{R^3}\right) \quad (51)$$

Specifically, they suggested that g was a decreasing exponential and that $\alpha = 2.28$.

This pioneering study was recently revisited in ref. [151]. This latest investigation was based on advanced sampling and thermodynamic reweighting techniques to probe ring configurations with volume up to ten times smaller than the one reached in the seminal studies of ref. [126]. In addition, the number of independent configurations sampled at the highest density was also increased by orders of magnitude. The dependence of the unknotting probability as a function of the ring length and radius of confining sphere is shown in Figure 32a. The enhanced thermodynamic sampling confirmed the validity of the general functional form of eq. (51) but with two important differences: the scaling exponent α is 2.15 and the scaling function is not a simple exponential, as shown in Figure 32b.

The enhanced sampling allowed us to investigate not only how the probability of occurrence of unknotted polygons depends on N and R , but also to repeat the analysis for more complicated knot types. Compared to the unknot case, the probability manifold of non trivial knots presents major differences. While the unknot manifold is always monotonically decreasing as a function of $1/R$ at fixed N , (and vice-versa), for non trivial knots one observes a "shoulder", as is readily appreciated in probability of trefoil formation shown in Figure 33a.

This peak can be explained with the following argument. For non-trivial knots, the non-monotonic dependence of the probability distributions as a function of N in the unconstrained case, $1/R = 0$, is a well-known fact. It reflects the intuitive expectation that, as longer and longer

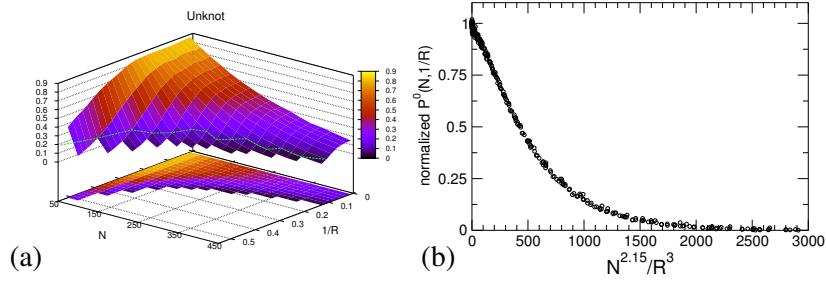


Figure 32: (a) Unknotting probability, $P^0(N, 1/R)$, for equilateral freely-jointed rings of N bonds (of unit length) confined inside a sphere of radius R . Below the thin green line, the fraction of unclassified knots is greater than 10%. (b) All data points in the manifold in panel (a) can be collapsed in a simple curve by plotting the normalised unknotting probability, $P^0(N, R)/P^0(N, 1/R = 0)$ as a function of $N^{2.15}/R^3$. Adapted from ref. [151].

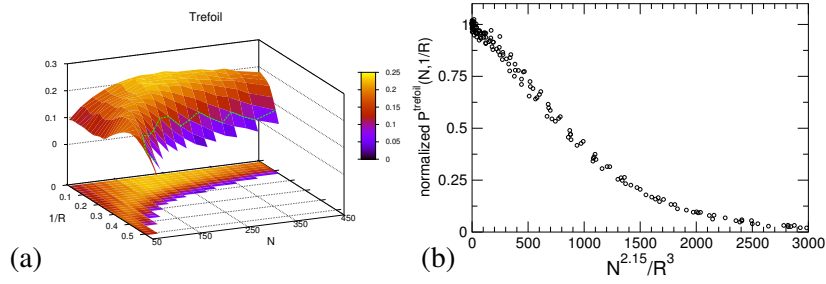


Figure 33: (a) Trefoil probability, $P^3(N, 1/R)$, for freely-jointed equilateral rings of N bonds (of unit length) confined inside a sphere of radius R . Below the thin green line, the fraction of unclassified knots is greater than 10%. (b) The data points for $N > 250$ in the manifold in panel (a) can be approximately collapsed in a simple curve by plotting the normalised probability, $P^3(N, R)/P^3(N, 1/R = 0)$ as a function of $N^{2.15}/R^3$. Adapted from ref. [151].

chains are considered, more complicated knots appear at the expense of simpler ones. Consistent with this fact, the location of the peaks at $1/R = 0$, is shifted towards higher and higher values of N for knots of increasing complexity. The presence of the shoulder at fixed small values of N as a function of $1/R$ is explained with an analogous intuitive argument. In fact, upon increasing confinement, simpler knots are progressively superseded in frequency of occurrence by more complicated knots.

The presence of the shoulder in the manifolds of Figure 33a suggests that the simple scaling function of eq. (51) cannot govern the behaviour of the probability functions of non-trivial knots for all values of N . It is noticed, however, that for sufficiently large N (for example for $N > 250$ for trefoils) the manifolds have a monotonic dependence on both N and $1/R$, analogously to the unknot case.

It is therefore natural to pose the question of whether the same scaling behaviour for unknots is valid for trefoils too. Figure 33b shows indeed that the trefoil probability data do collapse if they are plotted as a function of $N^{2.15}/R^3$. Notice that the latter quantity is the argument of the scaling function used for unknots, and is not fine-tuned to achieve a good collapse of the trefoil data. The scaling function, g , see eq. (51), where the data collapse, does not have a simple form; in particular it is not described by a single exponential.

Due to the more limited statistics of trefoils compared to unknots, the quality of the collapse is not as good as the one shown in Figure 32b, but it is nevertheless significant and indicative that the scaling relation of eq. (51) has a range of applicability wider than originally hypothesized by Michels and Wiegel. At present, no simple argument can be offered for explaining the scaling relation and for tying the scaling exponent, α , to the other relevant exponents governing the occurrence of knots in either unconstrained or confined rings or the length of the knotted region itself. In this respect, we mention that for unconstrained trefoil-knotted rings embedded in a cubic lattice, the length of the knotted region has been argued to scale as N^t , with $t \approx 0.75$. Based on this result (which is reported at length in section 17) one could envisage that the exponent α reflects the scaling of the knotted region volume; indeed the numerical value $3t = 0.225$ is remarkably close to the previously-reported value of the Michels and Wiegel exponent. While this argument is appealing we mention two difficulties that deserve further investigations. In fact, on the one hand, the exponent $t \approx 0.75$ describes the scaling of the trefoil knot length in the unconstrained region only, while the Michels and Wiegel relationship appear to hold for various degrees of compactness. In addition, it appears difficult to extend the previous argument, which is tailored to rings with a given non-trivial topology, to unknots, for which the Michels and Wiegel relationship was first formulated.

In recent years, the confinement-induced knotting of ring polymers was studied not only in the context of freely-jointed chains, as discussed above (and more recently in ref.[152]) but also for semi-flexible chains endowed with excluded-volume interactions and a finite bending rigidity.

For example, the study of ref. [153] specifically addressed the knotting probability of a semi-flexible thick chain subject to a progressive spatial confinement.

This type of investigation can provide some insight into a problem of high biological interest, namely the occurrence of knots in DNA molecules that are tightly packed inside viral capsids, which is discussed hereafter.

10. DNA knotting inside viral capsids

The problem of characterizing the extent to which knots, and other types of entanglement, arise in biomolecules such as DNA emerges quite naturally if one considers that, in all types of organisms, the genomic material is subject to a very high degree of confinement [85, 154].

For example, in eukaryotic cells, DNA molecules with a contour length as large as $\sim 1\text{m}$ are packed in a nucleus of diameter of about $1\ \mu\text{m}$. In bacteria, mm-long DNA is typically hosted in μm size cells. At the smallest scale, we have viruses, such as bacteriophages, whose μm -long genome is packed inside capsids having diameter of about 50nm .

Upon considering the degree of packing common to all above types of organisms, the consideration of the extent to which the spatial confinement of the genome is accompanied by the self-entanglement, and particular knotting, of the involved DNA filaments emerges naturally.

The understanding of the genome organization across eukaryotic, bacterial and viral organisms is far from being complete. Arguably, one of the best characterised systems is represented by the smallest types of organisms, namely bacteriophages. The latter, in fact, have been probed in recent years by the most advanced experimental techniques. This has provided a wealth of information about the detailed structure of the capsids and, to a more limited extent, of the organization of the genome held inside.

Prototypical examples are provided by bacteriophages such as $\epsilon 15$, which have been resolved by means of cryo-em techniques. These experiments, which did not enforce any *a priori* symmetry on the resolved structure, have revealed a highly ordered organization of the DNA contained

in the capsid interior. In particular, the genome arrangement was compatible with that of an inverse spool with a progressive increase of disorder moving towards the interior of the capsid.

The degree of order of the packaged DNA is affected by specific details of the capsid and of the surrounding solvent. Computer models of packaged DNA have shown, for example that the presence of an inner core inside the capsid favours the increase of DNA order [155]. The degree of oblateness or prolateness of the ellipsoid approximating the capsid, is also known to influence the specific DNA arrangement [156]. In addition, the presence of counterions in solution, which can diffuse through the capsid walls can affect the DNA self-repulsion and hence produce different arrangements [157].

Upon considering the high degree of order observed in several experimental measurements one might expect a low incidence of knots in the packaged DNA. Model arrangement of well-ordered inverse spools show, in fact, the virtual absence of knots after circularization [158]. The necessity to avoid knots inside capsids might, at first sight, also appear to be a biological necessity as the viral genome needs to be ejected through a narrow channel (the virus tail) into the infected bacterial cell and knots in the genome could obstruct the exit channel thus preventing the infection [159].

These two observations are challenged by a series of measurements carried out on tailless mutants of the P4 virus. In these mutants, the two complementary ends of DNA can anneal inside the capsid (in wild-type viruses one end would be anchored to the tail) producing a circular DNA molecule. The knotted state of the latter, which does not change unless the molecule is broken, is revealed through gel electrophoresis [65, 160, 161, 162]. The experiments have revealed a very high fraction (95%) of knotted molecules, unlike what was predicted on the basis of ordered spool models of packaged DNA. It is important to remark that a smaller, but still large percentage of knotted DNA molecules was observed in wild-type P4 genome where circularisation occurs after the destruction of the capsid. The knotted DNA molecules therefore reflect a fairly high degree of entanglement already present inside the capsid. We remark here that this aspect is not necessarily in contradiction with the fact that DNA needs to be delivered efficiently through the phage head. Indeed, it is known that knots occurring in (unconstrained) chains tend not to be localised [43], and a highly delocalised knot may be fully compatible with the genome exiting from the tail without occurrence of obstructions.

Before discussing the details of the knot spectrum of P4 DNA molecules we shall first attempt to relate the findings with the results discussed in the previous section about knots in confined rings.

For the purpose of this comparison, and following Vologodskii et al. [53], the 10Kb-long circularised P4 genome (corresponding to a contour length of $3.4\mu\text{m}$) was modeled as a flexible ring of $N = 200$ cylinders. The cross-sectional diameter, or thickness, of the cylinders was set to 2.5 nm which corresponds to the diameter of hydrated double-stranded DNA. Between consecutive cylinders a bending rigidity was introduced appropriate to reproduce, within Kratky-Porod models, the nominal dsDNA persistence length of 50nm.

The equilibrium properties of the model were studied with an advanced sampling technique analogous to those described in the methods sections (particularly multiple-Markov chains at various confining pressures and reweighting techniques) [153].

In accord with what was established for the confined freely-jointed rings, also for the thick flexible ring of cylinders it was seen that, for increasing spatial confinement, the knot spectrum is shifted towards higher complexity with a similar progression of complexity. In particular, it was seen (again consistent with the freely-jointed rings case), that among the knots with five minimal crossings, the torus knot 5_1 is systematically about half as probable than knot 5_2 over a wide

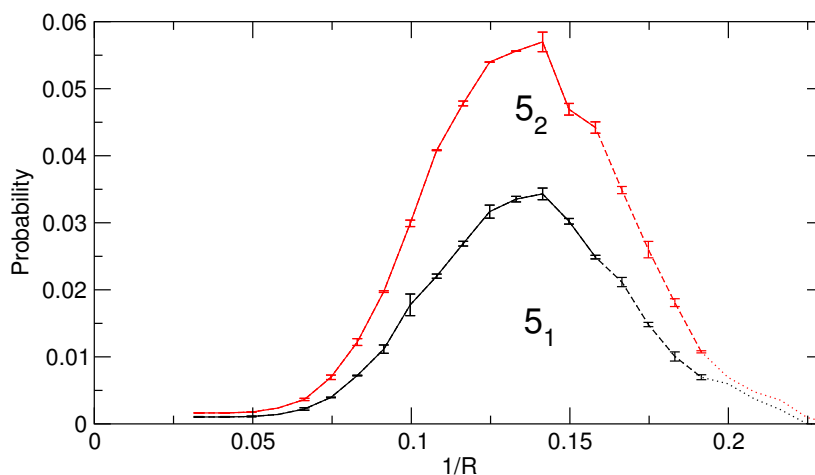


Figure 34: Probability of formation of knots of type 5_1 and 5_2 in flexible rings of cylinders of $N = 200$ bonds (of unit length) confined in a sphere of radius R . The bending rigidity of the rings and the thickness of the cylinders has been set to match those of circular DNA molecules of the P4 bacteriophage (see ref. [153] for details). Dashed [dotted] lines are used to indicate the regions where the knot complexity becomes so high that 10 [50] % of the rings form knots that could not be classified after simplification. Figure adapted from ref. [153].

range of $1/R$ values, see Figure 34.

This aspect appears profoundly different from what was established experimentally for the knotting of the P4 genome. A series of experiments, in fact, have shown that, among the simplest types of knots, torus knots are much more abundant than twist ones. In particular, the knot of type 5_1 was present in much higher abundance than 5_2 , which, in fact, was virtually absent from the measured spectrum. The bias in favour of torus knots is accompanied by another apparent bias, namely the one in favour of chiral knots. It is seen, in particular that knot 4_1 appears much less frequently than simpler or more complex knot types (e.g. 3_1 and 5_1).

This result then leads to the question of whether the knot spectrum of DNA phage might at all be explained via a model of confined polymers in thermodynamic equilibrium. One possibility is that the phage knot “selection” is a consequence of a certain degree of ordered spooling in the DNA conformations, which, while not large enough to drive the formation of a perfect unknotted spool, may still provide a measurable bias towards chiral and torus knots. For instance, Arsuaga and Diao recently showed that fluctuating, hence imperfect, DNA spools generate a knot spectrum closer to the experimental one [163]. However the generation of DNA spools came from a mathematical algorithm rather than a force field or potential, so it remained unclear what physical mechanism, kinetic or thermodynamic, provides the ultimate driver for the bias towards torus and chiral knots.

These biases are indirect clues about how DNA is organised inside the capsid; in particular they are suggestive of certain degree of ordered spooling, as this would be intuitively accompanied by a bias in chiral and torus knots. The discrepancy of experiments and computational predictions based on the simplified DNA models poses the interesting question of what specific aspects of DNA self-interaction and/or the genome packaging process need to be accounted for in order to explain the observed measurements.

In a very recent contribution, we provided quantitative evidence supporting the scenario that the biases in the knot spectrum may be explained via a more accurate force field which takes into account DNA self-interactions in a more realistic way [164]. The main novelty in Ref. [164] is the introduction of a chiral potential which favours a small twist angle between spatially contacting DNA segments. This potential would promote a cholesteric apolar ordering of DNA (with a pitch is in the $\sim \mu\text{m}$ range, hence much larger than the phage size). Such a chiral ordering *is* commonly observed in sufficiently concentrated DNA solutions *in vitro* (see e.g. Ref. [165]). This additional chiral interaction is also needed in models to discuss DNA in solutions at high enough densities to form a cholesteric phase, and is well documented in that literature [166, 167, 168, 169]. In the context of phage DNA, this interaction was never considered in simulations. Its effect is dramatic: the ordering increases so that DNA conformations now resemble much more fluctuating spools, and the main “selection rules” found in the experimental knot spectrum are very well reproduced, as the 4_1 and 5_2 twist knots are now extremely rare, and knots are typically chiral. Torus knots outnumber twist knots in the simulations even for more complicated knots, such as 7-crossing ones, which were not analysed in detail experimentally. Note that, for computational reasons, instead of the P4 genome a mutant containing half the genome (and preserving the main features of the knot spectrum, as demonstrated in [170]).

A remaining intriguing question is how phages are able to efficiently eject their DNA, which is the first step in the infection of a bacterial host, given that their genome is knotted with large probability, at least in the case of the P4 phage. The detailed simulations of Ref. [164] suggest a possible resolution of this seemingly paradoxical issue. By analysing the knotted configurations, it was found that the knots generated using the chiral interaction just described are highly delocalised (see Section 17 for a definition and discussion of knot localisation). This is very different to what occurs in DNA knots in swollen, uncompact configurations, which are (weakly) localised. The delocalisation of the knot makes so that the local conformation which is found close to the opening of the phage where the DNA gets out is not appreciably affected by the knot state of the DNA, which is a global topological characteristic of the molecule. On the other hand, it is these local entanglements which are likely to impact on ejection dynamics, and hence knot delocalisation renders ejection relatively insensitive to the DNA topology. More computational studies would be needed to further elucidate the interesting problem of knot ejection.

The latest theoretical and computational investigations provide quantitative evidence in favour of the fact that the experimental spectrum reflects specific aspects of DNA self-interaction (namely cholesteric ordering) that emerge at high DNA packing densities [164].

11. Knotting of polymer rings undergoing adsorption transition

It is well known that if a long polymer chain is in proximity of an attractive impenetrable surface, it may undergo a conformational transition from a *desorbed phase*, where the chain likes to be extended in the bulk, to an *adsorbed state* [50, 79, 171] where it is essentially localized at the surface.

Therefore, the attractive substrate can be regarded as a means to realize polymer confinement. The average degree of adsorption of a long polymer is expected to depend significantly on the temperature of the system [50]. The latter, in fact, controls the balance between the loss of configurational entropy when the polymer adheres to the surface rather than being free in the bulk, and the energy gain, ϵ , for each monomer that is in contact with the attractive substrate.

A crude estimate for this balance can be given by considering the entropy per monomer of the free polymer in three-dimensions, μ_{3d} , and in two dimensions, μ_{2d} (clearly $\mu_{3d} > \mu_{2d}$). The free

energy per monomer of the fully desorbed and adsorbed states are, respectively, $f_d \approx -T \ln \mu_{3d}$ and $f_a \approx -\epsilon - T \ln \mu_{2d}$. Accordingly, at temperatures lower than $T_c = \epsilon / \ln(\mu_{3d}/\mu_{2d})$ the polymer is expected to be fully adsorbed on the surface. The above estimate for T_c is admittedly crude as the adsorption is treated as an *all or none* process as a function of temperature. As a matter of fact, more accurate theories [50, 79, 172] and computational studies [88, 173] indicate that below a critical temperature, T_c , the fraction of polymer models adsorbed on the surface increases continuously from zero to 1.

Extending considerations from the case of linear polymers to rings with unconstrained topology, i.e. where “virtual” strand passages are allowed so to establish an equilibrium population of knots (see Section 7) brings additional elements of interest.

In particular, it is most interesting to analyse how the fraction of knotted rings varies with temperature. The salient physical mechanisms at play in this problem are best formulated by considering a partitioning of the ensemble of circular polymers into knotted and unknotted rings.

The first observation is that for each of these two sub-ensembles one can define a critical temperature for adsorption. In general these two temperatures are not expected to coincide. The second observation regards the relative weight between the population of knotted and unknotted rings. From what was discussed in Section 7 we know that in bulk (above the adsorption temperature for both sub-ensembles) the knotted population will outweigh the unknotted one for sufficiently long chains. At the same time, the lowest energy configurations, which dominate the system thermodynamics at sufficiently low temperatures, can only correspond to adsorbed *unknotted* rings. Only the latter, in fact, can be perfectly flat and thus guarantee that each single monomer is in contact with the surface. It is therefore to be expected that, as $T \rightarrow 0$, (i.e. well below the adsorption temperature for both sub-ensemble), the fraction of unknotted rings approaches 1.

Because of the complicated interplay of the two effects mentioned above, no clear prediction can be made for how the knotting probability depends on temperature in the neighborhood the adsorption transition(s).

For polygons on the cubic lattice it is however possible to show that, for every finite value of T , the probability that a N -edge configuration is knotted goes to one as N goes to infinity [174]. So except in the limiting case of zero temperature, when the polygon flattens completely by fully adhering to the surface, the polygon is knotted with high probability.

Numerical calculations [175] indicate that, for a fixed value of the adsorption energy, ϵ , the knotting probability of sufficiently-long polymers is described by the following functional form:

$$P_N(T) = 1 - e^{-\alpha_0(T)N + o(N)} \quad (52)$$

where N is the number of polymer monomers.

It is readily realised that the above expression generalises the expression for the knotting probability of unconstrained rings in three dimensions, see eq. 22. Indeed, for temperatures above the adsorption transition(s) $\alpha_0(T)$ is found to be independent of temperature and equal to the bulk value. Notably, a shoulder in proximity of the adsorption transition was observed even if the data were not sufficiently asymptotic to discriminate between the presence or the absence of a maximum around the critical temperature T_c [174]. In particular it was not possible to decide whether the adsorption transition of unknotted polygons differs from the one of polygons with unrestricted topology. Finally, consistent with previous observations $\alpha_0(T)$ was found to approach the zero value as $T \rightarrow 0$.

Further interesting observations, pointing to open problems could be made about the model system. For example, a preliminary investigation on the knot complexity shows that it decreases

as T decreases. No clear results are however available for the knot distribution as a function of T in the adsorbed regime. The limited number of theoretical investigations of the subject (which include the above mentioned works and the study in [176]) have left many open questions deserving more in-depth investigations. A summary of these open issues is provided below:

- it is unclear whether the adsorption transition depends on knot type. More stringent numerical investigations are needed in this respect.
- up to now, the knotting probability in adsorbed polymers has been studied only for lattice polygons. It appears necessary to extend the investigation to off-lattice models of ring polymers. This would also allow a more stringent comparison with the novel experiments of knotted circular DNA adsorbed on mica surfaces [75] or with future experiments based on single molecule imaging techniques [177, 178, 179];
- even for lattice polygons the knotting probability and the knot spectrum have not been characterized extensively neither in proximity of the adsorption transition nor in the fully-adsorbed phase, where a possible comparison with the model of *flat knots* [180] can be pursued (see section 17.2);
- in the adsorption problem discussed so far it was assumed that the surface exerts its attractive action over a lengthscale comparable to the typical size b of the monomers (short range potential). It would be interesting to examine how the entanglement of the rings is affected by extending the range of the attractive potential [171];
- so far very dilute solutions have been considered. In the case of adsorption transition from semi-diluted solutions it would become necessary to account for the mutual entanglement of polymer rings. This problem leads to the largely-unexplored issue of how ring linking probability depends on the polymer concentration in proximity of the attractive surface, and on the strength of the adsorption itself.

12. Knotting of polymers under tension

A further notable means of imposing spatial constraints on polymers is based on their direct *mechanical* manipulations. Owing to technological advancements introduced in the past decade, it is presently possible to apply a variety of controlled types of confinement on few, or even single biopolymers [66, 81]. Examples range from microfluidic devices [181, 74] which are used to force polymers into channel or slab-like geometries to experiments where one of the polymer ends (the other being anchored to a surface) is pulled by an AFM tip or by means of optical or magnetic tweezers [80, 76, 182, 68]. The latter two types of probe are particularly interesting in the present context as the “topology” of the stretched chain is not fixed (at variance with the AFM case) [82].

The variety of available experimental setups provide concrete contexts for validating or challenging the theories that had been developed for the response of polymers to mechanical probes either in the bulk [183, 50] or in confined geometries [184, 146, 185].

Arguably, the most common type of mechanical probe is the application of a stretching force at the two ends of a polymer. The application of the force, which couples to the end-to-end distance of the chain, reduces the chain configurational entropy. It is therefore interesting to

analyse how the equilibrium degree of entanglement of the chain is affected by the application of the tensile force.

The latter question has been investigated for the case of lattice polygons [186, 187]. The model was formulated so that the effects of both stretching and compression could be treated on common grounds. Specifically, the compressing/stretching force along the z direction was coupled to the calliper size, s , of the polygon measured along the z direction. In other words, because the concept of end-to-end separation is not applicable to closed polymers, the force is coupled to the largest distance projected by the ring polymer along the z direction. The calliper size therefore measures the width of the smallest slab (with plates perpendicular to the z axis) which accommodates the polymer configuration.

In the *constant force ensemble*, if we denote by $p_N(s)$ the number of lattice polygons with calliper size s , the equilibrium properties of the system are aptly encoded in the canonical partition function

$$Z_N(\tilde{f}) = \sum_s p_N(s) e^{f s} \quad (53)$$

where $f = \tilde{f}/k_B T$ is the *reduced force* and \tilde{f} is the applied force (in this way reduced forces are measured in units of inverse length). The unconstrained case is recovered for $f = 0$ where $Z_N(0) = p_N$. For $f < 0$ (*compressing regime*) the polygons are squeezed along the z direction while for $f > 0$ (*stretching regime*) conformations elongated along the z -direction will be favored⁴. By concatenation arguments the existence of the limiting free-energy

$$F(f) = \lim_{N \rightarrow \infty} \frac{1}{N} \log Z_N(\tilde{f}) \quad (54)$$

of this system for any (finite) values of the force can be determined [186].

The metric properties of the stretched chains have been explored by numerical simulations [187]. In particular it is interesting to study how the average extension of the polygons along the direction of application of the force:

$$\langle R_f \rangle = \frac{\partial}{\partial f} \log Z_N(f) \quad (55)$$

depends either on the applied force f or on N .

A valuable theoretical framework for characterizing the behaviour of linear (non closed) chains subject to a tensile force is provided by the scaling analysis of Pincus [183, 50]. This theory identifies two characteristic length scales in the problem: the average modulus of the end-to-end distance in the unconstrained case, $\bar{R} \propto N^\nu$, and the so called tensile screening length $\xi = 1/f$. The cases of weak and strong stretching forces correspond respectively to the conditions $\bar{R}/\xi \ll 1$ and $\bar{R}/\xi \gg 1$. According to Pincus [183] three specific stretching regimes should be observable for polymers in good solvent (see ref. [188] for discussion of bad solvent effects).

- *Weak force regime.*

⁴Note that the statistical ensemble of the rings compressed by a constant negative force ($f < 0$) is the conjugate of the statistical ensemble of rings confined in a slab of constant width. The properties of either ensembles can be recovered from the other through an appropriate reweighting technique (see Section 6.2). This correspondence is exploited in Section 8.3 to achieve an efficient computational sampling of rings confined in a slab.

For small forces one should expect a linear increase in the extension R_f as f increases (Hooke's law). Assuming the validity of the scaling relationship:

$$\langle R_f \rangle = R \Phi(\bar{R}/\xi), \quad (56)$$

where $\Phi(x)$ is a dimensionless scaling function, one can recover Hooke's law if $\Phi(x \rightarrow 0) \sim x$ so that

$$\langle R_f \rangle \propto R^2 f = N^{2\nu} f. \quad (57)$$

Note that for chains with no excluded volume interaction (ideal chains) $\nu = 1/2$ and $\langle R_f \rangle$ is linear in N at low forces. For self-avoiding walks $\nu \approx 0.588$ and the average extension is a nonlinear function of N . In the ideal case the force is transmitted along the backbone while for self-avoiding walks the transmission is also through contacts between pairs of monomers due to excluded volume interactions. Notice that scaling (57) implies

$$f = K \langle R_f \rangle, \quad (58)$$

so that the effective spring constant controlling the Hookean behaviour, K , decreases with the polymer length as $N^{-2\nu}$. It is important to notice that this Hookean regime should not necessarily be interpreted as arising from an effective increase of the average distance of the two chain ends. This point is best illustrated for a chain that is mildly pulled at both ends (which at low stretching forces can be slightly different from our case where the chain is pulled at the points with maximum and minimum values of z). The mild pulling at both chain ends leaves unaffected the end-to-end separation to leading order in f . In fact, it merely causes the end-to-end distance vector to rotate towards the stretching direction. This rotation produces in turn the linear (Hookean) increase of the projection of the end-to-end vector along the z axis [189, 190].

- *Intermediate force regime.* In the regime, which arises for intermediate forces, the value of $\langle R_f \rangle$ can be obtained according to a "blob" interpretation similar to the one described for polymers in confined geometries. The application of the theory can be argued as follows. As we discussed above, the presence of small-enough stretching forces does not alter the shape of the polymers but causes a rotation towards the stretching direction. As the force is progressively increased, the shape will eventually distort so that the polymer will extend along the stretching direction and grow thinner perpendicularly to it. This thinning is expectedly uniform along the polymer producing a situation similar to the tube-like confinement where the blob picture was first introduced.

Analogously to the scheme outlined in Section 8.1.1 the chain subjected to mechanical tension can be broken into a succession of tensile blobs along the z axis. The typical blob size is $\xi \sim f^{-1} = (\tilde{f}/k_B T)^{-1}$ (see Figure 35). The blobs do not interact with one another and the monomers contained in each blob behave as unperturbed self-avoiding walks. That is $\xi \sim g^\nu$ where g is the number of monomers in each blob. Since each chain is a stretched array of tension blobs, their average extension along the direction of force application is the product of the tensile screening length ξ and the number of these blobs, N/g per chain

$$\langle R_f \rangle \sim \xi N/g \sim N f^{1/\nu-1} \sim N f^{2/3}, \quad (59)$$

where in the last term we have used the Flory value of the exponent $\nu = 3/5$. This is the so-called Pincus regime. In this case

$$f = K \langle R_f \rangle^{3/2} \quad (60)$$

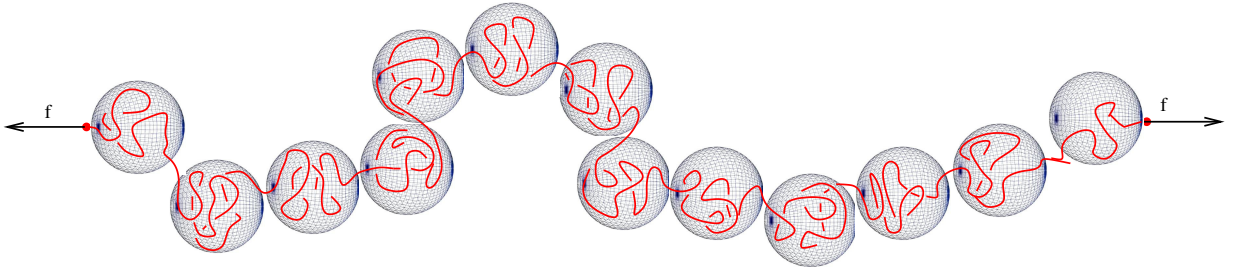


Figure 35: Blob picture of stretched polymers in the intermediate force regime.

with $K \sim N^{-3/2}$.

- *Strong force regime.* For extremely large forces excluded volume effects become irrelevant since the bonds of the polymer are fully aligned along the stretching direction and monomers do not interact with one another. In this case $\langle R_f \rangle$ becomes comparable to N and the force-extension relation for the chain is dominated by the bonding potential between consecutive monomers. As a result the force-extension curve would be model dependent.

Figure 36 shows $\langle R_f \rangle / N^\nu$ vs $f N^\nu$ where $\nu = \nu_{saw} \approx 0.588$ for positive forces. For relatively small positive forces, as N increases, the data collapse onto a single curve. In this weak force regime the behaviour is linear as suggested by the dashed straight line. For larger values of f the curves collapse nicely if we plot $\langle R_f \rangle / N$ as a function of f (see Figure 37). The dashed curve represents the best fit of the data to a power-law behaviour, $A N^c$. The estimate $c \approx 0.64$ is close to the value $2/3$ which characterizes the Pincus regime. In these data the values of f are not large enough to see the strong force, non-universal, regime. Notice that longer polygons reach the scaling regime at weaker forces. Indeed the rigidity of a long chain is smaller than that of short chains and this makes longer polygons more easily deformed. In the contractile region, $f < 0$, no scaling theory is available.

For the knotting probability some rigorous results are available [186]. In particular, for f positive and sufficiently large it was possible to prove a pattern theorem for stretched polygons. A key element of the proof is the notion of a cut plane, that is a plane orthogonal to the stretching direction that separates independent sub-parts of the polygon, in analogy with the blobs in the Pincus scaling argument [183]. The proof relies on the fact that, for typical polygon conformations, cut-planes occur with a finite density along the stretching direction.

The pattern theorem can be used to prove the FWD conjecture also for sufficiently-stretched polygons. This result can be stated as follows: for arbitrary large positive, though finite, values of the stretching force, the probability that a stretched polygon is knotted approaches 1 as the length of the polygon (at fixed f) increases. In other words, for $f > f_0$ the following large N behaviour for the unknotting probability holds

$$P_N^0(f) = e^{-\alpha_0(f)N + o(N)}. \quad (61)$$

Note that that eq. (61) can be proved for $f > f_0 = 4\kappa$. On the other hand a proof exists for $f = 0$ (see section 7) and it is quite intriguing that in the intermediate region $0 < f < f_0$ no proofs are

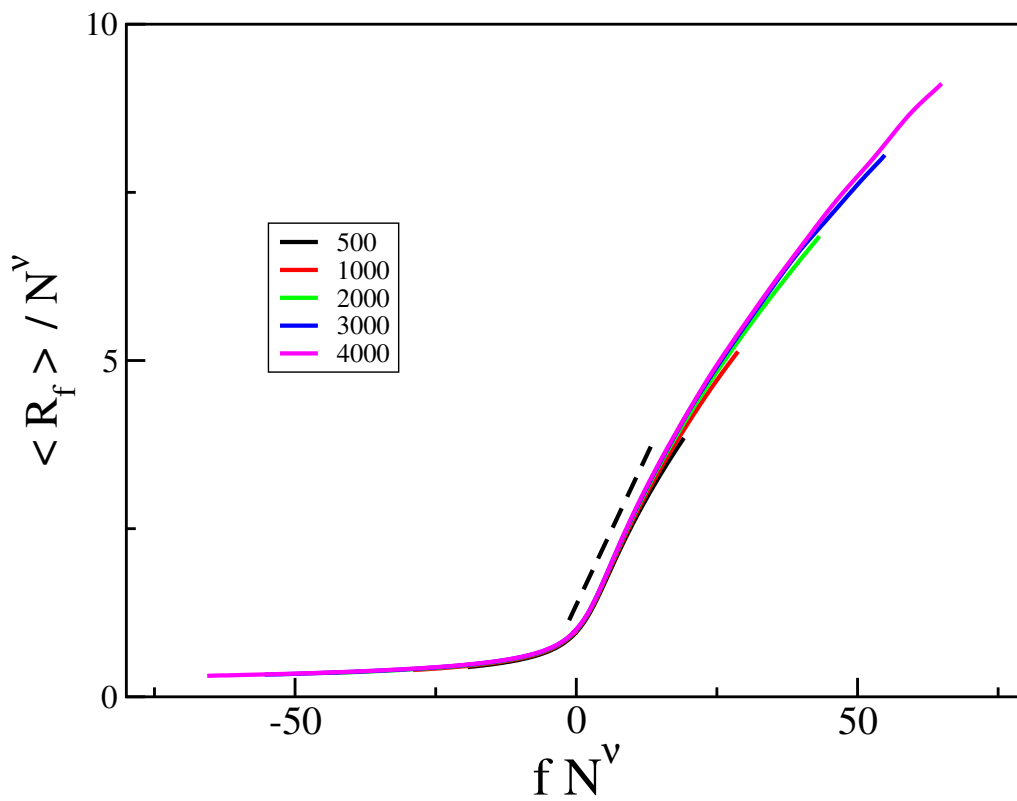


Figure 36: Plots of $\langle R_f \rangle$ vs f for stretched polygons of different values of N . To underlying the weak adsorption regime the average extension along the force direction has been scaled by n^ν whereas the force is multiplied by n^ν . (The value of ν used is $\nu \approx 0.588$). The dashed straight line indicates the expected linear behaviour for small values of f .

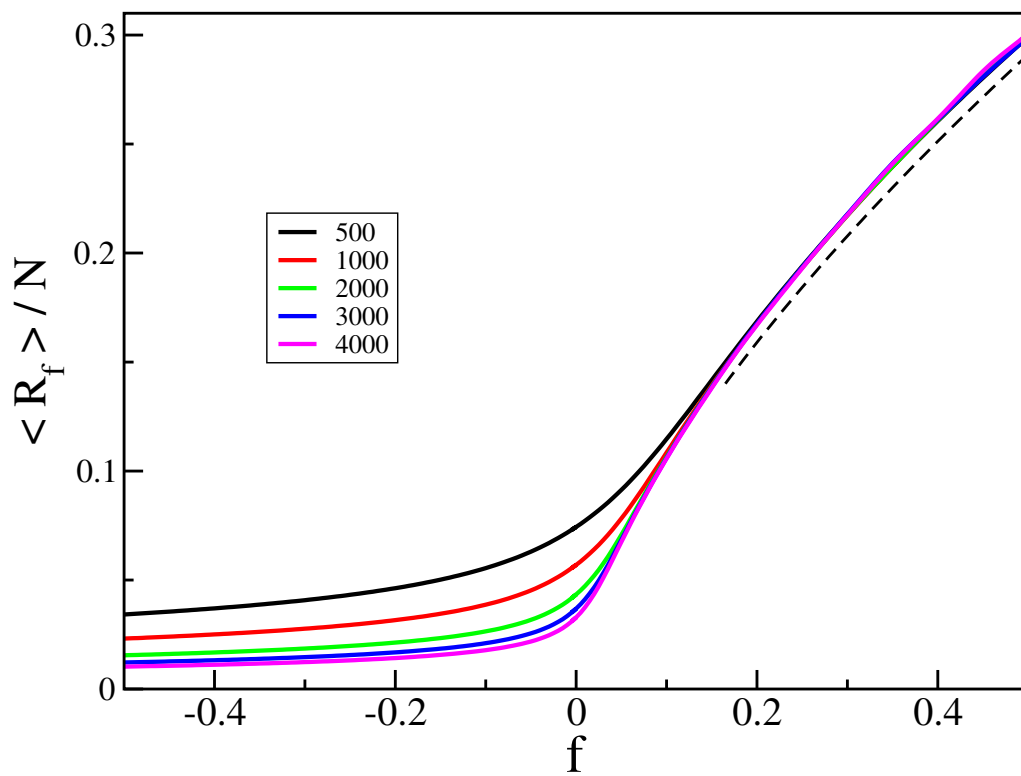


Figure 37: Same data of the previous Figure. Now $\langle R_f \rangle$ is divided by N to highlight the Pincus regime. The dashed curve correspond to the fit $A N^{0.66}$ done on the $N = 4000$ data.

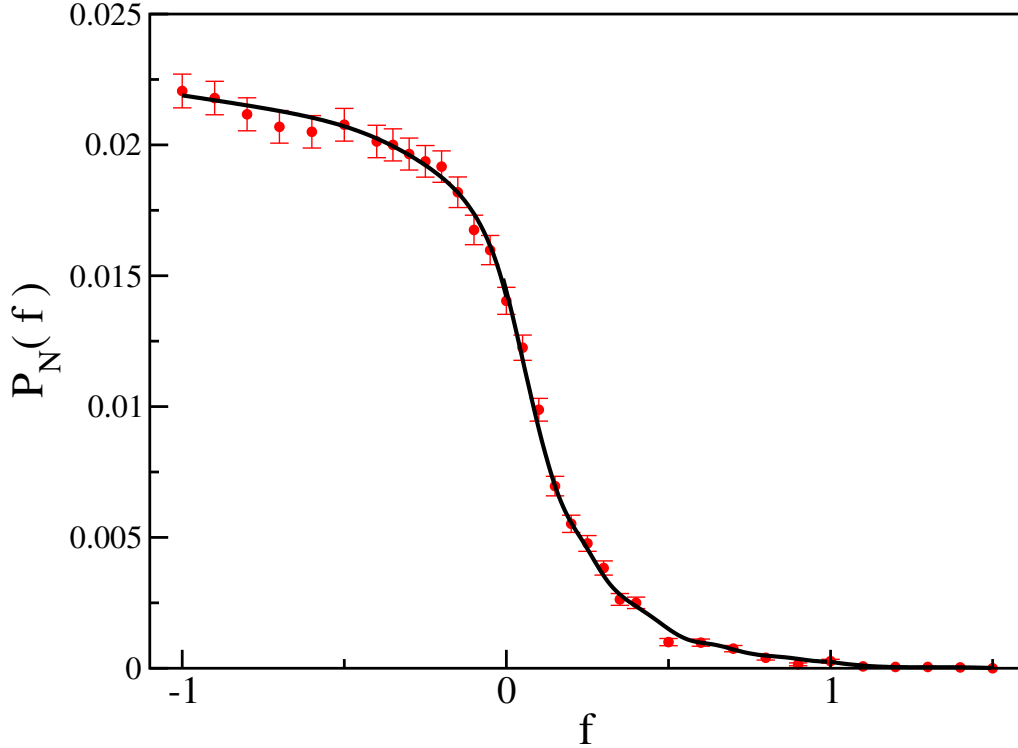


Figure 38: Knotting probability for $N = 3000$ bonds polygons subject to an external force f coupled to the span s of the polygon along the z direction.

at the moment available⁵. This unknown region could correspond to the weak stretching regime where the Pincus blob picture may not be valid. For negative values of f no rigorous results are available to present day.

The problem can, however, be investigated numerically by Monte Carlo simulations [187]. A typical approach is based on the two-point pivot algorithm implemented on the importance sampling techniques with weight proportional to e^{fs} . A MMC sampling method is then performed on the space of f . Once a reasonable number of uncorrelated configurations are sampled at a given f , the knotting probability is computed by using the Alexander polynomial (see Section 3) as knot detector. The results show a knotting probability that, at fixed N , decreases rapidly as the stretching force increases while it increases (although very slowly) in the compressive regime (see Figure 38). For fixed values of f the exponential decay (61) is confirmed in the *whole range of f* and an estimate of $\alpha_0(f)$ is obtained.

In addition to the case of rings mentioned above there are models of linear chains under mechanical stress for which a non-ambiguous definition of knottedness can be introduced. Examples are walks spanning a slab and whose ends are anchored to the walls or walks in which

⁵A pattern theorem for biased self-avoiding walks has been proven in [191] for all values of $f > 0$. If the technique in [191] were applicable to models of pulled polygons one should be able to prove (61) for all positive values of f

both extremities are anchored to an impenetrable surface (loops) [192]. For these models both the thermodynamic and the entanglement properties have been explored either by rigorous arguments or by Monte Carlo simulations. A thermodynamic phase transition from swollen to ballistic (i.e. where the end to end distance grows with N) phases) has been proved to exist for $f = 0^+$ and the unknotting probability has been confirmed, numerically, to follow the law (61) for the all range of positive and negative values considered [192]. Polygons can also be stretched by confining them into a tube and by applying a force along the axis of the tube. In this case the geometrical constraint helps in proving a pattern theorem *for any positive values of f* and, consequently, an extension of the FWD conjecture to polygons stretched through a tube [193].

With the exception of the studies just mentioned, the knotting probability of polymers under tension and in general the dependence of the entanglement complexity on the external force remains a rather unexplored topic that deserves a more in-depth investigation.

For example very little is known on the knot spectrum as a function of f and there are no results available (neither analytical nor numerical) for the knotting probability for off-lattice models of polymers under tension.

13. Third part: Mutual entanglement of several polymer chains

The third part consists of Section 14 and is devoted to discussing the occurrence of a particular topological state in a polymer melt, that is the *mutual entanglement* of several polymeric chains (linking). Historically, this is arguably the oldest topic in the topology of closed curves: in fact its origins can be traced back to Gauss [194].

The mutual entanglement of chains and filaments that are densely packed in the same region of space is known to affect their rheological and elastic properties [195, 196]. The topologically-entangled states of two or more circular polymers are called links (or catenanes) [18, 16]. Links are of interest to chemists [61, 197, 198], but are also frequent in biology. For example, linked pairs of DNA rings occur in the mitochondria of malignant cells and are intermediates in the replications of circular DNA [199]. Linked rings are also present in trypanosomes, microorganisms associated to leishmaniasis and Chagas disease. In these organisms there are organelles, called kinetoplast, which house thousands of DNA circles which can be interlinked to form a network resembling chain mail [200].

In solutions with a sufficiently-high concentration of linear polymers cyclization reactions will produce linked states of two or more chains. In analogy with the case of knots, is natural to ask how frequently, in thermodynamic equilibrium, a linked state would occur compared to the unlinked one and how this linking probability and linking complexity depends on polymer concentration, solvent condition and degree of polymerization.

As for knots, linked states are not easily described in terms of local variables and with the exception of analytical work based on the Gaussian integral measure of links (linking number) [201, 202, 203] the linking probability of circular polymers in free solution has been investigated mainly by numerical simulations and in the simplest case in which only two rings are involved (two components links) [204, 205, 206]. Similar investigations have then been carried out for polymers in a melt [207, 208] but, with the exception of few studies on simplified models [209, 210, 211, 212] the linking probability and link spectrum of rings in confined geometries is an issue that remains mostly unexplored. This subject is discussed in Section 14.

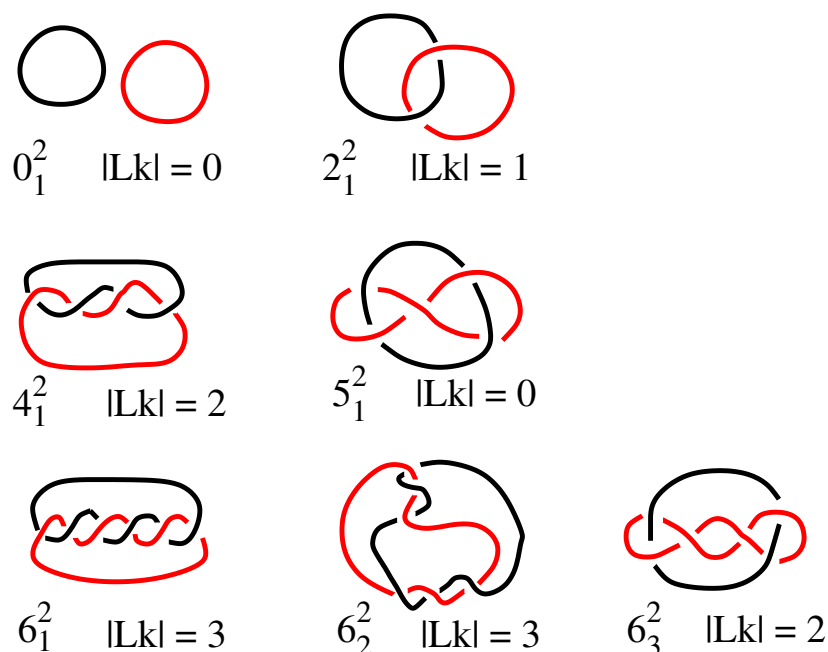


Figure 39: The simplest two-components links with their symbol and linking number.

14. Mutual entanglement between polymer rings in solution: linked states

In solutions with sufficiently-high concentrations of linear polymers, a circularization reaction will usually trap the chains in mutual entanglement producing various topological states, known as *links* (see Section 3).

Although the links arising from the ring-closure operation may involve several chains, we will primarily focus on two-components links which are made by a pair of chains. Such links are easier to define and detect than generic multi-component links. Furthermore the latter can be often characterized in terms of their pairwise subcomponents, as we shall discuss later.

Consider two simple closed curves, C_1 and C_2 that are disjoint, i.e. with no points in common, and embedded in three-dimensional space. The curves are said to be *topologically linked* or, more simply, *linked* if no smooth deformation exists by which they can be pulled apart so that they lie in two different half-spaces separated by a plane. In Figure 39 we show the diagrammatic representation of the simplest types of 2-components links. Notice that, while for isolated closed curves, the salient topological information was contained in the *self-crossings* of their diagrammatic representations, for links, the topological state is additionally specified by the *reciprocal* crossings between the curves. As reported in the figure, the standard nomenclature for links parallels the one of prime knots with the addition of a superscript to denote the number of link components so that, e.g. the unlink is denoted as 0_1^2 . For future reference, we point to the reader's attention the links 2_1^2 and 5_1^2 are known respectively as the *Hopf link* and the *Whitehead link*.

Links between pairs of polymer chains are of paramount interest from the chemico-engineering

point of view, especially regarding the synthesis of macromolecular compounds with so-called catenane units, see refs. [213, 61] [197, 198, 214]. Examples of naturally-occurring links are common between nucleic acids molecules and also protein complexes. For the latter case a remarkable example is provided by the protein capsid of bacteriophage HK97 whose resistance to degradation results from the mutual linking of its tiling proteins [215]. Intriguingly, the introduction of *de novo* designed links in proteins has now been proposed as an effective method for stabilizing protein complexes against thermal and chemical denaturation [216, 217].

DNA molecules too offer several examples of topological linking. For example, linked pairs of DNA rings are found in mitochondria of malignant cells [218]. In bacteria, DNA linking inevitably occurs during the replication process of the circular genome [5, 199]. The removal of the resulting entanglement is essential for the successful completion of the replication process and is provided by enzymes, aptly named *topoisomerases* because they are capable of modifying the topological linked status of DNA rings by suitably “cutting and rejoining” DNA strands [5, 199, 9, 219, 11].

As for the case of knots, there exist no general prescriptions or algorithms that can be used to classifying exactly the topologically state of a link starting from an arbitrary diagrammatic representation. There are, however, several partial descriptors based on *link invariants* that can classify two-component links up to a given degree of complexity. However, the most powerful descriptors are also highly complex from the algorithmic point of view. Consequently it is often necessary to strike a balance between the power of the employed descriptor and the computational cost of its evaluation.

The link invariant that requires the least amount of computation is the *linking number*. Loosely speaking it corresponds to the effective algebraic number of times the one curve winds around the other, and viceversa. For two piecewise linear curves, C_1 and C_2 , the linking number is conveniently evaluated by first choosing an orientation for each curve and next projecting them onto a plane avoiding intra- and inter-curve degenerate vertices. To each crossing point where, say, C_1 underpasses C_2 we assign +1 or -1 value according to the crossing orientation (see Figure 9 where in this case the strand labelled k belongs to C_1). The sum of these signed crossings is the linking number $Lk(C_1, C_2)$ between the two curves. Figure 39 shows examples of two-component link diagrams and the associated linking number. Note that instead of focussing on the under-crossings of C_1 one can compute the sign of all the, say K , crossings between the two curves. In this case the linking number is given by the formula

$$Lk(C_1, C_2) = \frac{1}{2} \sum_{i=1}^K \sigma_i, \quad (62)$$

where σ_i is the sign of the i -th crossing. We emphasize that, at variance with the case of single-component link (i.e. a knotted closed curve) where standard topological invariants are independent of the choice of orientation of the curve, the value of Lk does depend on how the two curves are oriented. For polymers that can be oriented based on properties of their chemical sequence it is meaningful to consider the signed value of Lk . In more abstract or general contexts, where the choice of orientation is subjective, it is more appropriate to consider only the absolute value $|Lk|$ which is obviously independent of the curves orientation.

For completeness we mention that there exist other algorithmic formulations of the linking number which are equivalent to the one given above [18]. One that is particularly useful for analytic calculation on smooth curves is the definition introduced by Gauss in terms of the double

integral

$$Lk_G(C_1, C_2) = \frac{1}{4\pi} \int_{C_1} \int_{C_2} d\vec{r}_1 \times d\vec{r}_2 \frac{\vec{r}_1 - \vec{r}_2}{|\vec{r}_1 - \vec{r}_2|^3} \quad (63)$$

where \vec{r}_1 (\vec{r}_2) defines a point on the curve C_1 (C_2). The integral $Lk_G(C_1, C_2)$ is usually referred to as the *Gauss linking number*, after Gauss who introduced it to characterize the entanglement of the orbits of heavenly bodies. Consistent with the former definition of linking number, the above integral returns an integer value whose sign depends on the orientation of the two curves.

The limitations of the linking number as a descriptor of topological-linking are illustrated in Figure 39 which portrays a Whitehead link 5^2_1 . Although this link has a non-trivial topology, its linking number is zero as is the linking number of the unlink 0^2_1 . This ambiguity has made necessary the introduction of the concept of *homologically linked* curves which is used to denote two curves C_1 and C_2 having $|Lk(C_1, C_2)| \neq 0$. Homologically-linked curves are also referred to as being *algebraically linked*, in contrast to topological or geometrically linked ones. Indeed, pairs of curves that are homologically linked are guaranteed to be topologically linked but, as shown by the previous example, the converse is not true.

Despite the above limitations, the linking number is very commonly employed as a detector of the concatenation of two curves. This is because it is algorithmically simple to code and can be evaluated with a negligible computational cost. Secondly, the linking number is often a complete descriptor for the type of linking arising in certain contexts, particularly biomolecular ones (e.g. DNA catenanes). Finally, in the context of double-stranded DNA circles, the linking number of the two DNA strands is important. This is because the linking number is a *topology-dependent* quantity which matches the sum of two important *geometrical* quantities, namely local twist and the writhe of the DNA duplex [220, 221].

More complete descriptors of topologically-linked states between two curves are usually based on generalised polynomial invariants such as the two-variable Alexander polynomial $\Delta(s, t)$ [222] or, better, the HOMFLY polynomial reported in Section 3. A detailed discussion of how to compute the two variable Alexander polynomial from a given 2-component link diagram is provided in ref. [204].

14.1. Linking statistics of two rings in unconstrained spaces

Consider the case where the linked state between two rings is not fixed but can fluctuate in equilibrium or in steady-state conditions. A concrete example of the latter situation can be provided by a solution of circular DNA molecules in the presence of topoisomerase II enzymes which continuously process the molecules cutting and rejoining DNA strands. The action of the enzymes would therefore change the initial topological linked state of the DNA circles producing a steady-state distribution of linked or knotted molecules [219]. Analogously, it is possible to envisage an equilibrium linking probability for confined linear polymers whose termini can attach to/detach from one of the bounding surfaces (which provide a “closure” for the chains).

In these and similar cases it natural to ask how frequently the equilibrated, or steady-state, configurations display a linked state and how complex it is. It is reasonable to expect that these properties depend on several factors such as the degree of overlap between rings, the quality of the solvent, the degree of confinement etc. In the following we will review the salient available theoretical results on this problem.

14.1.1. Some analytical and rigorous results

Because of the complexity of the problem, only a limited number of analytical results are available for the statistics of two-component links for rings in free space. Early attempts were

aimed at characterizing the probability distribution of the linking number between two closed rigid curves randomly displaced in \mathbb{R}^3 [201, 202]. In particular in [201], the Gauss integral representation of the linking number was used to compute the *squared linking number* averaged over all relative rotations and translations of the two curves and over all the possible reciprocal orientation. The formula for the second moment of the Lk probability distribution function was subsequently re-discovered and generalized to space curves without a plane symmetry by using Fourier transform techniques [202]. A different derivation and a further generalization to closed manifolds in \mathbb{R}^n was later provided [203].

As intuitively expected, one of the difficulties of characterizing the *Lk* probability distribution for two curves in free space lies in the fact that for the overwhelming majority of their possible relative configurations, the two curves will be too far apart to be linked.

A more natural formulation of the linking problem is obtained by introducing an external constraint limiting the phase space of possible relative displacements of the two curves. A commonly-employed scheme is to prevent the separation of the centers of mass of the two curves from largely exceeding the average size of the rings.

An alternative, more rigorous formulation of the problem consists of considering the ensemble of *fixed linking type* and calculating the limiting entropy of a system of two rings with a definite linked (non trivial) state. This approach has been used for linked pairs of polygons in the simple cubic lattice [205] and the results obtained are summarised hereafter.

Let us denote by $p_{NN}^{(2)}(\tau)$ the number of polygons pairs, each of N bonds, forming a specific type of topological link (meaning their type of concatenation), τ . When no restriction is introduced for the knot type of each component, it is expected that:

$$\lim_{N \rightarrow \infty} \frac{1}{2N} \log p_{NN}^{(2)}(\tau) = \kappa \quad (64)$$

i.e. the limiting entropy of a two-component (non trivial) link equals the one of the single polygon, independently on the link type.

Different results are obtained when the knot type of both components is kept fixed. Suppose, for example, that neither of the two rings is knotted and let $p_{NN}^{(2)}(\tau|0, 0)$ be the number of such embeddings in the cubic lattice. In this case it is possible to prove that, independently of the two-component link type τ , the following inequality holds:

$$\lim_{N \rightarrow \infty} \frac{1}{2N} \log p_{NN}^{(2)}(\tau|0, 0) = \kappa_0 < \kappa . \quad (65)$$

In other words, the key feature affecting the limiting entropy of a two-component link is not the topological linked state between the two rings but the requirement that *both* components are unknotted. One may *conjecture* that this holds true also if both components have a fixed non-trivial knot type σ :

$$\lim_{N \rightarrow \infty} \frac{1}{2N} \log p_{NN}^{(2)}(\tau|\sigma, \sigma) = \kappa_\sigma . \quad (66)$$

This result, albeit being a plausible generalization of what was established for unknotted polygons, has not been proved rigorously because of the difficulty in proving the existence of the following limit,

$$\lim_{N \rightarrow \infty} \frac{1}{N} \log p_N(\sigma) = \kappa_\sigma . \quad (67)$$

Inequality (65) can be used to establish how the knotting probability $P_{NN}^{(2)}(\tau)$ that *both* components of the link of type τ are knotted grows as a function of N . One has, in fact, that

$$P_{NN}^{(2)}(\tau) = 1 - e^{-\alpha_0 N + o(N)} \quad (68)$$

when $N \rightarrow \infty$. This results is straightforwardly generalized to k -components links as follows. If k unknotted polygons, each of N bonds, form a k -component link of type τ , then

$$\lim_{N \rightarrow \infty} \frac{1}{kN} \log p_{N,N,\dots}^{(k)}(\tau|0, 0, \dots, 0) = \kappa_0 \quad (69)$$

irrespectively of the k -component link type, τ . Extension of these results to the links of higher dimensional structures (p -spheres) can be found in [223].

Arguments similar to those in refs. [205] and [223] can be used to establish that the exponential growth rate of the number of topologically linked polygon pairs is equal to that of topologically unlinked polygon pairs. Therefore, unlike the knotting probability, it cannot be concluded that all but exponentially few sufficiently-long pairs of polygons are linked, even if the distance constraint is taken into account. This leaves open the possibility that the linking probability could still approach unity as $N \rightarrow \infty$ but in this case it would not do so exponentially. It is important to stress once more that all the results presented above have been obtained by assuming that both rings have the same number of bonds, N .

14.1.2. Numerical results on linking probability

The linking probability of two rings clearly depends on their spatial separation. When the distance of the centers of mass of the rings is much larger than the sum of their gyration radii, the linking probability of the rings will be zero. As the distance is progressively reduced it is intuitively expected that the linking probability increases. It is therefore interesting to examine, by computational means, whether the expected monotonic increase is indeed observed within an equilibrated ensemble and whether the limiting value of the linking probability is 1.

The first numerical investigation of these two aspects was carried out by Vologodskii et al. [204] who considered random (non self-avoiding) polygons embedded on a body-centred cubic lattice. A Monte Carlo scheme, based on a chain-growth algorithm, was first used to sample unrestricted conformations of a single polygon of N bonds. Next, several pairs of uncorrelated polygons were picked from the Monte Carlo generated ensemble. Each pair was embedded in the lattice so that the centers of mass of the polygons were at a pre-assigned distance, d , and their linked state was established by using the two-variable Alexander polynomial $\Delta(-1, -1)$. By repeating the process for each pair of rings the linking probability $P_{NN}^{(2)}(d)$ it was finally estimated. For ring lengths up to $N = 80$ the numerical data were well-consistent with an exponential dependence of the linking probability on the separation, d :

$$P_{NN}^{(2)}(d) \sim Ae^{-\alpha_L d^3} . \quad (70)$$

The effect of the excluded volume interaction on the pairwise linking probability of self- and mutual-avoiding rings (on the simple cubic lattice) was later studied in [205]. Because of the self-avoiding nature of the rings, the efficiency of the simple sampling technique used in [204] is poor. An importance sampling method was used instead where polygon pairs, deformed by two-point pivot moves, were accepted according to a probability density that decreases rapidly with the separation of the rings centers of mass. Suitable reweighting techniques (see Section 6)

were next used to remove the effect of the external bias and compute the equilibrium ensemble averages.

The linked state of each pair was probed by computing both the linking number (homological linking) and the Alexander polynomial $\Delta(-1, -1)$ (topological linking). For pairs of polygons, each with up to $N = 1800$ edges, the homological and topological linking probability as a function of d were calculated. In analogy with the knotting of ring polymers in confining geometries, the degree of the mutual entanglement turned out to be governed by the competition between two length scales, namely the gyration radius, proportional to bN^ν , and the ring separation, d . The linking probabilities calculated for various values of d and N are compatible with the following simple scaling relationship:

$$P_{NN}^{(2)} \sim f\left(\frac{d}{bN^\nu}\right) \quad (71)$$

which, in fact, yields a good collapse of the numerical data points for $P_{NN}^{(2)}(d)$ obtained for various values of N and d .

The scaling relation of eq. (71) is consistent with the vanishingly small probability of having two polygons linked when their separation largely exceeds their typical size, i.e. when $d/bN^\nu \gg 1$, and also captures the fact that upon bringing the rings progressively closer, the linking probability increases and ultimately reaches 1. Using numerical means the conditional probability that two topologically-linked rings (i.e. $\Delta(-1, -1) \neq 0$) are also homologically linked (i.e. $|Lk| \neq 0$) was also analyzed. At large separations ($d/bN^\nu \gg 1$) this conditional probability was found to be zero. On the other hand, as d/bN^ν decreased, the fraction of topologically linked polygons pairs that are also homologically linked increasingly approached unity for $d/bN^\nu \ll 1$. This behaviour, which is not evident *a priori*, suggests that the linking number is a very good indicator of topological linking for pairs of polygons that strongly interpenetrate. By converse, the linking number is a poor proxy for topological linking when the ring separation is large.

The impact of mutual excluded-volume interactions on the linking probability between 2 self-avoiding rings has been recently re-examined in [206] in off-lattice contexts by using the rod-bead model (see Section 4.1). In this study the linking probability was monitored as the radius of the bead Δ_2 was varied from zero (equilateral random polygons with no excluded volume) to nearly 1. In a fashion similar to the study of ref. [204] single-ring configurations were first generated using simple sampling techniques. The rings were not subject to any spatial confinement but the sampling was limited to unknotted rings. Next, pairs of single-ring configurations were randomly picked from the sample and put at a given distance d . The topologically-linked state of each pair was established using $\Delta(-1, -1)$ and finally the linking probability, $P_{NN}^{(0,0)}(d)$, was computed. The superscript 0,0 is used to remind of the unknotted topology of each component.

Throughout the explored range for r_e it was confirmed that $P_{NN}^{(0,0)}(d)$ is vanishingly small for $d/bN^\nu \gg 1$. Remarkably, at variance with the lattice model of ref. [205], it was found that for $r_e \geq 0.2$, i.e. where excluded volume effects become relevant, the linking probability is no longer a monotonic function of d , but has a maximum at d/bN^ν . Furthermore, Hirayama *et al.* [206] observe the breakdown of the scaling assumption (71) for $r_e < 0.2$ i.e. in the regime where excluded volume interactions are negligible.

The comparison of these findings with those of ref. [205] suggests that salient aspects of the linking probability are strongly affected by the introduction of topological constraints, such as specific knotted states, on the individual components. Future investigations of the problem ought to shed light on this problem, possibly in connection with the expectedly important role played

by the size of the knotted region (see Section 17).

14.2. Linking probability in confined geometries

14.2.1. Statistics of two-components links confined in a cube

As anticipated, it is particularly interesting to characterize the linking probability of fluctuating rings that are spatially constrained to lie in a region of width comparable to the average size of unconstrained chains.

To the best of our knowledge, the first investigation of the linking probability in confined geometry was discussed in [205]. In this study, Monte Carlo simulations were used to compute the linking probability of two N -edged polygons embedded on a cubic lattice of lattice spacing b and confined inside a cube with linear size equal to D .

Pairs of confined polygons were generated using the scheme similar to ref. [204] that is by first generating individual polygons in free space (using two-point pivot moves), then by using rejection techniques to pick pairs of polygons which have total calliper size (i.e. the calliper size of the pair) not larger than D in all three Cartesian directions.

All configurations of the two polygons that could fit in the D -cube were enumerated. As the embedding space is finite, two configurations of the polygon pairs that differ for rigid translations along the lattice axes are considered inequivalent.

The linked state of each polygon pair was probed using both the homological and topological indicators, that is the linking number and the Alexander polynomial $\Delta(-1, -1)$. In analogy with the case of knotting of individual polygons subject to geometrical confinement, the occurrence of the two rings linking was found to depend on the interplay of the average ring size, bN^ν , and the average confining length scale, D .

In particular, the linking probability was found to be a function of adimensional ratio $D/(bN^\nu)$. If $D \gg bN^\nu$ (mild confinement) the linking probability is essentially zero whereas as $D/(bN^\nu)$ decreases the linking probability increases monotonically.

Regarding the viability of using linking number as a proxy for topological linking, it was found that when the spatial confinement is mild then almost all topologically-linked pairs (i.e. those with $\Delta(-1, -1) \neq 0$) have linking number equal to zero. On the other hand as $D/(bN^\nu)$ decreases the two rings start to strongly interpenetrate each other and, in analogy with the case of unconstrained rings brought in close proximity, the resulting topological linking is associated to a non-zero linking number.

This finding is not only interesting *per se*, but can be exploited to speed up the computational detection of topological links in systems with a high density of rings/polygons as it suggests that the computational-effective linking can be reliably used.

By considering polygons without excluded volume interactions, Arsuaga et al. [210] characterized the linking probability for densities (polygon bonds per unit volume) much higher than those examined in ref. [205] for self-avoiding polygons. More precisely, in ref. [210] the uniform random polygon (URP) model was used [224]. In this model the polygon configurations are obtained by joining N points picked with uniform probability in the unit cube (plus the closure condition). The polygons are clearly non-equilateral and the bonds are considered as being infinitely thin. In the limit of high densities, the probability of two URPs to be homologically linked was found to approach 1 linearly, with slope proportional to $1/N$.

Because of its simplicity of formulation, the URP model lends to analytical characterizations and, in [210] it was rigorously shown that linking probability between a fixed closed curve in the unit box and a uniform N -bonds random polygon approaches 1 at a rate at least of order $1/\sqrt{N}$.

We stress that this result refers to a single uniform random polygon in presence of a *fixed* curve and, up to now, this has not been extended to the more interesting case of two uniform random polygons mentioned before. Finally, we mention that in the same study, it was rigorously shown that, for two N -bonds URP in the unit box, the second moment of the linking number distribution is proportional to N^2 .

14.2.2. Statistics of two-components links in D -slabs and (D_1, D_2) -prisms

Very few results are available for the linking probability of two rings confined in D -slabs and (D_1, D_2) -prisms. In [209] this problem was tackled numerically for polygons embedded in the cubic lattice with lattice spacing b . To overcome the sampling difficulties arising in confined geometries, a hybrid stochastic scheme was used. The method combined the strategy of pairing unrestricted single-ring conformations and the method of generating compact structures of individual rings described in section 6.2. Specifically, polygon pairs are first generated using importance sampling techniques according to the biasing weight $w = \exp(-d^2/d_0^2)$, where d is the distance of the rings centers of mass and d_0 is a preassigned mean target distance. Next, from the set of sampled polygon pairs, only the ones that fit into a D -slab or (D_1, D_2) -prism were retained (rejection technique).

The global qualitative features observed in [209] for the linking probability bear strong analogies to those observed for the knotting probability of a single ring subject to spatial confinement. In particular, the linking probability of polygon pairs confined in a D -slab or (D_1, D_2) -prism does not have a monotonic dependence on D . In fact, there is a maximum value for a specific value of D which depends on the polygon length, N , but is independent of the scaling variable $D/(bN^\nu)$. This indicates that the knotting and linking probabilities (respectively for a single ring and a pair of them) are influenced in analogous ways by the introduction of geometrical constraints such as slabs or prisms.

One of the latest investigations of this subject were carried out by Soteros *et al.* [211] who studied, by rigorous arguments, the linking probability of pairs of mutually-avoiding polygons confined within a tube and having the same calliper size along the tube direction (tube spanning constraint).

The additional spanning constraint causes each bond of one polygon to be within a preassigned distance (related to the tube diameter) of bonds belonging the other polygon. This is a more stringent distance constraint than the one described before, which pertained to the centres of mass of the two rings. In this confining geometry rigorous results can be obtained for the linking probability of polygon pairs in a (D_1, D_2) -prism. In particular it is obtained that the *homological* linking probability goes to one at a rate at least of order $(1/\sqrt{N})$ (analogously to what was discussed before for the URP model) while the *topological* linking probability goes to one exponentially rapidly [211]. Furthermore the linking number grows (with probability one) faster than any function $f \propto o(\sqrt{N})$ but it cannot grow faster than linearly in N because of the prism constraint. It is interesting to notice that no linear upper bound exists without the prism constraint since the number of crossings can grow as fast as $O(N^{4/3})$ for a knot [225] or link [226] with length N .

14.3. Mutual entanglements for polymers in concentrated solution

All the results presented in the previous sections pertain to two isolated rings brought in spatial proximity. These systems, while interesting *per se* can be viewed as a first approximation to more realistic systems where several rings can mutually entangle. In practical contexts, these

topological entanglements can occur when, for example, linear polymers in a concentrated solution undergo a closure reaction thus turning the geometrical entanglement of the open chains into linked states of high topological complexity. The problem of mutual entanglement is manifestly important in the equilibrium and dynamical properties of concentrated solutions of polymers [50, 227, 228, 196].

However, a topological characterization of this entanglement in equilibrium conditions is still largely unexplored and most of the available results have been established either numerically [229, 230]) or, in the case of melts, in the context of the tube model [50, 227]. This model postulates that the mutual avoidance of the chains in a melt generates spatial constraints which effectively force each chain to reptate through a meandering tubelike region [50, 228]. One of the main reasons for the widespread use of these concepts is that the geometrical constraint given by the tubular neighborhood is much easier to handle, and more amenable to calculations and simulations, than the topological constraints [184]. A notable example is provided by the primitive-path method introduced a few years ago to analyze numerical simulations of dense polymer melts [231]. The method allows to characterize the viscoelastic behaviour of the melts in terms of properties of the network of the coarse-grained paths traced by polymers chains.

An attempt to probe directly the topological complexity of concentrated polymer solutions and melts was carried out in refs. [207, 232] The method consisted of considering a specific configuration of the concentrated solution and to randomly “drilling out” from it a prism (tube). Next, the chain portions trapped in the prism are analysed. Most of these trapped chains have their ends at the prism boundaries. These sub-chains can be both self-entangled and mutually entangled and this entanglement can be properly defined in terms of knotting and linking by bridging the two ends of each chain outside the prism (see Figure 40 panels (a) and (b)). Sometimes it is necessary to introduce extraneous crossings outside the prism but this number can be easily controlled (see below).

By repeatedly applying this procedure it is possible, for example, to compute the probability that a certain type of chain linking is found in randomly-drilled prism etc. It is interesting to notice that, within this approach, the complicated problem of characterizing the equilibrium topological properties of concentrated solutions of polymer chains can be, to some extent, reduced (or at least compared to) to the simpler problem of the linking probability of k -components rings in (D_1, D_2) -prism.

The above approach was further simplified in ref. [207, 232] where the extracted prisms were subdivided into smaller pieces, such as cubes. In this case, each cube and the k sub-chains within it form an entangled structure of k strings where knotted and linked state can be rigorously defined (see Figure 40). The topological properties of the entire prism can be inferred by properly identifying the boundary faces of the elementary cubes. A possible way of describing this system, that is also amenable of numerical and possibly analytical calculations, is in terms of a set of k self- and mutually-avoiding walks on a cubic lattice suitably embedded in a cube of linear size D . This model has been explored in details by Monte Carlo simulations and scaling arguments in [207, 232]. In these studies it was calculated the linking number between two chains embedded in a cube and with their ends joined by arcs external to the cube. As mentioned above it is possible that an additional, extraneous, crossing is introduced during the closure outside the box. If this is the case the sign of this extra crossing is chosen at random with probability 1/2.

This measure was later extended to k chains by computing the $\binom{k}{2}$ linking numbers between pairs of chains. The absolute values of these $\binom{k}{2}$ linking numbers were finally summed algebraically so to obtained a single-valued measure, L , of the degree of entanglement of a given

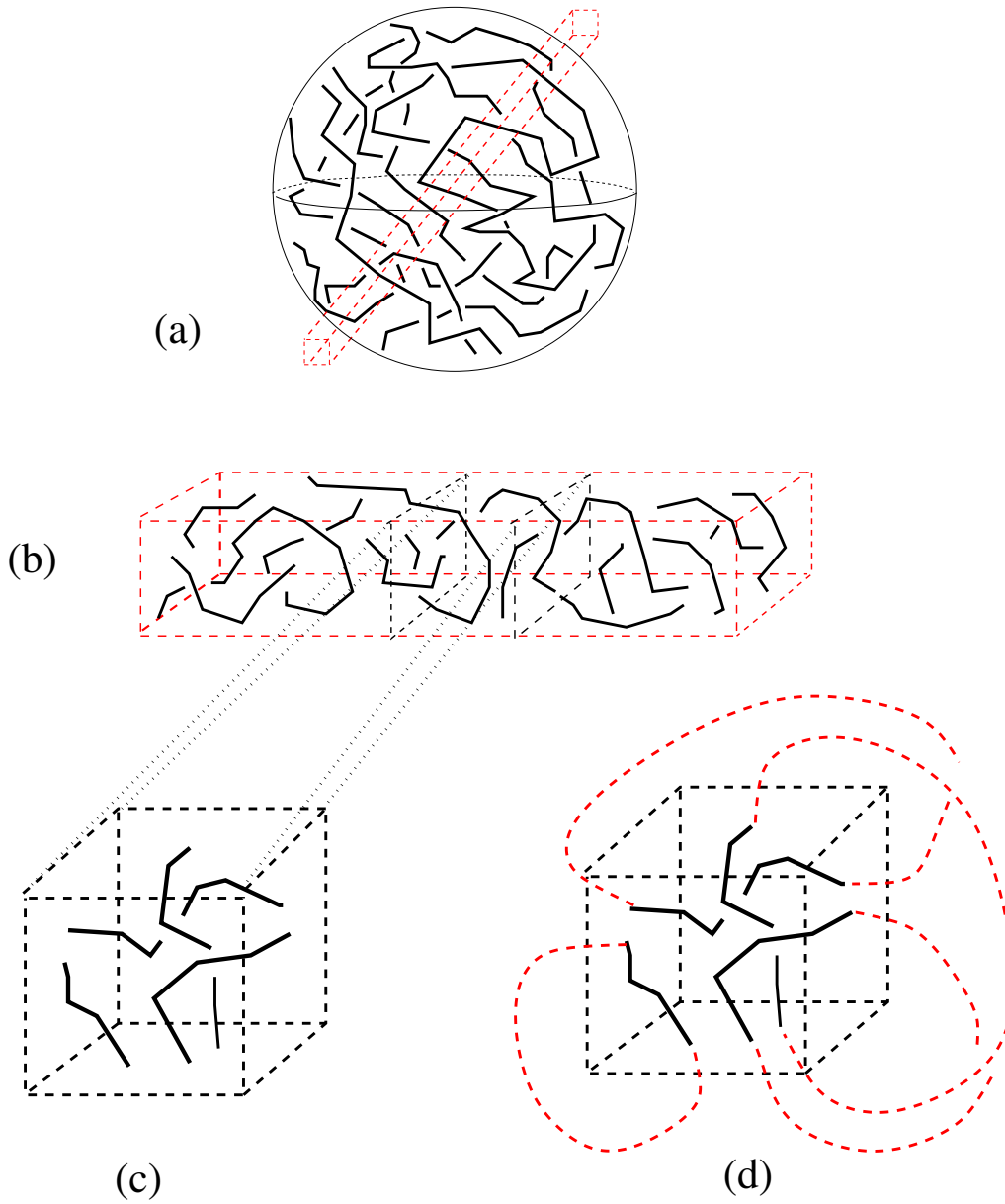


Figure 40: (a) A carrot is extracted from a concentrated solution of polymers. (b) The carrot is sectioned in smaller boxes (c). The entanglement of the sub-chains within an elementary box is determined by computing the linking number between the rings obtained by closing outside the cube the sub-chains.

arrangement of k chains inside the D -cube. Note that for $k = 2$ the measure L reduces to the linking number between two rings.

The quantity L was then averaged over the sampled configurations to form the statistical average $\langle L \rangle$. It turns out that for each D and k there is an initial set of values of the monomer density ρ at which $\langle L \rangle / \binom{k}{2}$ is approximately zero, and then increases roughly linearly with ρ . As D increases, the linear part of the curve becomes steeper and sets in at smaller values of ρ . One expects that, in the regime where $\langle L \rangle / \binom{k}{2}$ is close to zero, the k chains will occupy essentially disjoint regions of space, while when $\langle L \rangle / \binom{k}{2}$ is linear in ρ the regions occupied by the chains will have substantial overlap. This corresponds roughly to the distinction between the dilute and semi-dilute regimes in polymer solutions [50, 227]. In this situation, two length scales are competing: one is the box dimension D while the second is the average extension R of the single polymer chain in free space, $R \sim bN^\nu$, where N is the number of polymer monomers. Linking is expected to occur rarely when $R \ll D$, and to be frequent when $R \sim D$. Since $N = \rho D^3/k$, at fixed D the density ρ^* at which linking is expectedly important is given by

$$D \sim bN^\nu \sim b(\rho^* D^3/k)^\nu \quad (72)$$

so that

$$\rho^* \sim b^{-1} D^{(1-3\nu)/\nu} k. \quad (73)$$

Note that ρ^* is the critical value of the density above which the system is in the semidiluted regime [50, 227]. It is natural to formulate the hypothesis that the mutual entanglement $\langle L \rangle / \binom{k}{2}$ is a function of the ratio of the two competing length scales, D and R :

$$\langle L \rangle / \binom{k}{2} = f\left(\frac{D}{bN^\nu}\right). \quad (74)$$

Using the fact that $N = \rho D^3/k$ one has $\frac{D}{bN^\nu} \sim \left[\rho b^{1/\nu} D^{(3\nu-1)/\nu}/k\right]^{-\nu}$ the dependence of L on D can be recasted in terms of a new function, g :

$$\langle L \rangle / \binom{k}{2} = g\left(\rho b^{-1} D^{(3\nu-1)/\nu}/k\right) = g(\rho/\rho^*) \quad (75)$$

Using Flory's value $\nu = 3/5$ this implies

$$\langle L \rangle / \binom{k}{2} = g\left(\rho b^{-1} D^{4/3}/k\right) \quad (76)$$

The validity of the above scaling relationship is confirmed by the good collapse of the numerical data points obtained by plotting $\langle L \rangle / \binom{k}{2}$ as a function of $\rho D^{4/3}/k$. The collapse is particularly good for densities ρ up to about $4\rho^*$. At higher densities, the collapse deteriorates, probably due to the onset of the melt regime ($\rho > \rho^{**}$) [227] where the efficiency of the Monte Carlo algorithm starts to deteriorate. More sophisticated sampling techniques are then necessary to look at the scaling regime of $\langle L \rangle / \binom{k}{2}$ in the, still unexplored, region $\rho \gg \rho^*$.

A further possible extension of the above-mentioned problem is the study of the probability of occurrence of self-entanglement (i.e. knotting) and how this depends on melt concentration. In principle this could be done by joining the two ends of the same walk by an arc outside the cube, and calculating (for instance) the one-variable Alexander polynomial of the resulting simple closed curve.

15. Fourth part: properties of polymers with fixed topology

The fourth part of this review, which comprises sections 16 and 17 departs from the topics covered so far and which largely dealt with the characterization of the topological state of polymer chains that circularise in equilibrium. It is equally interesting, however, to characterize the physical properties of polymer chains whose topological state is fixed and cannot be altered during the equilibrium fluctuation dynamics of the chain (e.g. because the circularization occurs via a covalent bonding which is very resilient at room temperature). In this case, it is clearly not meaningful to investigate the knot spectrum. Instead it is interesting to examine how the topological constraint affects the accessible configurational space of the polymer and, in turn, how this affects the polymer dynamics and equilibrium metric properties. These issues are covered in this last part of the review. In particular, the following questions will be addressed:

- To what extent does the presence of topological constraints influence the equilibrium properties of a single ring or a melt of rings?
- Are the limiting configuration entropy and the average extension of rings with fixed topology different from the unconstrained counterparts?
- Is there any dependence on the type of topological constraint imposed on the system? In particular, do unknotted rings behave differently from rings with a nontrivial knot type?
- More generally, what are the salient configurational features of a spatially confined molecule with a given topology?

A good prototypical example of how the salient physical properties of a polymer ring can be influenced by fixing its topological state is provided by the gel electrophoresis [233] or stretching experiments [2] where a detectably different response is associated to various knot types.

The presence of a topological constraint can have an even deeper impact if the chain is geometrically confined into thin slabs, narrow channels or small containers. This is because, in addition to the relevant lengthscales of the problem, i.e. the contour length, persistence length and width of the confining region, fixing the topological state introduces a further lengthscale, namely the size of the knotted region. For a knotted ring or a linear polymer the competition between topology and confinement can dramatically affect the translocation ability [219, 234]. This has profound implications for the passage of a macromolecule through a narrow hole or channel, a phenomenon that is ubiquitous in biological systems.

Furthermore, for a *melt* of rings in confined geometries the topological constraints can strongly enhance the effective (entropic) repulsion between rings which can dramatically affect their spatial arrangement. Indeed, this mechanism is believed to be an important ingredient in the spatial organization and segregation of highly confined DNA molecules such as bacterial chromosomes [235] and eukaryotic chromosomes during interphase [236, 85] (see the discussion in Section 16.4).

The available results on the subject are accompanied by a general overview of the main theoretical and computational challenges that arise in systems of fixed topology. In brief, the challenges on the analytical side arise from the fact that the (global) topological constraints prevents exploitation of the mapping between the statistics of rings with unrestricted topology and critical magnetic systems. Field theory arguments cannot be applied any more[50].

By necessity, most of the theoretical approaches to the problem therefore start from the assumption that it is possible to transfer scaling arguments developed in the unconstrained case

to the fixed-topology one [237, 238, 239] and use numerical computation to support or verify *a posteriori* the validity of this hypothesis [240, 241, 242]. In turn, from the numerical perspective the difficulty stems from the fact that it is difficult to ensure *a priori*, that all the relevant configurational phase space is explored by stochastic modification of polymer rings which respects the given topological constraint.

A conceptually-important feature of the fixed-topology problem answers the question of how large a fraction of the ring is occupied, on average, by a given knot type [43].

More precisely the following questions can be addressed:

- For knotted rings at equilibrium is the knot segregated into a small region in which all the topological details are confined or is it loosely spread over the entire chain ?
- Does the average length of the knotted region depends on physical parameters such as the polymerization degree, the stiffness of the chain, the quality of the solvent etc etc ?
- For knotted rings confined within thin slabs, narrow channels or closed small containers, is the typical size of the knot altered by the degree of confinement ?

All previous issues implicitly build on the notion that it is possible to measure the size of the knotted region within a ring. Actually, this is a delicate conceptual point since the most natural way to perform this measure consists of extracting arcs from the full ring and looking for the presence of the knot within each of the excised arcs. This scheme makes manifest the ambiguity of the definition of the knot length because, as already mentioned, the notion of knottedness of an open arc cannot be generally established except for very special circumstances, such as when the termini are subjected to suitable constraints, on in case of strong adsorption [75, 180]. In other circumstances, there is no unique way to establish the knotted state of an open arc. As will be discussed in the review, this ambiguity can actually be exploited to define a probabilistic notion of knottedness of a given arc with a given (fixed) configuration, and valuable insight into the fixed-topology problem can be thus obtained. This is the subject of Section 17.

16. Equilibrium properties of topologically constrained polymers

In this section we shall report on the results available for topologically constrained rings. We shall first consider the case of isolated rings whose knotted state is fixed, and next move on to the case of several rings with a fixed type of mutual linking. These two situations are expected to arise from the polymer circularization in, respectively, dilute and dense polymer solutions.

16.1. Ring polymers in diluted solution: fixed knot type

We first consider the case the of isolated self-avoiding rings of fixed knot type.

16.1.1. Limiting entropy and entropic exponents of rings at fixed knot type

In principle, the equilibrium properties of a ring with a given knot type, τ , can be obtained by considering, in place of the full ensemble of configurations (microstates), only those with the correct knot type τ . The introduction of this restriction usually makes it impractical to characterize analytically the equilibrium properties. The difficulty arises because the “knottedness” is a global property of the chain and, for example, cannot be accounted for by adding to the energy function terms that favour/disfavour specific local geometries of the ring. For this reason there are very few theoretical results based on analytical and/or rigorous approaches.

From the FWD theorem (see Section 7) it is known that the limiting entropy of unknotted self-avoiding polygons, κ_0 , exists and satisfies the inequality

$$\kappa_0 < \kappa, \quad (77)$$

where κ is the limiting entropy of the whole set of rings (i.e. summed over all the topologies). The question that rises naturally from inequality (77) is the following: is it possible to prove rigorously the existence of the limiting entropy κ_τ for rings with a given knot type τ ? Moreover: is the strict inequality (77) still valid if one replaces κ_0 with κ_τ ? While a complete answer to the problem is still lacking, the following rigorous results have been established. Let $p_N(\tau)$ be the number of N -bonds polygons whose knot type is τ . Since all, but exponentially few polygons contain at least one copy of, say, a knot τ' different from τ , we have:

$$\limsup_{N \rightarrow \infty} \frac{1}{N} \log p_N(\tau) < \kappa. \quad (78)$$

In other words, self-avoiding polygons with a particular knot type τ are exponentially rare [243]. This number can be compared to the number of unknots by noticing that a subset of N -bond polygons with knot type τ can be obtained by concatenating M -edges polygons with knot type τ and $N - M$ edge unknotted polygons. This yields the following inequality [243],

$$p_N(\tau) \geq \frac{1}{2} p_M(\tau) p_{N-M}(\emptyset). \quad (79)$$

By recalling the FWD result about the existence of the limiting entropy of unknotted self-avoiding polygons, κ_0 , one has that, for fixed M and $N \rightarrow \infty$ the previous inequality can be recasted as

$$\liminf_{N \rightarrow \infty} \frac{1}{N} \log p_N(\tau) \geq \kappa_0. \quad (80)$$

The last inequality shows that, to exponential order, there are at least as many polygons with knot type τ as unknots. Notice that \liminf and \limsup are used because the limit $\lim_{N \rightarrow \infty} N^{-1} \log p_N(\tau)$ is not guaranteed to exist.

It would be interesting to establish whether eq. (80) holds as an equality. At present, the only available rigorous result, based on the existence of the limiting entropy κ for the space of *all* unrooted polygons, is that

$$p_N \sim A e^{\kappa N + o(N)}. \quad (81)$$

where p_N is the number of all such polygons.

On the other hand, field-theory arguments, based on the mapping between the statistics of self-avoiding rings and the $O(n)$ model for $n \rightarrow 0$ [50] give a more detailed asymptotic behaviour for p_N ,

$$p_N = AN^{\alpha-3} e^{\kappa N} \left(1 + \frac{B}{N^\Delta} + CN^{-1} + o(N^{-1}) \right) \quad (82)$$

where α and Δ are respectively the *entropic* and the *correction to scaling* exponents. They are known to be universal quantities, in that they depend only on fundamental properties of the system (such as the space dimensionality, d) and not on model details. For unknotted self-avoiding polygons we know rigorously the existence of κ_0 but there is no field theory result available in this case since, for the statistics of self-avoiding unknotted rings, no mapping to the a $O(n)$ -like model has been devised.

Nevertheless, it appears reasonable to conjecture that:

$$p_N(\emptyset) = A(\emptyset)N^{\alpha(\emptyset)-3}e^{\kappa_0 N} \left(1 + \frac{B(\emptyset)}{N^{\Delta(\emptyset)}} + C(\emptyset)N^{-1} + o(N^{-1}) \right). \quad (83)$$

For self-avoiding polygons with a given knot type τ no rigorous proof of the existence of the limiting entropy κ_τ exists, though it appears plausible that it obeys a scaling form analogous to the above one,

$$p_N(\tau) = A(\tau)N^{\alpha(\tau)-3}e^{\kappa_\tau N} \left(1 + \frac{B(\tau)}{N^{\Delta(\tau)}} + C(\tau)N^{-1} + o(N^{-1}) \right). \quad (84)$$

Assuming the validity of eq. (84) then eq. (78) implies that $\kappa_\tau < \kappa$ for every knot type τ .

The validity of the above assumptions can be tested using numerical simulations. Two different schemes (each with different advantages and drawbacks) can be used to sample polygons (or in general rings) with fixed knot type.

One possibility is to sample extensively the space of all polygons (for example by using two-point pivot moves that change the knot type). *A posteriori*, considerations can then be restricted to only those conformations that have the desired knot type (identified, for example, through the computation of knot polynomials). The advantage of this approach is that algorithms based on pivot moves are ergodic in the whole class of polygons and are also quite efficient. Aside from considerations about the use of imperfect topological indicators, a major drawback of this scheme is that, according to (78), the number of polygons with a fixed knot type τ is, in the limit $N \rightarrow \infty$, exponentially rare with respect to whole class so an exponentially-diverging (in polygon length) simulation time is need to collect a reliable statistics for a given τ . On the other hand, for fixed (but large enough) N , a reasonable amount of knots can be sampled obtaining a good statistics for at least the simplest knot types. Notice that for polygons on the cubic lattice the population of trefoil knots is non-negligible for $N \sim 10^5$ whereas for off-lattice equilateral rings, the maximum incidence of trefoils (corresponding to a probability of about 25 %) is observed for $N \approx 300$.

The second approach consists of sampling configurations always remaining in the region of phase space associated with the given knot type, τ . The spirit of these (generalizable [244]) approaches is aptly illustrated in lattice contexts. Polygons at fixed knot type on the cubic lattice can be sampled using the BFACF algorithm [108, 109, 110] described in Section 6.3.

The BFACF algorithm is, indeed, a viable tool for sampling polygons with a fixed knot type though it can lead to long correlation times. The severity of the latter problem can be largely reduced using the Multiple Markov chain method (see Section 6) where various copies of the system are run at different values of the bond fugacity [147]. In [240, 241], by using the BFACF algorithm, the scaling hypothesis (84) has been tested for different knot types. Within numerical uncertainty, it was found that

$$\kappa_\tau = \kappa_0 \quad \text{and} \quad (85)$$

$$\alpha(\emptyset) = \alpha. \quad (86)$$

Moreover

$$\alpha(\tau) = \alpha(\emptyset) + N_f \quad (87)$$

where N_f is the number of prime factors in the knot decomposition of τ . Equation (87) implies that $\alpha(\tau)$ is independent of τ if τ is a prime knot. Similar results have been later found for off-lattice models of knotted rings as Gaussian random polygons and rod-bead rings [121]. In this

study the sampling of rings with fixed knot type was based on the first approach described above, i.e. a stochastic generation of rings with free topology and subsequent selection of configurations of a given knot type detected by topological invariants such as the Alexander and the Vassiliev polynomials.

The results of eq. (87) can be understood if one assumes that knots are tied relatively tightly in the polygon. To turn this observation into a more quantitative statement let us consider a simple closed curve, ω , in three-dimensional space, having the topology of prime knot, τ . Consider a geometric sphere, S , intersecting ω in exactly two points, dividing ω into two 1-balls, ω_1 and ω_2 . Suppose that ω_1 meets S at its two boundary points but is otherwise inside S and that ω_2 meets S at its boundary points but is otherwise outside S , see Figure 41. Next, convert ω_1 into a simple closed curve ω'_1 by adding a curve on the sphere S so to join the end points of ω_1 . The same construction converts ω_2 to a simple closed curve ω'_2 .

If ω'_1 has knot type τ and ω'_2 is unknotted then we can say that the knot is *localized* inside S . Let the total length of the knotted segment ω_1 be m_τ , and assume that ω has a total contour length equal to N , as sketched in Figure 41. Define M_τ to be the infimum of m_τ over all possible intersections with geometric spheres which cut ω in exactly two points. Define N_τ to be the expected value of M_τ taken uniformly over all polygons of knot type τ . If $N_\tau = o(N)$, i.e. $\lim_{N \rightarrow \infty} N_\tau/N = 0$, then in the large N limit, the ‘‘average’’ knotted polygon looks like an unknotted polygon with a small sphere containing a knotted arc (of known knot type!) attached to it. In this case the knot τ is said to be *tight* (or *localized* or *segregated*). An extreme case would be when N_τ is a constant independent on N . If the knot is tight we expect that the number of inequivalent places where it can be accommodated along the ring grows proportionally to the ring length itself. In other words there exists a positive number $\epsilon < 1$, such that there are of order ϵN positions in the ring where the knot can be created by concatenating a small polygon of knot type τ and N_τ edges and an unknotted polygon with N edges. This gives

$$p_{N_\tau+N}(\tau) \sim \epsilon N p_N(\emptyset) \quad (88)$$

and from the scaling form (84) we have

$$\alpha(\tau) = \alpha(\emptyset) + 1, \quad (89)$$

if τ is a prime knot. Note that we have implicitly assumed $\kappa_\tau = \kappa_0$ but, rigorously, we only know that $\kappa_\tau \geq \kappa_0$ ⁶. This argument can be similarly generalized to cases where τ is a knot with N_f prime factors. It is indeed sufficient to choose N_f out of ϵN locations in about $(\epsilon N)^{N_f}$ ways and the rest of the argument is the same giving the result in (87).

Because in the large N limit the statistics of topologically unconstrained polygons is dominated by composite knots then, if eq. (87) holds one would be expect to see a significant difference between the values α and $\alpha(\emptyset)$. This is, however, not the case; indeed there is strong numerical evidence supporting the validity of relation (86).

A full comprehension of this result is presently lacking, although some notable progress in this direction was made in the context of subclasses of lattice animals partitioned with respect to their cyclomatic index (i.e. the number of independent cycles), which, although having different entropic exponents altogether make up the class of animals with entropic exponents equal to those of lattice trees [245].

⁶A. Y. Grosberg has given a qualitative argument for which the equality $\kappa_0 = \kappa_\tau$ holds: see A.Y. Grosberg, in *Ideal Knots*, Series of Knots and Everything, vol. 19, World Scientific 1998

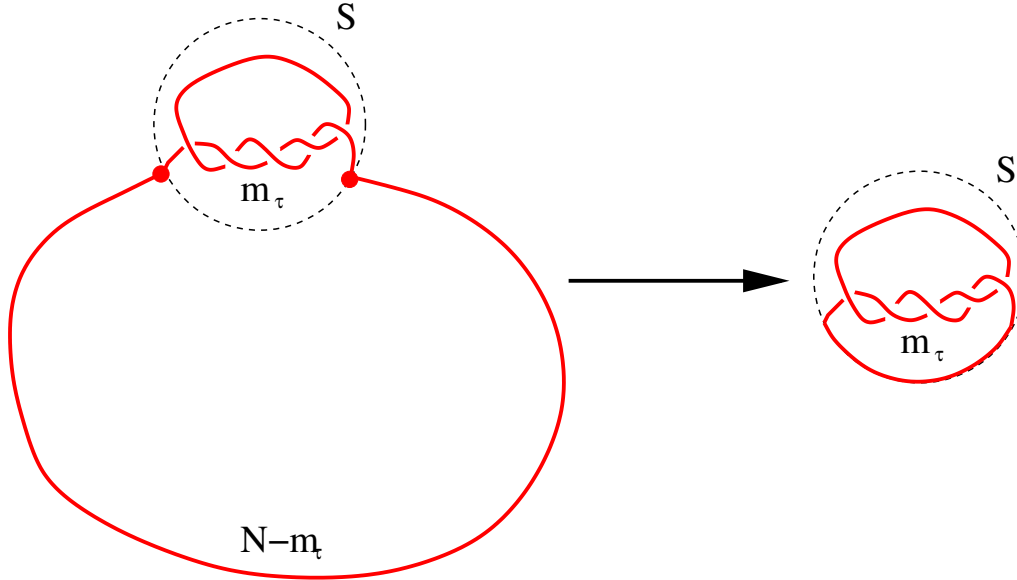


Figure 41: The sphere S separates the knotted region into two arcs, one of which will be knotted with knot type τ (5_1 in the figure) if it is closed by an arc on the sphere.

16.1.2. Metric properties of rings at fixed knot type.

The above argument on the localization, or segregation, of the knotted portion of the chain not only provides a basis to rationalise eq. (87) but has also important implications on the metric properties of self-avoiding polygons of fixed knot type, in particular regarding the mean square radius of gyration, $\langle R_N^2 \rangle$ (see eq. 2). For the whole (i.e. topologically-unconstrained) class of self-avoiding rings, field theory arguments suggest the asymptotic form

$$\langle R_N^2 \rangle = A_\nu N^{2\nu} \left(1 + B_\nu N^{-\Delta} + C_\nu N^{-1} + o(N^{-1}) \right), \quad (90)$$

where the subscript ν is used to distinguish the A , B and C coefficients of eq. (90) from those in eq. (82). Available theoretical estimates [246] for the exponents ν and Δ yield:

$$\begin{aligned} \nu &= 0.5882 \pm 0.0010 \\ \Delta &= 0.478 \pm 0.010 \end{aligned} \quad (91)$$

whereas the best available numerical estimates for the self-avoiding walk are as follows

$$\begin{aligned} \nu &= 0.587597 \pm 0.000007 \quad [49] \\ \Delta &= 0.56 \pm 0.03 \quad [247]. \end{aligned} \quad (92)$$

As for the case of $p_N(\tau)$, no field theory argument is available for the scaling behaviour of the mean squared radius of gyration $\langle R_N^2(\tau) \rangle$ for self-avoiding rings at given knot type τ . However, analogously to eq. (84) it is plausible to expect that

$$\langle R_N^2(\tau) \rangle = A_\nu(\tau) N^{2\nu(\tau)} \left[1 + B_\nu(\tau) N^{-\Delta(\tau)} + C_\nu(\tau) N^{-1} + o(N^{-1}) \right]. \quad (93)$$

The validity of the above scaling hypothesis can be ultimately checked using numerical simulations. Specific aspects of the above relationship can, however, be checked for consistency against the localization assumption discussed before.

In particular, if knots were subject to the discussed localization, then, in the large N limit, a polygon with knot type τ consisting of N_f prime knot components should be statistically similar to an unknotted ring with N_f roots (i.e. distinguishable vertices). On the other hand, since rooted polygons have a different entropy with respect to un-rooted ones and yet have the same average extension, we should expect $\nu(\tau) = \nu(\emptyset)$ and $A_\nu(\tau) = A_\nu(\emptyset)$ for all τ . Note that neither the metric exponent ν (universal quantity) nor the amplitude $A_\nu(\tau)$ should depend on the knot type. It is however possible that the topological constraint affects the higher order correction to the scaling relation of eq. (93) but, in order to get a more definite answer on this question a direct measure of the size of the knot within the ring is needed. The numerical investigations performed up to now by different groups and on different models of self-avoiding rings have shown a good agreement on the independence of ν on the knot type τ [248, 249, 241, 250, 251, 252]. For the amplitude the numerical evidence $A_\nu(\tau) = A_\nu(\emptyset)$ is less sharp [249] but results obtained with more asymptotic values of N seems to confirm that the amplitude A_ν is constant over τ .

Compared to available theoretical results, there are very few experiments that, up to now, have explored the influence of the topological constraints on the equilibrium properties of isolated rings. The main reason resides in the extreme difficulty in synthesizing highly purified unknotted and unconcatenated rings [253]. In the few cases when these conditions could be met it was indeed found by viscosity measurements [254], that the average size of isolated unknotted rings is the same as for (isolated) linear chains. While the topological constraint of being unknotted does not seem to change the average extension of these rings there are indications that it entails a decrease of the θ temperature, which is the temperature at which the second virial coefficient becomes zero signalling the occurrence of a coil-collapse transition [50, 79]. The decrease of θ was found by measuring the rheological properties of unknotted ring polystyrenes in cyclohexane [255, 256] and was later confirmed by light scattering measurements of the second virial coefficient of highly-purified ring polystyrenes in cyclohexane [257].

The fact that the unknottedness constraint affects the θ temperature, where the equilibrium statistics of the rings is compatible with that of ideal chains, suggests that the effective topologically-dependent interactions are very weak compared to excluded volume interactions and that they may manifest themselves when the latter can be neglected.

At the θ point, in fact, the metric exponent ν for all rings is $1/2$ since the ensemble essentially corresponds to random walks conditioned to return to the origin.

For infinitely-thin rings with trivial topology it was conjectured that the average size scales as $N^{\nu(\emptyset)}$ with $\nu(\emptyset) = \nu_{SAW} \approx 0.588 \approx 3/5$. This conjecture builds on the seminal work of des Cloizeaux who studied the conformational properties of linked rings and concluded that topological constraints on a long flexible ring have a similar effects as excluded volume interactions [258]. On the basis of this observation, for rings with no excluded volume interactions, the exclusion of all non-trivial knots from the statistics is expected to be equivalent to the introduction of an effective *topological repulsion* that swells the infinitely-thin unknotted rings up to an average size that scales as the one of self-avoiding rings (although corrections to the asymptotic scaling point at a different universality class for self-avoiding rings and infinitely-thin unknotted ones[259]).

This conjecture was later supported by scaling arguments [239] leading to a more specific

prediction for infinitely-thin unknotted rings:

$$\langle R_N^2(\emptyset) \rangle = \begin{cases} (b^2/12)N & \text{if } N \ll N_0 \\ A(b^2/12)N^{2\nu_{SAW}} & \text{if } N \gg N_0 \end{cases} \quad (94)$$

where $N_0 = 1/\alpha$ is the characteristic length of the unknot, i.e. it appears in the exponential decay of the unknotting probability, $\exp(-N/N_0 + o(N))$. Expression (94) suggests a crossover from a small N regime, where the knotted infinitely-thin ring is characterised by the random walk exponent $\nu = 1/2$, to a large N regime in which the average size scales as the one of self-avoiding walks. Evidence in favour of the scaling relation of eq. (94) was subsequently provided by extensive simulations [260, 261, 242].

Notably, these studies suggest that the above mentioned-relationship also holds for any set of infinitely-thin rings with fixed knot type. At present, no exact result is available to confirm the asymptotic validity of the numerical findings. A number of arguments have however been suggested, ranging from the relative strength of topological and excluded volume interactions [262, 263, 260] to considerations made on the fraction (and size) of rings that, compared to the average case, are under- or over-knotted [242]. Interestingly, the latter argument predicts that the ν exponent for sufficiently long rings of a given knot type would be directly inherited from the asymptotic one of the unknotted rings, $\nu(\emptyset)$.

16.2. Knotted rings in proximity of an impenetrable surface

As previously discussed, the configurational entropy of a spatially-confined chain is clearly smaller than when it is unconstrained in the bulk. A ubiquitous type of polymer confinement is obtained in proximity of a surface. As the chain approaches the surface, the chain configurational entropy decreases producing a soft entropic force pushing the polymer away from the surface [264].

The case when the ring approaching the surface is knotted, and cannot change the knot type, is a notable example of the interplay that can arise between geometrical and topological constraints. In particular, one may ask what free energy loss, or equivalently entropic repulsive force, is experienced by surface-adsorbed polymers with different topologies. Is this force large enough to be detectable in single-molecule experiments (which would hence provide a new means of detecting the ring topologies)?

To quantify the impact that topology can have on the free energy cost of placing a polymer close to a wall, consider the particularly simple case of a freely-jointed chain, made up of N statistically-independent links, each of length b , and rooted at a point at a distance x_0 from an impenetrable wall, which for definiteness we may take parallel to the yz plane and placed at $x = 0$. It is a simple polymer physics exercise to find the partition functions of a linear open and a ring polymer rooted, e.g. via the so-called image method [227, 265], in the continuum limit (valid for $N \gg 1$). These are respectively given by

$$Z_{\text{open}}(N, x_0) \propto \text{erf}\left(\frac{\sqrt{3}x_0}{b\sqrt{2N}}\right) \quad (95)$$

$$Z_{\text{loop}}(N, x_0) \propto \left[1 - \exp\left(-\frac{6x_0^2}{Nb^2}\right)\right] \quad (96)$$

where erf denotes the error function, and we have omitted a constant which does not depend on x_0 .

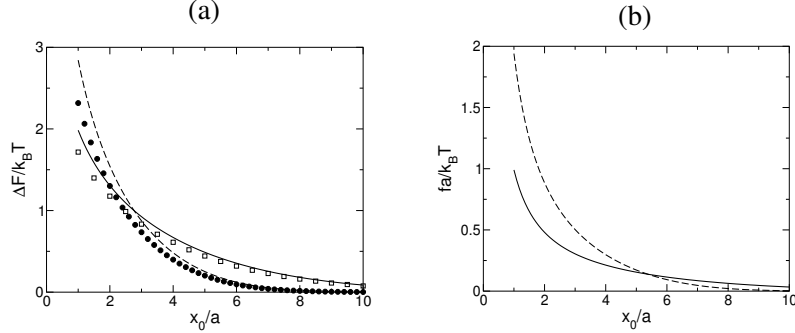


Figure 42: Plot of (a) the free energy which is lost, and (b) the force required to keep the polymer in place, when a linear (solid lines) and a looped (long dashed lines) freely-jointed chain with $N = 100$ are placed at a distance x_0 (in units of the Kuhn length) from a solid wall, according to Eqs. 97,98. In (a) we also show the numerical estimate for the free energy loss for a linear (open squares) and a looped (filled circles) chain with same contour length. The difference between these and the analytical calculations is due to finite size effects.

From the partition function one can then find both the free energy loss due to the decrease in configurational entropy, and the repulsive entropic forces (this is the derivative of the free energy with respect to distance from the wall). After some algebra it is possible to show that the repulsive force, for open and looped configurations, is respectively given by (note that we keep the dependence on N and x_0)

$$f_{\text{open}}(N, x_0) = k_B T \frac{\partial \ln Z_{\text{open}}(N, x_0)}{\partial x_0} = \frac{2\sqrt{3}k_B T \exp\left(-\frac{3x_0^2}{2Nb^2}\right)}{\sqrt{2\pi}Nb \operatorname{erf}\left(\frac{\sqrt{3}x_0}{\sqrt{2}Nb}\right)} \quad (97)$$

$$f_{\text{looped}}(N, x_0) = k_B T \frac{\partial \ln Z_{\text{looped}}(N, x_0)}{\partial x_0} = \frac{12x_0 k_B T \exp\left(-\frac{6x_0^2}{Nb^2}\right)}{Nb^2 \left(1 - \exp\left(-\frac{6x_0^2}{Nb^2}\right)\right)} \quad (98)$$

These forces are plotted in Figure 42. It can be seen that the repulsive force builds up first for the open chain, whose statistical size is larger. However, upon close approach it is the ring which feels a stronger repulsive force. This different trend may be understood by comparing the change in the entropic exponent, γ , for a ring and an open chain when they are tied to a wall [264]. It is actually possible to show that, at least in the thermodynamic limit, the more complex the topological constraints are, the steeper the entropic repulsive force will rise for $x_0 \rightarrow 0$. Thus, for a network of freely-jointed chains locally made of n_L rings and n_M linear branches tied together at a common root held at distance x_0 from the surface, we find, for $x_0 \rightarrow 0$, $f(N, x_0) \sim \phi k_B T / x_0$, with $\phi = 2n_L + n_M$ through an analysis similar to the one above.

Therefore entropic forces for different network topologies are different. What about the case of a fixed knot type approaching a solid wall? In order to answer this question, it is necessary to compute the free energy loss, or equivalently the partition function, of a ring with fixed knot type as a function of x_0 (and N). This may sound like a difficult task, but in this case it can be realised via a small change in a standard knot generation algorithm. In particular, in Ref. [264] we have generated several fluctuating freely-jointed rings with Monte-Carlo simulations, and we have computed how the probability of having the topology of an unknot, or a simple prime knot

changes with the distance to the wall, x_0 . The free energy of a polymer chain with knot type τ as a function of x_0 is then equal, up to an additive constant, to minus the logarithm of the probability of forming knot type τ if the root is a distance x_0 from the solid wall. The constant can be adjusted so that the free energy loss is 0 as $x_0 \rightarrow \infty$. It is then straightforward to compute the entropic forces and in particular the difference between forces felt by different knot types. In order to reduce the statistical errors in the force curve and enhance the signal to noise ratio it is useful to employ additional tricks, which are however not important conceptually – the reader interested in or needing these may consult Ref. [264] for more technical details.

Figure 43 shows an example of the results which can be obtained. This figure shows how the unknotting and trefoil formation probability change with respect to their bulk value (panels a and b respectively), and also shows the difference in the free energy (panels c and d) and in the force (panels e and f) “approach curves” for two polymers of different given knot types. From the figure it is apparent that all the computed probabilities are non-monotonic with respect to x_0 . The unknot probability (panel a) decreases for intermediate x_0 and then increases for very small x_0 , to slightly higher values compared to the bulk one. The deviation from the bulk value increases with the size of the ring. For small chains ($N = 50$ and $N = 100$), the qualitative behaviour of the trefoil (panel b) and the 4_1 knot is the same, and is opposite to that of the unknot – these probabilities display a *maximum* for intermediate x_0 (or even oscillations for larger N). From the knotting probabilities one can extract the difference in free energy losses for different knot types. It can be seen that these have a maximum value of $0.1 K_B T$, and decreases with N , so that they would vanish in the thermodynamic limit. However real polymers are often less than 100 Kuhn lengths long and for those the difference in free energy losses might be picked up by single molecule experiments.

There are several open problems having to do with knots in restricted geometries which could be studied within a similar framework. For instance, it would be interesting to analyze the free energy profile as a function of position in suitably-patterned microchannels and microdevices. For instance, in a sinusoidal or ratchet-shaped channel the free energies of different knot types will be different from each other and depend on height. Is it possible to sort knots in this way? Eventually, it would be also interesting to study the dynamical properties of knots in these geometries, for instance when they are subjected to a uniform stretching flow. Clearly in these cases the Monte-Carlo algorithm may only be used to generate initial conditions, which then need to be evolved via a dynamic algorithm (e.g. Brownian dynamics or Lattice Boltzmann according to whether hydrodynamic interactions can be neglected as a first approximation or need to be included). While it may be that these more complicated microfluidic geometries will actually be more readily studied or more interesting for experiments, understanding the case of an impenetrable surface, as discussed above, is a necessary first step.

16.3. Topological and volume exclusion interaction between pairs of rings

We now turn to the case of a semidilute solution of rings. It is interesting to characterize the behaviour of two or more nearby rings with fixed topology, that is of given knotted and linked state.

Let us first consider a system consisting of only two unlinked rings which fluctuate in equilibrium subject to the constraint that the distance of their centers of mass, r is held fixed (see section 14.1).

When the distance r is larger than the average size of each ring the two rings are statistically independent. Upon decreasing r , the two rings start to feel each other and mutual self-avoidance interactions become important. In addition the constraint of keeping the two rings unlinked

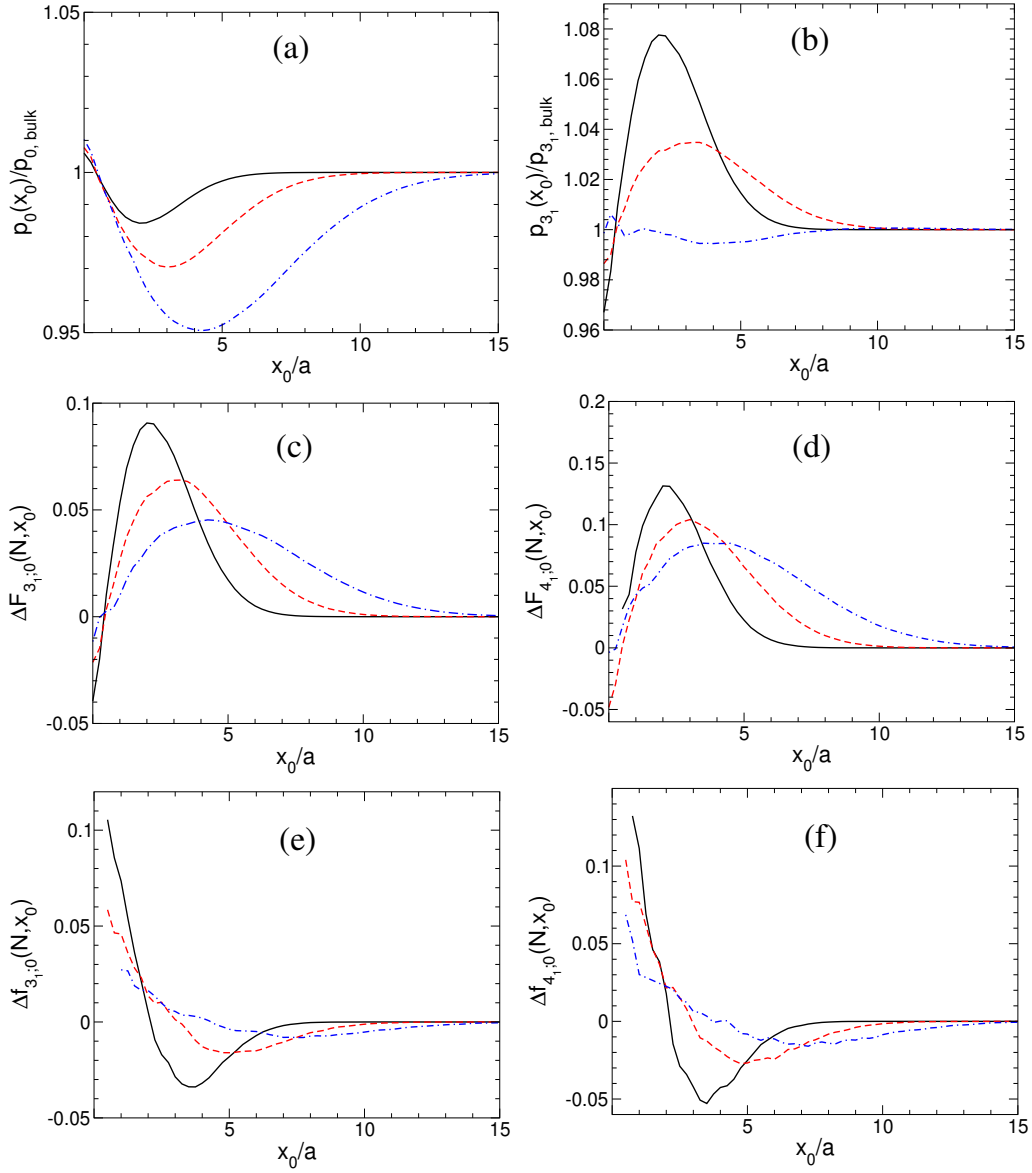


Figure 43: Panels (a) and (b): plots of the knotting probabilities (normalised to their bulk value) for polymers of given knot type approaching a wall ((a) refers to the unknot and (b) to the trefoil). Panels (c) and (d): plots of the differential free energy for a trefoil (c) and a 4_1 knot (d) approaching a wall. The free energy differences are computed with respect to the free energy spent for the case of the unknot. Panels (e) and (f): differences between the force felt by a trefoil and unknot when they are approaching the wall (e), and between a 4_1 knot and an unknot. Solid, dashed and dot-dashed lines respectively correspond to chains with $N = 50$, $N = 100$, and $N = 200$ Kuhn lengths. Figure reproduced from Ref. [264].

further decreases the number of configurations that would be accessible to each of the isolated rings. This *topological entropy* (or free energy) loss $\Delta F_{topo}(r) = F_{SAW}(r) - F_{unlink}(r)$ gives rise to an effective repulsive potential $U_{topo} = \exp(-\Delta F_{topo}(r)/k_B T)$ and, consequently, to a *topological second virial coefficient*, $B_{topo}^{(2)}$, which adds to the second virial coefficient arising from excluded volume:

$$B_{topo}^{(2)} = 2\pi \int_{\mathbb{R}} r^2 [1 - \exp(-\Delta F_{topo}(r)/k_B T)] dr. \quad (99)$$

The quantity $B_{topo}^{(2)}$ can be estimated by considering the linking probability between two rings [266, 267, 268]. Starting from the fact that the linking probability between two rings whose centers of mass are held at a distance r , $P_{link}(r)$ follows the Mayer relation, $P_{link}(r) = 1 - \exp(-\Delta F_{topo}(r)/k_B T)$.

This scheme was first explored in ref. [204] where $P_{link}(r)$ was numerically investigated for random polygons on a centred cubic lattice (see Section 14.1.2). The numerical data suggested that $P_{link}(r)$ had the following functional dependence on r ,

$$P_{link}(r) = 1 - A_0 \exp(-\alpha_0 r^3) \quad (100)$$

from which the following topological second virial coefficient was obtained:

$$B_{topo}^{(2)} = \frac{2}{3} \pi \frac{A_0}{\alpha_0}. \quad (101)$$

Note that for random polygons the second virial coefficient due to excluded volume interactions is zero and only $B_{topo}^{(2)}$ is present. If, on the other hand, real polymer rings are considered (i.e. with excluded volume) the effect of $B_{topo}^{(2)}$ would be to shift the value of the temperature at which the total second virial coefficient $B_{SAW}^{(2)} + B_{topo}^{(2)}$ is zero [266, 267]. This value would correspond to the new θ point value for unlinked and unknotted rings [206] discussed at the end of Section 16.1.2.

A related problem was considered in ref. [269], which focused on two approaching *rooted* lattice rings. In this case, in place of the distance between the rings centres of mass, the distance between the two rooting points, r , was used. By comparing the free energy losses upon close approach of both linked and unlinked rings, it was possible to separate the topological and excluded-volume contributions to the repulsive entropic force between the rings. Interestingly, we found that the effect due to mutual avoidance dominates the topological contribution by about an order of magnitude.

The system considered has a loose analogy with a situation that may be realised experimentally, namely by allowing/disallowing topoisomerase enzymes, such as topo-II, to act *in vitro* on circularized DNA molecules. In the presence of ATP, the topo-II strand-passage action can link/unlink and knot/unlink the DNA rings [9].⁷ When topo-II does not act, then the linking state of the circular DNA molecules cannot change. Based on the previous theoretical consideration (but bearing in mind that they pertain to an equilibrium situation, which is unlike the steady state action of topo-II) it could be anticipated that the free energy/forces recorded when the two loops are placed close together should not differ much whether or not topo-II or other similar enzymes are included in the experiments.

⁷The topo-II action therefore produces a steady-state probabilities for linking and knotting circular DNA molecules that are significantly lower than those measured when DNA circularization occurs in equilibrium.

Interestingly, the rooted polymer simulations (unlike the ones in which the centres of mass are controlled) can be used to test field-theoretical predictions on the entropic exponents of polymeric networks, which rely on renormalisation group estimates. Thus, observing that when the two roots approach each other the two rings locally look like a 4-leg branch point, one can use the formulas in Ref. [270, 271] to predict the following scaling for the free energy loss ΔF in the limit $x \rightarrow 0$:

$$\Delta F \propto -\frac{2\gamma_2 - \gamma_4 - 1}{\nu} \log(x) \quad (102)$$

where $\gamma_2 = 1$ and $\gamma_4 = 1/2$ are the ϵ -expansion estimates of the entropic exponents for 2- and 4-leg branch points (see Ref. [271] for details). Remarkably, simulations confirm the field theory scaling close to $x_0 \rightarrow 0$ to a very good approximation. This is particularly notable, as the theory does not fix either the knot type of each of the rings, or their linking number.

At the same time, the field theory predicts $\Delta F \propto \log N$, so it only costs a few $k_B T$ to position the two roots very close together, and there is only a very weak logarithmic dependence on polymer size. While this value is experimentally detectable, it does not ensure ring segregation in semidilute equilibrium solution (in other words thermal fluctuations lead to ring interpenetration, as they do for linear polymers [272]).

It is also interesting to consider the approach of ring pairs when they are in the globular phase [273, 269] and intrachain interactions dominate over interchain ones. In that case the range of the entropic/topological repulsion is smaller compared to the case of two polymers in the swollen phase, but the force is “harder” and increases much more steeply. This case may be more relevant for nearby interphase chromosomes segregating into territories during interphase (see below for more details on this application of linking and entanglement in semidilute suspensions) [274]. Finally, the case of several rings coming together, possibly by entropic forces [275, 276], to form a rosette is also considered – even in this more complicated case field-theoretical estimates work semiquantitatively.

16.4. Topological constraints in concentrated solutions.

We have seen that the topological entropic repulsion arising between two unlinked rings brought in spatial proximity, does not appreciably alter the salient equilibrium properties, such as the ν exponent, of the two-rings system. The situation may, however, dramatically change in concentrated solutions or melts of rings [228, 196].

The effects of topological constraints where many chains are close together is difficult to investigate analytically and, with the exception of few findings based on perturbation analysis on an effective field theory of unlinked rings [208], all the known results have been obtained by numerical investigations and scaling analysis [277, 237, 278, 251]. Within these approaches it was found that unknotted and unlinked rings in concentrated solutions are more compact than their linear counterparts. In particular the mean squared radius of gyration of a ring scales as N^ν with ν between 0.40 and 0.42 [277]. This value is significantly smaller than the Gaussian value $1/2$ expected in concentrated solutions and has a theoretical explanation based on the following Flory-like argument [237].

In Section 16.3 we discussed the entropy loss of two unlinked rings brought progressively close. This entropy costs would give rise to an effective topological repulsion that adds to the mutual excluded volume interaction. While in dilute solutions this repulsion is overwhelmed by self-avoidance, in concentrated solutions it becomes more important, presumably because the crowded environment limits severely the amplitude of the conformational fluctuations of the rings.

For an N -monomer ring of size R , the intensity of this effect should be a function of the average number of overlapping rings k that, in arbitrary dimension d , should scale as $R^d \frac{\rho}{N}$. The k neighbours act as obstacles for the given ring decreasing its conformational entropy. This gives a contribution to the free energy proportional to $k_B T R^d / N$. This term favours a compact spatial organization of the ring. On the other hand an entropic penalty has to be paid if the ring is confined within a spherical cavity of radius $R < bN^{1/2}$. This penalty was estimated in the context of the Flory theory for the coil-globule transition and scales as $k_B T \frac{Nb^2}{R^2}$. By minimizing the sum of these two terms with respect to R one obtains $R \sim N^\nu$ with $\nu = \frac{2}{d+2}$. Note that in $d = 3$ this gives $\nu = 2/5$, i.e. a value that closely agrees with the numerical estimates found in simulations [277, 278, 251] and with recent small-angle neutron scattering experiments carried out on cyclic polydimethylsiloxane (PDMS) [279]. Later numerical investigations with higher values of N and more detailed scaling arguments [280, 281] have revealed that actually the value $\nu = \frac{2}{d+2}$ describes the data in a crossover region of N values separating the short N regime, in which the topological interactions are weak and rings appear to be Gaussian (as their linear counterpart in concentrated solution), and the large N regime in which the rings assume a more globular structure with $\nu = 1/3$. Note that this large N regime can be described in terms of a ring squeezed within a network of topological obstacles created in a self-consistent way by the surrounding rings [282, 283].

16.4.1. Out-of-equilibrium and entropic effects in chromosome territories

A notable system where the above mentioned effects could be at play is given by chromosome territories.

Most of a cell's life is spent to perform a variety of functions, including preparation for cell division. This phase of the cell cycle is known as *interphase* – whereas division occurs during *mitosis* [219]. Interphase and mitosis are arguably the most important of the phases in the cell's cycle. Most of us associate chromosomes with elongated X-like structures: however these shapes are only observed during mitosis, when chromosomes condense and become more readily visible. On the other hand, during interphase, chromosomes are better described as swollen polymers with thickness of approximately 30 nm (the diameter of the chromatin fiber) and persistence length in the 40-200 nm range, confined in a quasi-spherical volume (the eukaryotic nucleus) [284, 285]. While theory predicts that linear polymers should strongly intermingle in confinement if in thermodynamic equilibrium (see e.g. the discussions in [284, 85, 286, 287, 288]) chromosomes instead segregate into spatially distinct regions, or *territories*.

A possible explanation to this effect is that the physics of interphase chromosomes is strongly dominated by out-of-equilibrium effects. This is at the basis of the proposal by Rosa and Everaers in [284], who suggest that the observed segregation is kinetically driven. The key idea behind the simulations in [284] is that chromosomes enter interphase (the “ordinary” cellular phase and hence the one with the longest time duration) after the mitotic chromosome separation. Therefore, the starting mitotic chromosome configurations are compact and well segregated. Consistently with this fact, Rosa and Everaers chose the initial configurations of the model chromosome as solenoidal structures in which loops are stacked up in a cylindrical state. By means of large scale parallel simulations, the authors managed to follow the dynamics of one or a few polymers as long as a human chromosome starting from a mitotic state. Periodic boundary conditions were introduced to model what happens in the nucleus where chromosomes are close to each other. Such long polymers were found to not be able to equilibrate and intermingle, so that they remain segregated as in the initial mitotic configuration, at least when interstrand crossing was

disallowed. Interestingly, yeast chromosomes are about two orders of magnitude shorter than human ones, thus equilibrate much faster – indeed neither molecular dynamics simulations nor experiments show territories in yeast chromosomes.

Chromosome territories, however, may also originate from *thermodynamic* forces. In this case, it is topological and entropic repulsion which can lead to segregation [289, 290, 285, 281, 291]. According to this explanation, there are scaffolding DNA binding proteins which act as ties [292] forcing a looped topology on chromatin in interphase chromosomes. Simple steric repulsion between rosettes on different chromosomes made up by joining several loops can then be estimated to lead effectively to segregation [290, 285, 269]. In particular, Ref. [289] also considered an ensemble of equilibrated unlinked freely-jointed loops and demonstrated that these too can segregate, which shows that segregation can be purely topologically driven. Lattice simulations of very long ring polymers also support this view [277, 281]. Of course, the kinetic and thermodynamic explanation are not necessarily mutually exclusive and in reality they could complement each other.

In any case, our understanding of the physical and topological properties of interphase chromosomes is still far from conclusive, and both theoretical and experimental breakthroughs are in order before a satisfactory picture can be reached. For instance, the role of the looping proteins, or “ties” mentioned above might lead to interchromosomal, as well as intrachromosomal, contacts. How is this avoided in practice? Apart from the segregation into territories, what is the local and global organization of one interphase chromosome? It is likely that in order to answer questions like these a serious revision of the force field used to characterise confined DNA will be needed. Once more, large scale simulations may safely be anticipated to be the primary method of investigation.

It is also interesting to compare the problem of chromosome segregation in eukaryotes to that in prokaryotes. In bacteria like *E. coli*, the genome is circular, and replication is concurrent with the segregation of the sister chromosomes [154]. Apart from the topology of the genome, looped versus linear, there is also a fundamental generic difference between chromosome segregation in bacteria and in eukaryotes: the geometry of confinement. While the nucleus is essentially spherical, bacterial cells which contain the DNA are typically elongated: for instance *E. coli* may be modelled as an ellipsoid with one major axis and two nearly degenerate minor ones. The ratio between major and minor axes varies between 2 and 4 in the wild-type (the variability is due to the fact that the cells grow while replicating). These two differences both help segregation and it has recently been proposed in [235, 154], on the basis of scaling arguments and numerical simulations, that entropic forces alone (i.e. self-avoidance) are enough to lead to chromosome segregation in a slowly dividing *E. coli*. This is mainly because an elongated geometry entropically favours configurations where the two sister chromosomes do not mix. Although the scenario may thus seem simpler in bacteria, the number of open questions is just as impressive as for the eukaryotic case [293]. For instance, in the lab *E. coli* cells usually divide much more rapidly than in a minimal medium, with the “firing” of multiple replication origins, which leads to the coexistence of more than two chromosomes in a cell. What happens in this case, which is topologically more complex than the one considered in Ref. [235]?

Furthermore, most experimental evidence points to the fact that the DNA in bacteria is strongly supercoiled, and it would be extremely interesting to understand how this impacts the structure of the bacterial DNA during replication. The development of ever more accurate bacterial cell biology experiments is also likely to shape our understanding of the biophysics of the bacterial genome. For example, in an interesting recent study [294] White *et al.* have shown experimental evidence which suggests that chromosome segregation in *E. coli* is not random but

is driven in a manner that results in the leading and lagging strands being addressed to particular cellular destinations. It may therefore be that entropic forces are complemented by active ones (e.g. due to a segregation protein machinery) in order to ensure an error-free cell replication.

17. The size of knots

In Section 16.1, in order to understand the scaling behaviour of the entropic and metric properties of polymer rings with fixed knot type, we used the working hypothesis that knots are tightly tied in the chain. This assumption could be verified *a posteriori* by looking at the statistics of the effective size of the knotted region within the chain. Questions that may be relevant in this respect are for example the following:

- What is the average size of the knotted portion of a ring in equilibrium?
- What is the fraction of the chain contour length that is taken up by the knot?
- How do the above properties depend on external conditions such as the quality of the solvent, the degree of a spatial confinement, the intensity of an applied stress etc?

The above questions can be made more precise if formulated through the notion of the *degree of localization of a knot*. In the following we shall denote with N the total number of bonds in the ring, and with $\langle N_\tau \rangle$ the average length (in unit of chain bonds) of the region where the knot of type τ resides. Three possible scenarios can occur:

- I. when, upon increasing N , $\langle N_\tau \rangle$ increases more slowly than any power of N , then the knot is said to be *strongly localized* within the ring. Note that this definition includes either the situation where $\langle N_\tau \rangle$ grows as any power of $\log N$ or the case in which $\langle N_\tau \rangle$ is independent on N .
- II. When $\langle N_\tau \rangle$ is $o(N)$ but yet grows as N^t , with $0 < t < 1$, then the the knot is said to be *weakly localized*. In this situation it is possible that short chains display knotted region that are comparable in size with the whole chain and only for very large (depending on t) values of N the knotted region becomes negligible relatively to the chain contour length.
- III. Finally, when $\langle N_\tau \rangle$ is proportional to N then the knot is said to be *delocalized*.

17.1. Knotted arc

The major difficulty one encounters in estimating $\langle N_\tau \rangle$ relies on the notion of *knotted arc* that, in general, cannot be defined rigorously (see Section 3.6). Indeed, if we consider open equilateral chain the standard definition of knot type (see Section 3) will tell us that such curves are unknotted. This is because an open piecewise chain with a knot tied in it can be deformed, possibly with moves that do not preserve edge lengths, into a straight line without passing the curve through itself. Notice, however, that by using only edge-preserving moves it is not presently known whether an arbitrary configuration of an equilateral piece-wise linear chain can be deformed into a straight segment (and such deformations have been proven to be impossible for certain non-equilateral chain configurations) [295, 32].

There are cases, however, where the notion of knotted arc can be well defined. Simple examples are open chains in which the two extremities lay at the surface of a three-ball (i.e. homeomorphic to a the standard three ball $\{(x, y, z), x^2 + y^2 + z^2 \leq 1\}$) that contains all the rest of chain. Indeed, in this case the definition of knotted arc can be made rigorous through the idea of

knotted ball pair introduced in Section 9 and more carefully defined in [296, 113]. This can be easily seen for the class of *unfolded* self-avoiding walks since they can be uniquely completed to (3, 1) ball-pairs. To see how the construction works let us consider for example the set of *x-unfolded* walks [297]. They are characterized by having the x coordinates with the property $x_0 < x_i < x_N$ for $1 \leq i \leq N - 1$. We add half-edges in the negative and positive x -direction to the first and last vertices of the walk and construct a 3-ball with two parallel faces perpendicular to the x -axis, and four more faces (perpendicular to the remaining coordinate directions) so that the walk (and the added half-edges) is properly embedded in the 3-ball. The walk and the 3-ball containing it form uniquely a (3, 1) ball-pair for which the notion of knot is well defined. Unfortunately, although unfolded walks are not exponentially rare in the set of all SAWs [298], they are still too rare to search for them within a long walk as possible candidates of knotted regions. Even if the above scheme based on unfolded walk is not going to solve the problem of how define a knotted arc *for any arc* it does suggest some useful extensions [297].

- I. One idea is to choose a direction at random and construct two parallel rays, whose origins are the two extremities of a given walk and which are parallel to the chosen direction. Since all such rays will have irrational direction cosines they will not pass through any of the vertices of the cubic lattice. If we regard the two rays to join themselves at the point at infinity the resulting curve is a closed curve that will be, almost surely, simple. For this closed curve the topological entanglement is well defined and can be detected for example by computing some invariants. Note that in general the value of the invariant will depend on the chosen direction so it will be convenient to average over all directions. The main problem of this construction is that it can create or destroy entanglements. For instance, a knotted arc present in the chain may not be necessarily detected as being knotted upon closure, because one of the rays might pass through the 3-ball associated with the knotted arc thus unknotting the curve (see Figure 44). Despite these potential pitfalls, closing over all possible directions has been shown to yield robust results for both compact and unconstrained ring configurations. Its main limitation resides in the heavy computational cost associated with the repeated calculation of knot invariants. A robust and more computationally-effective alternative is offered by the minimal-entanglement closure scheme introduced recently by some of us[44].
- II. An alternative and apparently simpler closing scheme is to join the ends of the arc with a line segment. The immediate problem is that the added line segment will in general pass through vertices of the lattice and the resulting closed curve might not be a simple curve (i.e. not self-avoiding). One way to get around this problem is to add to the ends of the walk two parallel line segments (of length say $\epsilon < b$) in a direction with irrational direction cosines, and then join up the end points of the resulting object to form a closed curve that is almost always a simple closed curve. As for the previous scheme the knot detection may depend on the direction cosines chosen so that an averaging over them might be necessary. Clearly, also in this case the addition of the segment closing the curve may change the entanglement status of the starting arc.

It is clear from the schemes described above that the closing construction is not unique and so is the detection of the topological entanglement in the arc. This uncertainty poses severe problems for a "deterministic" definition of knotted arc. One may rely instead on a more probabilistic approach as suggested in [34] and outlined in section 3.6. The idea consists in analyzing the spectrum of knots generated by multiple closures of the same open chain. Each closure is obtained by connecting the ends of the chain to a point chosen (randomly) on the surface of a

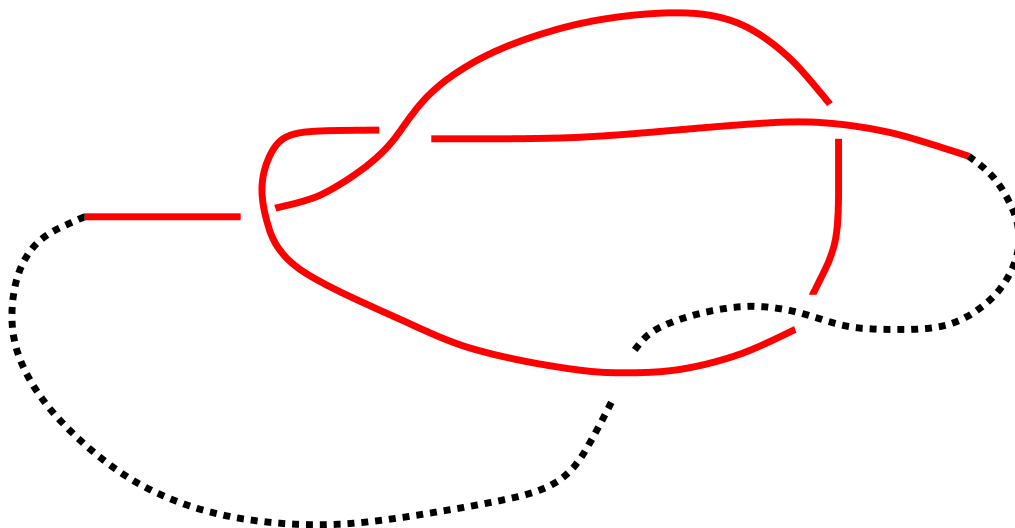


Figure 44: Example of an unknotted ring that contains a knotted region (solid line)

sphere that contains the walk. Different closures correspond to different chosen points on the sphere. For each fixed open chain a distribution of knots is estimated and the *most probable knot* gives the knot type of the open chain. Interestingly enough it turns out that the knot obtained by a simple direct end-to-end closure usually coincides with the knot type that dominates the random closure spectrum [34].

17.2. Flat knots

A definition of knotted arcs and knot size may be much easier to formulate for *flat knots* [180], a simplified model which has played an important role in the development of ideas concerning localization and delocalization properties of real knots in equilibrium [180, 299, 300, 301, 302]. Flat knots are closed curves in the plane, e.g. in the square lattice, that can be seen as quasi-2D projections of 3D knots. Physically they can be realized by adsorbing 3D polymer rings on a strongly attractive planar surface [75, 177] or membrane or by confining the polymer between two close parallel walls (see the model introduced in [176] and mentioned in Section 11). In these cases the flat knots can still equilibrate in 2D. Macroscopic realization of flat knots comes also from experiments in which macroscopic knotted chains are flattened by gravity onto a vibrating plane [303]. Flat knots have the advantage of being relatively easy to image by microscopy [75] and can be studied theoretically either by numerical or analytical approaches on properly defined two-dimensional models [304]. A model of flat knots on a lattice was first proposed in [180] where, the authors considered configurations embedded in the square lattice where the bonds lie on lattice edges except in correspondence of chain crossings (over/underpasses) where the diagonals of a *single* lattice square are used (see Figure 45a). With this model a numerical estimate of the entropy and the average extension of flat knots with a given fixed, topology was carried on. The stochastic sampling was based on BFACF plus some additional moves corresponding to lattice versions of Reidemeister moves on knot diagrams. These moves

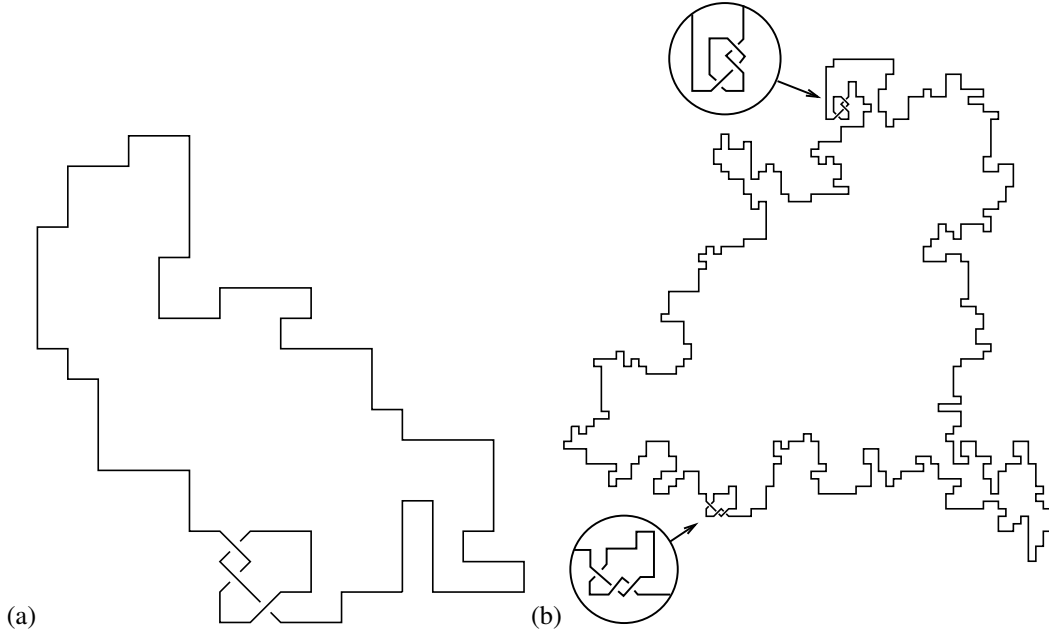


Figure 45: Examples of flat knots on the square diagonal lattice. The configuration in panel (a) has three crossings and has the topology of a (negative) trefoil knot. The one in panel (b) six crossings and has the topology of a composite knot $3_1\#3_1$. Note the localization (and the reciprocal separation) of the two prime knots.

assure a good mobility within the space of flat knots with a given knot type that is defined by the initial configuration corresponding to a projection of a knotted curve in 3-space.

This investigation shows that the connective constant of flat knots is independent of knot type, to numerical accuracy, and that

$$\alpha(\tau) = \alpha(\emptyset) + N_\tau \quad (103)$$

where N_τ is the number of prime components in the knot τ and $\alpha(\tau)$ is the exponent that enters in a scaling equation similar to (84) where $p_N(\tau)$ is replaced by the number of N -bonds flat knots with a given knot type τ . By computing the mean squared radius of gyration it was also shown that the critical exponent ν of flat knots is, within error bars, independent of the knot type. Although a detailed study of tightness was not carried out, in [180] it was observed that the knotted regions were typically very small compared to the rest of the ring (see Figure 45b for a typical configuration of the composite knot $3_1\#3_1$.) Note that all the results presented above for flat knots agree with the ones found for real knots in 3D (see Section 16.1) indicating that, at least for some properties, flat knots are a fair approximation of real knots. As for real knots the investigations in [180] refer to the asymptotic behaviour of the entropy and of the average size of flat knots. These furnish an indirect measure of the knot size. By exploring the properties of flat knots in the limit in which they display a minimal number of crossings it is possible to better characterize the size of the knotted region. This will be the subject of the next section.

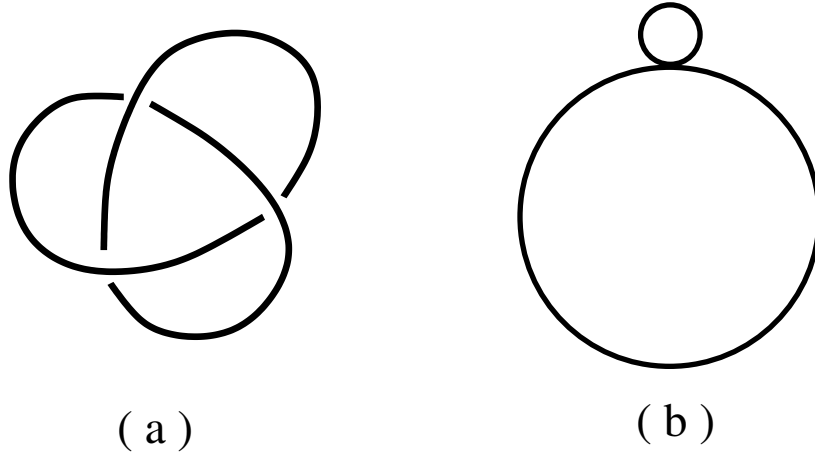


Figure 46: Uncontracted (original) flat trefoil configuration (a) and its figure eight contraction (b).

17.2.1. Size of flat knots

In the model presented in [180] the number of non essential crossings were free to fluctuate in the ensemble. If, on the other hand, the number of overlaps of the polymer ring with itself is restricted to the minimum compatible with the topology (e.g. 3 for a 3_1 knot) the flat knot model enjoys a drastic simplification. With this approximation an analytic approach to the problem of the size of a flat knot is possible [299]. The idea is to interpret the essential self-overlaps of the chain as vertices of a two-dimensional polymer network, for which a well developed theory exists (see for example, [271, 305] and [306]). By exploiting results coming from this theory it was possible to discuss the scaling of the length distribution of prime flat knots and predict a *strong localization regime* [299] (i.e. $\langle N_r \rangle = O(\log(N))$). This prediction was confirmed by Monte Carlo simulations [299].

The possibility of getting both analytical results and quite sharp numerical estimates on the localization of flat knots has recently stimulated an extension of this model that incorporates an attractive vertex-vertex interaction as a pseudo-potential to mimic poor solvent conditions. This gives the possibility of looking at the average size of the knotted regions as a function of the quality of the solvent and see, in particular if the knot localization property found in the swollen phase may be affected by the coil-globule (θ) transition [50, 79].

By simulating numerically this *self-attracting flat knots* model it was found [300, 302] that while in the good solvent regime the knots are strongly localized, consistent with the results of ref. [299], in the globular state flat knots are delocalized, (i.e. $\langle N_r \rangle = O(N)$). Right at the θ -temperature weak localization prevails with $t = 0.44 \pm 0.02$. This last result can be explained by extending the scaling theory of polymer networks of fixed topology at the θ point [307] and assuming that the configurations having the shape of a figure eight dominate the statistics in that regime [300, 302] (see Figure 46). This assumption, supported by the numerical data, leads us to speculate that the exact value of t is $3/7$ [300, 302]. If, on the other hand, the above assumption is rejected the leading scaling order of any prime flat knot is the uncontracted configuration (see Figure 46) that is delocalized, i.e. $t = 1$, also at the θ point [301].

17.3. The size of “real knots”

As anticipated in sections 3.6 and 17.1 the identification, in a knotted ring, of the shortest ring segment containing the knot is a difficult and, in general, ambiguous problem. For this reason the number of studies available on this topic is still limited and largely restricted to numerical investigations.

One of the earliest attempts to measure the length of the knotted region for polymer rings at equilibrium was done in [308]. This investigation was carried out with a Monte Carlo sampling of equilateral random polygons. In this work the identification of the *minimal knotted arc* was carried out following procedures (1) and (2) in section 17.1.

For polygons with $N = 500$ bonds it was found that the typical length of the minimal knotted arc were about 6 to 8 for trefoils, about 15 for figure eight knots and about 20 for 5_1 and 5_2 . Since this investigation was done for one value of N it is difficult to put these results within the context of knot localization. Nevertheless the general conclusion was that knots were typically tight.

In [309] a first study of knot localization for lattice polygons in a good solvent regime was carried out by Monte Carlo simulations using the BFACF algorithm. Since BFACF is ergodic within each knot class it was possible, for a fixed knot type τ , to consider several values of N and to explore properly the statistics of the knotted regions. These regions were detected by using a variant of the *cutting and closure* schemes outlined in Section 17.1 that allows one to minimize the risk of knot modifications or disentanglements during the closure of the subwalk. By detecting the minimal knotted arc in polygons having knot type 3_1 and with N up to 1500, it was found

$$\langle m_\tau \rangle \sim N^t \quad (104)$$

where $t \approx 0.75$ for the good solvent regime. This result turns out to be robust with respect to a change of prime knot type. For example by replacing the 3_1 with a 4_1 or 5_1 or 7_1 knot, the scaling behaviour (104) remains valid with the same (within error bars) estimated value of t [309, 310].

These results for the good solvent regime are qualitatively consistent with a molecular dynamics study by Mansfield [311] who, back in 1998, showed maximally-tight knots in a polymer becomes is loosened up by the dynamical evolution of the polymer (hence suggesting that equilibrated knots are not strongly localized).

At the same time it should be noted that a more recent study by Mansfield and Douglas [252] reported a value of $t = 0.54$ for trefoil knots occurring in self-avoiding rings on a cubic lattice. This value is appreciably different from the one reported before and prompts for further investigations of the source of this discrepancy. In particular, it is possible that the difference reflects the fact that in ref. [252], only a subset of the possible subportions of a ring are considered as candidate segments accommodating the knot. Specifically, considerations are restricted only to those ring segments that have both ends at the surface of the whole ring so to eliminate topological ambiguities upon closure. It is not implausible that introducing this selection criterion can result in different statistical properties of the shortest knotted segments.

17.3.1. The size of globular knots

It is important to stress that the above *direct* approaches to measuring the size of the minimal knotted arc strongly rely on the assumption that the closure procedure does not systematically introduce artifacts in the detection of the arc topology.

This condition ought to be realised in the good solvent regime where ring configurations are not compact. On the other hand, in situations such as the poor solvent regime where the whole

polymer is quite compact and strongly geometrically entangled, this condition is not expected to hold.

To circumvent the problem, Marcone *et al* [309, 310] recently proposed a novel strategy to identify the knotted arc of minimal length. The method exploits the so-called *entropic competition* between two unlinked, mutually-avoiding, knotted sub-loops obtained by introducing a *slip ring* in the full ring. The slip ring is small enough to prevent a complete migration of one sub-loop, or of its knot, into the other sub-loop (see also [195] and [312] for related works). The whole topology of the system is characterized by the knot types τ_1 and τ_2 , respectively, of the first and the second sub-loop, and by the linking state between the two loops.

In the formulation of Marcone *et al*, the rings in the poor solvent regime are described by polygons on the cubic lattice with an effective attraction between non consecutive vertices. This model is known to be adequate for reproducing the salient features of the coil-globule transition (θ point) and the equilibrium properties of the rings in the compact regime. By using a Monte Carlo approach based on BFACF moves the overall topology of the system was kept fixed and it was studied how the sub-rings shrunk or inflated depending on their topological state. We recall that the sub-rings are assumed to be unlinked. If a given prime knot τ is tied in each loop one can identify the average knot size $\langle m_\tau \rangle$ with the length of the smallest loop.

In the good solvent regime the above scheme yields $\langle m_\tau \rangle \sim N^t$ with $t \approx 0.75$. The results are in good agreement with the findings based on the closure scheme. For poor solvents the estimate was $t \approx 1$. This indicates that knots are weakly localized in the good solvent regime but are fully delocalized in the poor solvent regime. This behaviour was later confirmed in [313] for an off-lattice model.

Another approach that could be effective either in the swollen or in the compact regime is the one introduced in [244]. The method builds on the idea of quantifying the degree of tightness of knotted polymers by comparing the response to mechanical pulling (force-extension relation) of knotted and unknotted chains. By simulating rod-bead chains with N (the number of beads) up to 750 it was found $t = 0.4 \pm 0.1$ in the swollen regime [244]. This result agrees with the one in [309, 310] in showing that knotted polymers in the extended phase are weakly localized although the estimate of t is considerably smaller.

17.3.2. The size of adsorbed knots

A possible link between the theory of flat knots and knot localization in 3D is given by the phenomena of polymer adsorption onto an impenetrable plane [50, 79] (see section 11). It is known that, in the case of unrestricted topology, this system exhibits a phase transition between a *desorbed phase* (zero density of contacts with the surface) and an *adsorbed phase* where there is finite fraction of monomers at the surface. This fraction increases with decreasing temperature and at zero temperature the polymer is practically a fully adsorbed 2D object (see Section 11). If, on the other hand, the topology of the polymer is kept fixed, there will be a certain number of desorbed monomers. While the exact number of expected desorbed monomers cannot be predicted, it is plausible that it is simply related to the minimal number of crossings necessary to satisfy the given knot type. At very small temperature, the statistics should be dominated by fully-adsorbed configurations having the minimal number of desorbed monomers.

Thus, in adsorption conditions, it is possible to investigate how a knotted polymer (e.g. in good solvent) crosses over from the weak localisation regime found at high T to the strong localisation one corresponding to the occurrence of flat knots. In a recent study this interplay between topology and adsorption was investigated within a standard lattice polymer model [314]. Specifically, the polymer ring was described by *positive polygons* i.e. lattice polygons confined

to the half space $z \geq 0$ and with at least one vertex anchored at the $z = 0$ plane. For a given configuration an energy ϵN_a is assigned, where N_a is the number of vertices in the surface $z = 0$. Usually $\epsilon = -1$. The Monte Carlo sampling was based on BFACF moves while the determination of knot size was based on the cutting and closure scheme introduced in [309]. By exploring the whole adsorption phase diagram for the prime knots 3_1 , 4_1 , 5_1 and 5_2 , it was found that knots in the desorbed phase and right at the transition are weakly localised. Below the transition ($T < T_c$), the knot becomes more and more localised, reaching a strong localisation regime deep into the adsorbed phase. This crossover to more localised states is certainly triggered by the adsorption transition but turns out to be quite smooth as T decreases. In particular, on the basis of the collected data, it could not be ruled out that below T_c there is a continuous variation of the exponent t with the flat knot regime reached only in the limit $T \rightarrow 0$. An alternative scenario would be the existence of a genuine *localization* transition at some $T_{loc} < T_c$, where the region $T < T_{loc}$ would correspond to the strong localization regime. This appealing scenario is however less probable unless one assumes that the data in [314] are affected by strong finite-size corrections.

With the exception of the above cited study in [314] there are no other investigations on the interplay between topological constraints and polymer adsorption. It would be interesting, for example, to perform similar studies for off-lattice models of polymer rings in which self-avoidance and bending rigidity are taken into account. This would be an interesting issue to explore given that experimental results showing localization in adsorbed knots are nowadays available [75].

The above results indicate that the presence of a topological constraint introduces a new length scale $R_\tau \propto \langle m \rangle_\tau \sim N^{t\nu}$ into the problem that may affect the scaling properties of knotted rings at equilibrium. In the swollen phase, since $t \simeq 0.7 < 1$ (weak localization), the new length scale is subdominant and would not affect the leading behaviour of scaling laws such as eqs. (84) and (93). It may have, however, important consequences in the leading term of the correction to scaling expansion as shown in [310]. In the collapse regime, since $t = 1$, R_τ is comparable to the average extension of the whole polymer and changes in the scaling theory, already at leading orders may occur. For example, there are strong numerical indications that relation (87) is not valid for compact knotted rings [112].

The presence of a new, topological, length scale may also be important in determining the equilibrium properties of knotted polymer rings under geometrical confinement or under stretching forces. For example for polymers under geometrical confinement two crossover regimes may be considered. The first one occurs when the effective confining size, D , is comparable to R though still larger than R_τ . In this situation the knot, does not experience, on average, the confinement and the scaling behaviour such as eq. (26) should hold. If, on the other hand, $D < R_\tau < R$ then the knotted region will be affected by confinement. In this case it would be interesting to explore whether the knot would further localize or instead delocalize, as suggested by the numerical study of knotting in spherically-confined DNA molecules described in ref. [164].

A confinement-induced knot localization is probably at play in the case of polymer rings confined into slab as $D \rightarrow 0$ where we know from the theory of flat knots that almost $2D$ knots are strongly localized. Similar non trivial effects may be expected for stretched rings when the screening length $\xi = 1/f$ becomes comparable to the average knot size R_τ and a single knot cannot fit in a single blob of the Pincus argument. With the exception of very preliminary studies in [315] and [316, 317], these issues are still largely unexplored and would represent very appealing avenues for future research.

18. Summary and perspectives

The focus of review was mostly on the salient properties of polymers chains subject to spatial or topological constraints.

Although these systems are highly interesting from the theoretical and applicative points of view several of their key physical properties are still not fully understood. For example, the exact value of the metric exponent of infinitely-thin rings with a fixed knot type is still actively investigated and debated. An increasingly important avenue is also offered by biological systems, where spatially-confined long biopolymers (DNA and RNA) are ubiquitous. This poses the pressing need to understand the extent to which the *in vivo* organization of these biomolecules relies on “passive” physical mechanisms or “active” ones involving biological machinery.

The first three Chapters of the review provide a self-contained account of all the basic concepts and methodologies in polymer physics and topology that are necessary to tackle the state-of-the-art problems.

In particular, Sections 2 and 3 can be regarded as a primer to the topology of closed curves. Non-specialists will be progressively introduced to the topic starting from basic questions such as: what is a knot? What is the handedness of a given knot? How can we classify knots?

Next, in Section 4, we offer a didactical survey of the standard models that are used to characterise and study the kinetics and thermodynamics of polymers. Since we typically focus on universal, or transferable, physical properties of polymers subject to various constraints, we restrict considerations to *coarse grained* models. In these approaches, the polymer is described at a much coarser level than in atomistic approaches which are, in fact, more tailored to address the detailed properties of a specific type of polymer. The simplified nature of the models that we shall review, is not for the sake of a general and minimalistic statistical mechanical formulation of the problem; it is often an obligatory choice to keep the complexity of the problem at a manageable level. Indeed, global properties, such as polymer self-avoidance and spatial or topological constraints, are extremely difficult to deal within analytical approaches and can only be satisfactorily accounted for in extensive computational approaches.

In Section 6 we have accordingly reviewed the most advanced stochastic algorithms for studying the equilibrium properties of confined or entangled polymers. We note that there are additional methods which become relevant when non-equilibrium or kinetic effects become important. These methods typically involve Brownian or molecular dynamics simulations, or generalisations thereof. While we do report on selected problems where kinetic effects are important, we do not review these methods here, but refer the reader to the several authoritative methodological reviews that are presently available.

After introducing the fundamental theoretical concepts and methodologies, we first characterize the behaviour of a single polymer subject to geometric confinement. Specifically, in Sections 8 and 9 we discuss the statistical and topological properties of confined polymers and rings. Particular attention is paid to the so-called knot spectrum – that is the frequency of occurrence of various knot types – of confined polymers, starting from lattice models (for which analytical results are available) to more complex off-lattice models of flexible chains. The physical description of such systems is complicated due to the interplay of various length scales, i.e. the contour length, persistence length, excluded-volume interaction range, and finally the confining region size. In general, the effect of confinement is to make the incidence of knots much more frequent than in unconstrained cases.

As a matter of fact, quantitative estimates of the level of topological entanglement computed for standard models of DNA subject to high confinement (such as the genome of some viria)

largely exceeds the ones detected experimentally. In Section 10 we report on the quest that has been undertaken in recent years to bridge the gap between the theoretical and experimental data on DNA knotting and which has been instrumental in advancing the current understanding of the physics of confined DNA. Besides the open issues regarding DNA knotting in viria and in the cell, there are a number of outstanding questions regarding the topology of confined polymers in general. Among these we largely focused on the case of polymer confinement in slabs and prisms, which ought to acquire increasing importance with the advent of nano-fabrication techniques.

Likewise, when confinement is induced by an attractive interaction to a surface, which we study in Section 11, it is still unclear whether there is a topology-dependent character of the adsorption transition. As discussed in Section 12, little is known about how many and what knot types occur in stretched polymers. Again the latter may well be soon extensively characterized experimentally by means of single-molecule manipulation techniques.

The remainder of the review deals with cases where the entanglement is not driven by spatial confinement but rather by the proximity of other chains in concentrated solutions or cases where topological constraints affect the geometric properties of polymer rings.

The characterization of the equilibrium topological properties of polymers in concentrated solutions is given in Sections 13 and 14. In these sections the reader is first introduced to the concept of linked curves and to the various algorithms that have been designed by topologists to detect computationally the linked state of polymer rings. The presented results mostly focus on the linking probability of two or more rings as a function of the concentration. This topic has been actively investigated and several exact results are available for polymer on a lattice. Several major issues, including the impact that the linking or unlinking has on the configurational properties of polymers in dense solutions is still largely uncharacterised.

Sections 15 and 16 are devoted instead to the case where the topological state of the polymer(s) is fixed. In this case it is interesting to understand how and to which extent the topological constraint reverberates on the geometrical properties of the polymer chains.

These systems are challenging to simulate. In fact, it is typically necessary to sample the polymer configurational space by using topology-preserving polymer deformations which are, by necessity, local. This is reflected in the very long autocorrelation time of the stochastic Monte-Carlo or Molecular Dynamics simulation. At the same time, this type of problems is most interesting and connects to a number of open questions in polymer physics. These range from fundamental issues such as the determination of the universality class and critical exponents which characterise the infinitely-thin ring with fixed topology (see Section 16.1.2), to very applied and highly interdisciplinary problems, such as the segregation of chromosomes in eukaryotic and bacterial cells (this problem is reviewed in Section 16.4.1). Indeed, while in the nucleus and in the cell there are enzymes which allow crossing of DNA strands and hence the changing of the knot and link states of the genome, the action of these enzymes requires energy and time so that the fixed topology case is a good starting point and has been analysed with increasing attention by biophysicists. The problem of territories and in general of the structure and 3-dimensional organization of chromatin and bacterial DNA are fascinating open problems which have just now begun to be studied by physicists. Preliminary results suggest that confinement, crowding and topology should all be crucial to the understanding of these phenomena, and this area seems a particularly promising playground for the physics and topology of confined and concentrated polymers.

Finally, Section 17 introduces the study of the “length” of a knot in a single polymer, or equivalently the concept of localisation or delocalisation of knots. A knot is localised when the

portion of the chain that it occupies scales with a sublinear power of the total length of the polymer, and delocalised otherwise. While it is intuitive that stretched knots localise, other results on knot localisation are quite unexpected. For instance, knots in unconstrained polymers are weakly localised, and they delocalise below the theta temperature. Likewise, knots in bacteriophages appear to delocalise when they are inside the capsid, and this may be at the origin of the seemingly paradoxical observation that DNA can be ejected into the bacterial host even when it is highly knotted (see Sections 10 and 17.3). However, the interplay of knot size with confinement and concentration is poorly understood to date and will certainly attract more researchers in the years to come.

In summary, we have provided a survey of the methodology, the current results and the open problems in the physics and topology of confined and concentrated polymers. Most of the latest progress in this interdisciplinary area, which covers vital aspects of biophysics and technology, depends on the use of advanced theoretical and especially computational techniques. These have been covered in detail here with the aim of providing an organised summary of the state-of-the-art and an accessible guide for researchers entering in the field.

References

- [1] P. G. de Gennes, Tight knots, *Macromol.* 17 (1984) 703–704.
- [2] A. M. Saitta, P. D. Soper, E. Wasserman, M. L. Klein, Influence of a knot on the strength of a polymer strand, *Nature* 399 (1999) 46–48.
- [3] A. M. Saitta, M. L. Klein, Influence of a knot on the stretching-induced crystallization of a polymer, *J. Chem. Phys.* 116 (2002) 5333–5336.
- [4] J. C. Wang, DNA Topoisomerases, *Ann. Rev. Biochem.* 65 (1996) 635–692.
- [5] S. A. Wassermann, N. R. Cozzarelli, Biochemical topology: applications to DNA recombination and replication, *Science* 232 (1986) 951–960.
- [6] D. W. Sumners, Untangling DNA, *Math. Intelligencer* 12 (1990) 71–80.
- [7] D. W. Sumners, Knot theory and DNA, *New Scientific Applications of Geometry and Topology: Proceedings of Symposia in Applied Mathematics* 45 (1992) 39–72.
- [8] D. W. Sumners, Lifting the curtain: Using topology to probe the hidden action of enzymes, *Notices of the AMS* 42 (1995) 528–537.
- [9] V.V. Rybenkov, C. Ullsperger, A. V. Vologodskii, N. R. Cozzarelli, Simplification of DNA topology below equilibrium values by type II topoisomerases, *Science* 277 (1997) 690–693.
- [10] D. W. Sumners, C. Ernst, S. J. Spengler, N. R. Cozzarelli, Analysis of the mechanism of DNA recombination using tangles, *Quarterly reviews of biophysics* 28 (1995) 253–313.
- [11] Z. Liu, J. K. Mann, E. L. Zechiedrich and H. S. Chan HS, Topological information embodied in local juxtaposition geometry provides a statistical mechanical basis for unknotting by type-2 DNA topoisomerases, *J. Mol. Biol.* 361 (2006) 268–285.
- [12] Z. Liu, L. Zechiedrich, H. S. Chan, Action at hooked or twisted-hooked DNA juxtapositions rationalizes unlinking preference of type-2 topoisomerases, *J Mol Biol* 400 (5) (2010) 963–982, doi:10.1016/j.jmb.2010.05.007.
- [13] P. R. Cromwell, *Knots and Links*, Cambridge University Press, 2004.
- [14] G. Burde, H. Zieschang, *Knots*, Birkhuser, 2003.
- [15] K. Murasugi, *Knot theory and its applications*, Birkhuser, 1996.
- [16] C. C. Adams, *The Knot Book*, Freeman, 1994.
- [17] C. Livingston, *Knot theory*, The Carus Mathematical Monographs, Nr 24, Mathematical Association of America, Whashington DC, 1993.
- [18] D. Rolfsen, *Knots and Links*, Mathematics Lecture Series 7, Publish or Perish, Inc., Houston, Texas, 1976.
- [19] K. Reidemeister, *Knotentheorie*, Chelsea (New York) .
- [20] C. Ernst, D. W. Sumners, The growth of the number of prime knots, *Math. Proc. Cambridge Philos. Soc.* 102 (1987) 203–315.
- [21] D. J. A. Welsh, On the Number of Knots and Links, *Collq. Math. Soc. J. Bolyai* 60 (1991) 713–718.
- [22] M. Thistlethwaite, On the Structure and Scarcity of Alternating Links and Tangles, *J. Knot Th. Ramifications* 7 (1998) 981–1004.
- [23] J. Hoste, M. Thistlethwaite, J. Weeks, The first 1,701,935 knots, *Math. Intelligencer* 20 (1998) 33–48.

- [24] S. Rankin, O. Flint, J. Schermann, Enumerating the prime alternating knots, *J. Knot Theory Ramifications* 13 (2004) 57–100.
- [25] K. Perko, On the classification of knots, *Proc. Amer. Math. Soc.* 45 (1974) 262–266.
- [26] M. Scharlemann, Unknotting number one knots are prime, *Invent. Math.* 82 (1985) 37–55.
- [27] I. K. Darcy, Biological distances on DNA knots and links: Applications to XER recombination, *J. Knot Theory Ramif.* 10 (2001) 269–294.
- [28] A. Flammini, A. Maritan, A. Stasiak, Simulations of action of DNA topoisomerases to investigate boundaries and shapes of spaces of knots, *Biophys. J.* 87 (2004) 2968–2975.
- [29] K. Murasugi, On the braid index of alternating links, *Trans. Amer. Math. Soc.* 326 (1991) 237–260.
- [30] Kronheimer and Mrowka, Gauge theory for embedded surfaces, *Topology* 32 (1993) 773–826.
- [31] P. Pieranski, In search of ideal knots, *Ideal Knots*: edited by A. Stasiak, V. Katrich, and L. H. Kauffmann, *Series on Knots and Everything* 19 (1998) 20–41.
- [32] J. Cantarella, H. Johnston, Nontrivial embeddings of polygonal intervals and unknots in 3-space., *J. Knot Theory Ramifications* 7 (1998) 10271039.
- [33] F. Waldhausen, On irreducible 3-manifolds which are sufficiently large, *Annals of Math.* 87 (1968) 5688.
- [34] K. Millett, A. Dobay, A. Stasiak, Linear random knots and their scaling behavior, *Macromol.* 38 (2005) 601–606.
- [35] R. Potestio, C. Micheletti, H. Orland, Knotted vs. unknotted proteins: evidence of knot-promoting loops, *PLoS Comput Biol* 6 (7), doi:10.1371/journal.pcbi.1000864.
- [36] P. Virnau, A. Mallam, S. Jackson, Structures and folding pathways of topologically knotted proteins, *Journal of Physics: Condensed Matter* 23 (3) (2011) 033101, URL <http://stacks.iop.org/0953-8984/23/i=3/a=033101>.
- [37] W. R. Taylor, A deeply knotted protein structure and how it might fold, *Nature* 406 (2000) 916–919.
- [38] P. Virnau, L. A. Mirny, M. Kardar, Intricate knots in proteins: Function and evolution, *PLoS Comput Biol* 2 (9) (2006) e122. DOI: 10.1371/journal.pcbi.0020122, doi:10.1371/journal.pcbi.0020122.
- [39] R. C. Lua, A. Y. Grosberg, Statistics of knots, geometry of conformations, and evolution of proteins, *PLoS Comput Biol* 2 (5) (2006) DOI: 10.1371/journal.pcbi.0020045, doi:10.1371/journal.pcbi.0020045.
- [40] Y. L. Lai, S. C. Yen, S. H. Yu, J. K. Hwang, pKNOT: the protein KNOT web server, *Nucleic Acids Res* 35 (Web Server issue) (2007) 420–424, doi:10.1093/nar/gkm304.
- [41] F. Khatib, M. T. Weirauch, C. A. Rohl, Rapid knot detection and application to protein structure prediction, *Bioinformatics* 22 (14) (2006) 252–259, doi:10.1093/bioinformatics/btl236.
- [42] D. Bölinger, J. I. Sulkowska, H. P. Hsu, L. A. Mirny, M. Kardar, J. N. Onuchic, P. Virnau, A Stevedore’s protein knot, *PLoS Comput Biol* 6 (4), doi:10.1371/journal.pcbi.1000731.
- [43] E. Orlandini, A. L. Stella, C. Vanderzande, The size of knots in polymers, *Phys. Biol.* 6 (2009) 025012.
- [44] L. Tubiana, E. Orlandini and C. Micheletti, Probing the entanglement and locating knots in ring polymers: a comparative study of different arc closure schemes, *Prog. Theor. Phys.* accepted for publication.
- [45] P. J. Flory, *Statistical Mechanics of Chain Molecules*, Hanser, 1969.
- [46] J. Marko, E. Siggia, Stretching DNA, *Macromol.* 28 (1995) 8759–8770.
- [47] O. Gonzalez, J. H. Maddocks, Global curvature, thickness, and the ideal shapes of knots, *Proc. Natl. Acad. Sci. USA* 96 (1999) 4769–4773.
- [48] D. Marenduzzo, C. Micheletti, Thermodynamics of DNA packaging inside a viral capsid: the role of DNA intrinsic thickness, *J. Mol. Biol.* 330 (2003) 485–492.
- [49] N. Clisby, Accurate Estimate of the Critical Exponent ν for Self-Avoiding Walks via a Fast Implementation of the Pivot Algorithm, *Phys. Rev. Lett.* 104 (2010) 055702.
- [50] P.-G. de Gennes, *Scaling concepts in Polymer Physics*, Cornell University Press, Ithaca, New York, 1979.
- [51] N. M. Toan, D. Marenduzzo, C. Micheletti, Inferring the diameter of a biopolymer from its stretching response, *Biophys. J.* 89 (2005) 80–86.
- [52] N. M. Toan, C. Micheletti, Inferring the effective thickness of polyelectrolytes from stretching measurements at various ionic strengths: applications to DNA and RNA, *J. Phys. Condens. Matter* 18 (2006) S269–S281.
- [53] V.V. Rybenkov, N. R. Cozzarelli, A. V. Vologodskii, Probability of DNA knotting and the effective diameter of the DNA double helix, *Proc. Natl. Acad. Sci. USA* 90 (1993) 5307–5311.
- [54] A. Rosa, T. X. Hoang, D. Marenduzzo, A. Maritan, Elasticity of semiflexible polymers with and without self-interactions, *Macromolecules* 36 (2003) 10095–10102.
- [55] Y. D. Chen, Monte Carlo study of freely jointed ring polymers. I. Generation of ring polymers by dimerization method, *J. Chem. Phys.* 74 (1981) 2034–2038.
- [56] I. Carmesin, K. Kremer, The bond fluctuation method - a new effective algorithm for the dynamics of polymers in all spatial dimensions, *Macromolecules* 21 (1988) 2819.
- [57] J. M. Hammersley, Percolation processes II The connective constant, *Proc. Camb. Phil. Soc.* 53 (1957) 642–645.
- [58] E. J. Janse van Rensburg, A. Rechnitzer, Atmospheres of polygons and knotted polygons, *J. Phys. A: Math. Theor.* 41 (2008) 105002.

- [59] N. Clisby, R. Liang, G. Slade, Self-avoiding walk enumeration via the lace expansion, *J. Phys. A: Math. Theor.* 40 (2007) 10973–11017.
- [60] J. M. Hammersley, The number of polygons on a lattice, *Proc. Camb. Phil. Soc.* 57 (1961) 516–523.
- [61] H. L. Frisch, E. Wasserman, Chemical Topology, *J. Am. Chem. Soc.* 83 (1961) 3789–3795.
- [62] M. Delbruck, Knotting problems in biology, *Mathematical Problems in the Biological Sciences*, edited by R. E. Bellman, Proceedings of Symposia in Applied Mathematics, American Mathematical Society, Providence, Rhode Island) 14 (1962) 55–63.
- [63] D. W. Summers, S. G. Whittington, Knots in self-avoiding walks, *J. Phys. A: Math. Gen.* 21 (1988) 1689–1694.
- [64] N. Pippenger, Knots in random walks, *Discr. Appl. Math.* 25 (1989) 273–278.
- [65] S. Y. Shaw, J. C. Wang, Knotting of a DNA chain during ring closure, *Science* 260 (1993) 533–536.
- [66] C. Bustamante, D. Keller, Scanning Force Microscopy in Biology, *Physics Today* 48 (1995) 32–38.
- [67] H. G. Hansma, Atomic Force Microscopy of Biomolecules, *J. Vac. Sci. Technol. B* 14 (1996) 1390–1395.
- [68] J. R. Moffit, Y. R. Chemla, S. B. Smith, C. Bustamante, Recent Advances in Optical Tweezers, *Ann. Rev. Biochem.* 77 (2008) 205–228.
- [69] J. O. Tegenfeldt, C. Prinz, H. Cao, S. Chou, W. W. Reisner, R. Riehn, Y. M. Wang, E. C. Cox, J. C. Sturm, P. Silberzan, R. H. Austin, The dynamics of genomic-length DNA molecules in 100-nm channels, *Proc. Natl. Acad. Sci. USA* 101 (2004) 10979–10983.
- [70] W. Reisner, K. J. Morton, R. Riehn, Y. M. Wang, Z. Yu, M. Rosen, J. C. Sturm, S. Y. Chou, E. Frey, R. H. Austin, Statics and dynamics of single DNA molecules confined in nanochannels, *Phys. Rev. Lett.* 94 (2005) 196101.
- [71] D. Stein, F. H. J. van der Heyden, W. J. A. Koopmans, C. Dekker, Pressure-driven transport of confined DNA polymers in fluidic channels, *Proc. Natl. Acad. Sci. USA* 103 (2006) 15853–15858.
- [72] D. J. Bonthuis, C. Meyer, D. Stein, C. Dekker, Conformation and Dynamics of DNA Confined in Slitlike Nanofluidic Channels, *Phys. Rev. Lett.* 101 (2008) 108303.
- [73] W. Reisner, J. P. Beech, N. B. Larsen, H. Flyvbjerg, A. Kristensen, J. O. Tegenfeldt, Nanoconfinement-enhanced conformational response of single DNA molecules to changes in ionic environment, *Phys. Rev. Lett.* 99 (2007) 058302.
- [74] L. J. Guo, X. Cheng, C.-F. Chou, Fabrication of Size-Controllable Nanofluidic Channels by Nanoimprinting and Its Application for DNA Stretching, *Nano Lett.* 4 (2004) 69–73.
- [75] E. Ercolani, F. Valle, J. Adamcik, G. Witz, R. Metzler, P. De Los Rios, J. Roca, G. Dietler, Fractal Dimension and Localization of DNA Knots, *Phys. Rev. Lett.* 98 (2007) 058102.
- [76] T. R. Strick, J. F. Allemand, D. Bensimon, A. Bensimon, V. Croquette, The elasticity of a single supercoiled DNA molecule, *Science* 271 (1996) 1835–1837.
- [77] R. H. Austin, Nanopores: The art of sucking spaghetti, *Nat. Mat.* 2 (2003) 567–568.
- [78] C. Zurlan, T. Samuely, G. Bertoni, F. Valle, G. Dietler, L. Finzi, D. D. Dunla, Integration host factor alters LacI-induced DNA looping, *Biophys. Chem.* 128 (2007) 245–252.
- [79] C. Vanderzande, *Lattice Models of Polymers*, Cambridge University Press, 1998.
- [80] K. Svoboda, S. M. Block, Biological Applications of Optical Forces, *Ann. Rev. Biophys. Biomol. Struct.* 23 (1994) 247–285.
- [81] J. E. Bemis, B. B. Akhremichev, G. C. Walker, Single Polymer Chain Elongation by Atomic Force Microscopy, *Langmuir* 15 (1999) 2799–2805.
- [82] Y. Arai, R. Yasuda, K. Akashi, Y. Harada, H. Miyata, T. Kinoshita, H. Itoh, H. Tying a molecular knot with optical tweezers, *Nature* 399 (1999) 446–448.
- [83] X. R. Bao, H. J. Lee, S. R. Quake, Behavior of complex knots in single DNA molecules, *Phys. Rev. Lett.* 91 (2003) 265506.
- [84] T. Odijk, The statistics and dynamics of confined or entangled stiff polymers, *Macromol.* 16 (1983) 1340–1344.
- [85] D. Marenduzzo, C. Micheletti, E. Orlandini, Biopolymer organization upon confinement, *Journal of Physics: Condensed Matter* 22 (28) (2010) 283102.
- [86] W. M. Gelbart, C. M. Knobler, Virology. Pressurized viruses, *Science* 323 (5922) (2009) 1682–1683, doi: 10.1126/science.1170645.
- [87] J. I. Sulkowska, P. Sulkowski, P. Szymczak, M. Cieplak, Stabilizing effect of knots on proteins, *Proc Natl Acad Sci U S A* 105 (50) (2008) 19714–19719, doi:10.1073/pnas.0805468105.
- [88] K. De’Bell, T. Lookman, Surface phase transitions in polymer systems, *Rev. Mod. Phys.* 65 (1993) 87.
- [89] S. Chandrasekhar, Stochastic problems in physics and astronomy, *Rev. Mod. Phys.* 15 (1943) 1–89.
- [90] J. M. Hammersley and D. C. Handscomb, *Monte Carlo Methods*, Methuen & Co. London and John Wiley & Sons, New York, 1964.
- [91] C. Itzykson, J.-M. Drouffe, *Statistical Field Theory*, vol. II, Cambridge University Press, 1989.
- [92] K. Binder, D. W. Heermann, *Monte Carlo Simulation in Statistical Physics*, Springer-Verlag, 1988.
- [93] N. Madras and G. Slade, *The Self-Avoiding Walk*, Birkhäuser, 1993.
- [94] K. Kremer, G. Grest, Dynamics of entangled linear polymer melts: A molecular dynamics simulation, *J. Chem.*

- Phys. 92 (1990) 5057–5086.
- [95] S. Caracciolo and A. D. Sokal, Dynamic critical exponent of some Monte Carlo algorithms for the self-avoiding walk, *J. Phys. A: Math. Gen.* 19 (1986) L797–L801.
 - [96] M. P. Allen, D. J. Tildesley, *Computer Simulation of Liquids*, Clarendon Press, Oxford, 1987.
 - [97] N. Madras, A. D. Sokal, The pivot algorithm: A highly efficient Monte Carlo method for the self-avoiding walk, *J. Stat. Phys.* 50 (1988) 109–186.
 - [98] N. Madras, A. Orłitsky, L. A. Shepp, Monte Carlo generation of self-avoiding walks with fixed endpoints and fixed length., *J. Stat. Phys.* 58 (1990) 159–183.
 - [99] J. C. S. Alvarado, K. Millett, The Generation of Random Equilateral Polygons, preprint .
 - [100] M. L. Mansfield, Development of knotting during the collapse transition of polymers, *J. Chem. Phys.* 127 (2007) 244902.
 - [101] C. J. Geyer, Markov chain Monte Carlo maximum likelihood, *Computing Science and Statistics: Proc. 23rd Symp. on the Interface* (1991) 156–163.
 - [102] M. C. Tesi, E. J. Janse Van Rensburg, E. Orlandini, S. G. Whittington, Monte Carlo study of the interacting self-avoiding walk model in three dimensions, *J. Stat. Phys.* 82 (1996) 155–181.
 - [103] A. M. Ferrenberg, R. H. Swendsen, New Monte Carlo technique for studying phase transitions, *Phys. Rev. Lett.* 61 (1988) 2635–2638.
 - [104] Z. W. Salzburg, J. D. Jacobson, W. Fickett, W. W. Wood, Application of the Monte Carlo Method to the Lattice-Gas Model. I. Two-Dimensional Triangular Lattice, *J. Chem. Phys.* 30 (1959) 65.
 - [105] C. Micheletti, A. Laio and M. Parrinello, Reconstructing the Density of States by History-Dependent Metadynamics, *Phys. Rev. Lett.* 92 (2004) 170601.
 - [106] K. Koniaris, M. Muthukumar, Self-entanglement in ring polymers, *J. Chem. Phys.* 95 (1991) 2873–2881.
 - [107] M. Baiesi, E. Orlandini, S. G. Whittington, Interplay between writhe and knotting for swollen and compact polymers, *J. Chem. Phys.* 131 (2009) 154902.
 - [108] B. Berg, D. Foester, Random paths and random surfaces on a digital computer, *Phys. Lett. B* 106 (1981) 323–326.
 - [109] C. Aragao de Carvalho, S. Caracciolo, J. Fröhlich, Polymers and $g|\phi|^4$ theory in four dimensions, *Nucl. Phys. B* 215 (1983) 209–248.
 - [110] C. Aragao de Carvalho, S. Caracciolo, A new Monte Carlo approach to the critical properties of self-avoiding random-walks, *J. Physique* 44 (1983) 323–331.
 - [111] E. J. Janse van Rensburg, S. G. Whittington, The BFACF algorithm and knotted polygons, *J. Phys. A: Math. Gen.* 24 (1991) 5553–5567.
 - [112] M. Baiesi, E. Orlandini, A. L. Stella, F. Zonta, Topological signature of globular polymers, In preparation (2009) .
 - [113] E. Orlandini, S. G. Whittington, Statistical topology of closed curves: Some applications in polymer physics, *Rev. Mod. Phys.* 79 (2007) 611–642.
 - [114] H. Kesten, On the number of self-avoiding walks, *J. Math. Phys.* 4 (1963) 960–969.
 - [115] Y. Diao, N. Pippenger, D. W. Summers, On random knots, *J. Knot Theory Ramif.* 3 (1994) 419–429.
 - [116] Y. Diao, The knotting of equilateral polygons in \mathbb{R}^3 , *J. Knot Theory Ramif.* 4 (1995) 189–196.
 - [117] M.D. Frank-Kamenetskii, A. V. Lukashin, A. V. Vologodskii, A. V., Statistical mechanics and topology of polymer chains, *Nature* 258 (1975) 398–402.
 - [118] E. J. Janse van Rensburg, S. G. Whittington, The knot probability in lattice polygons, *J. Phys. A: Math. Theor.* 23 (1990) 3573–3590.
 - [119] A. Yao, H. Matsuda, H. Tsukahara, M. K. Shimamura, T. Deguchi, On the dominance of trivial knots among SAPs on a cubic lattice, *J. Phys. A: Math. Gen.* 34 (2001) 7563–7577.
 - [120] E. J. Janse van Rensburg, The probability of knotting in lattice polygons, *Physical Knots: Knotting, Linking, and Folding Geometric Objects in \mathbb{R}^3* , edited by J. A. Calvo, K. C. Millett, and E. J. Rawdon, *Contemporary Mathematics* 304 (2002) 125–135.
 - [121] T. Deguchi, K. Tsurusaki, Universality of random knotting, *Phys. Rev. E* 55 (1997) 6245–6248.
 - [122] K. Koniaris, M. Muthukumar, Knottedness in ring polymers, *Phys. Rev. Lett.* 66 (1991) 2211–2214.
 - [123] M. K. Shimamura, T. Deguchi, Characteristic length of random knotting for cylindrical self-avoiding polygons., *Phys. Lett. A* 274 (2000) 184–191.
 - [124] A. V. Vologodskii, A. V. Lukashin, M. D. Frank-Kamenetskii, V. V. Anshelevich, The knot problem in statistical mechanics of polymer chains, *Sov. Phys.-JETP* 39 (1974) 1059–1063.
 - [125] J. des Cloizeaux, M. L. Metha, Topological constraints on polymer rings and critical indices, *J. Physique* 40 (1975) 655–670.
 - [126] J. P. J. Michels, F. W. Wiegell, On the topology of a polymer ring, *Proc. R. Soc. Lond.* A403 (1986) 269–284.
 - [127] T. Deguchi, K. Tsurusaki, Topology of closed random polygons, *J. Phys. Soc. Japan* 62 (1993) 1411–1414.
 - [128] Y. L. Chen, M. D. Graham, J. J. Depablo, K. Jo, D. C. Schwartz, DNA Molecules in Microfluidic Oscillatory Flow, *Macromol.* 38 (2005) 6680–6687.

- [129] Y. Xia, G. M. Whitesides, *Soft Lithography*, *Angew. Chemie Int. Edit.* 37 (5) (1998) 550–575, ISSN 1521-3773.
- [130] R.M.M. Smeets, U. F. Keyser, D. Krapf, M. Y. Wu, N. H. Dekker, C. Dekker, Salt dependence of ion transport and DNA translocation through solid-state nanopores, *Nano Lett.* 6 (2006) 89–95.
- [131] E. R. T. Sakaue, *Polymer Chains in Confined Spaces and Flow-Injection Problems: Some Remarks*, *Macromol.* 39 (2006) 2621–2628.
- [132] A. Y. Grosberg, A. R. Khokhlov, *Statistical physics of macromolecules*, AIP series in polymers and complex materials, American Institute of Physics, New York, ISBN 1-56396-071-0, 1994.
- [133] J. Rudnik, G. Gaspari, The shapes of random walks, *Science* 237 (1987) 384–389.
- [134] C. Cordeiro, M. Molisana, D. Thirumalai, Shape of confined polymer chains, *J. Phys. II (France)* 7 (1997)(433-447).
- [135] J. van Vliet, G. ten Brinke, Orientation and shape of flexible polymers in a slit, *J. Chem. Phys.* 93 (2005) (1436-1441).
- [136] G. Morrison, D. Thirumalai, The Shape of a flexible polymer in a cylindrical pore, *J. Chem. Phys.* 122 (1990).
- [137] A. Y. Gorberg, K. A.R., *Giant Molecules*, 2nd Edition, World Scientific, Singapore, 2010.
- [138] T. Odijk, Scaling theory of DNA confined in nanochannels and nanoslits, *Phys. Rev. E* 77 (6) (2008) 060901, doi:10.1103/PhysRevE.77.060901.
- [139] H. Yamakawa, F. Motoharu, Wormlike chains near the rod limit: Path integral in the WKB approximation, *J. Chem. Phys.* 59 (1973) 6641–6644.
- [140] T. W. Burkhardt, Free energy of a semiflexible polymer in a tube and statistics of a randomly-accelerated particle, *J. Phys. A: Math. Gen.* 30 (1997) L167–L172.
- [141] F. Persson, P. Utko, W. Reisner, N. B. Larsen, A. Kristensen, Confinement spectroscopy: probing single DNA molecules with tapered nanochannels, *Nano Lett.* 9 (2009) 1382–1385.
- [142] J. M. Hammersley, S. G. Whittington, Self-avoiding walks in wedges, *J. Phys. A: Math. Gen.* 18 (1985) 101–111.
- [143] C. Soteris, S. G. Whittington, Polymers in slabs, slits and pores, *Israel J. Chem.* 31 (1991) 127.
- [144] C. Soteris, S. G. Whittington, Lattice models of branched polymers: effect of geometrical constraints, *J. Phys. A: Math. Gen.* 27 (1989) 5259–5270.
- [145] J. van Vliet, M. Luyten, G. ten Brinke, Scaling behaviour of dilute polymer solutions confined between parallel plates, *Macromolecules* 25 (3802-3806).
- [146] F. Wagner, G. Lattanzi, E. Frey, Conformations of confined biopolymers, *Phys. Rev. E* 75 (2007) (050902).
- [147] E. Orlandini, Monte Carlo study of polymer systems by multiple Markov chain method, *Numerical Methods for Polymeric Systems*, edited by S. G. Whittington, IMA Volumes in Mathematics and Its Application 102 (1998) 33–58.
- [148] M. C. Tesi, E. J. Janse Van Rensburg, E. Orlandini, S. G. Whittington, Knot Probability for Lattice Polygons in Confined Geometries, *J. Phys. A: Math. Gen.* 27 (1994) 347–360, ISSN 0305-4470.
- [149] C. Soteris, Knots in graphs in subsets of \mathbb{Z}^3 , *Topology and geometry in polymer science*, edited by S. G. Whittington, D. W. Sumners and T. Lodge, IMA Volumes in Mathematics and Its Application 103 (1998) 101–133.
- [150] C. Soteris, D. W. Sumners, S. G. Whittington, Entanglement complexity of graphs in \mathbb{Z}^3 , *Math. Proc. Camb. Philos. Soc.* 111 (1992) 75–91.
- [151] C. Micheletti, D. Marenduzzo, E. Orlandini, D. W. Sumners, Knotting of random ring polymers in confined spaces, *J. Chem. Phys.* 124 (2006) 64903–64903.
- [152] D. Reith, P. Virnau, Monte Carlo simulations of a single polystyrene chain in spherical confinement, *Computer Physics Communications In Press* (2010) 800, doi:DOI: 10.1016/j.cpc.2010.12.002.
- [153] C. Micheletti, D. Marenduzzo, E. Orlandini, D. W. Sumners, Simulations of knotting in confined circular DNA, *Biophys J.* 95 (2008) 3591–3599.
- [154] S. Jun, A. Wright, Entropy as the driver of chromosome segregation, *Nat Rev Microbiol* 8 (8) (2010) 600–607, doi:10.1038/nrmicro2391.
- [155] C. Forrey, M. Muthukumar, Langevin dynamics simulations of genome packing in bacteriophage, *Biophys J* 91 (1) (2006) 25–41, doi:10.1529/biophysj.105.073429.
- [156] A. S. Petrov, M. B. Boz, S. C. Harvey, The conformation of double-stranded DNA inside bacteriophages depends on capsid size and shape, *J Struct Biol* 160 (2) (2007) 241–248, doi:10.1016/j.jsb.2007.08.012.
- [157] A. Leforestier, F. Livolant, Structure of toroidal DNA collapsed inside the phage capsid, *Proc Natl Acad Sci U S A* 106 (23) (2009) 9157–9162, doi:10.1073/pnas.0901240106.
- [158] J. Arsuaga, R. K. Tan, M. Vazquez, D. W. Sumners, S. C. Harvey, S. C., Investigation of viral DNA packaging using molecular mechanics models, *Biophys. Chem.* 101-102 (2002) 475–484.
- [159] R. Matthews, A. A. Louis, J. M. Yeomans, Knot-controlled ejection of a polymer from a virus capsid, *Phys. Rev. Lett.* 102 (2009) 088101.
- [160] A. Stasiak, V. Katritch, J. Bednar, D. Michoud, J. Dubochet, Electrophoretic mobility of DNA knots, *Nature* 384 (1996) 122–122.
- [161] J. Arsuaga, M. Vázquez, S. Trigueros, D. W. Sumners, J. Roca, Knotting probability of DNA molecules confined

- in restricted volumes: DNA knotting in phage capsids, *Proc. Natl. Acad. Sci. USA* 99 (2002) 5373–5377.
- [162] J. Arsuaga, M. Vázquez, P. McGuirk, S. Trigueros, D. W. Sumners, J. Roca, DNA knots reveal a chiral organization of DNA in phage capsids, *Proc. Natl. Acad. Sci. USA* 102 (2005) 9165–9169.
- [163] J. Arsuaga, Y. Diao, DNA knotting in spooling like conformations in Bacteriophages, *J. Comp. Math. Meth. Med.* 9 (2008) 303–316.
- [164] D. Marenduzzo, E. Orlandini, A. Stasiak, d. W. Sumners, L. Tubiana, C. Micheletti, DNA-DNA interactions in bacteriophage capsids are responsible for the observed DNA knotting, *Proc Natl Acad Sci U S A* 106 (52) (2009) 22269–22274, doi:10.1073/pnas.0907524106.
- [165] E. Grelet, S. Fraden, What is the origin of Chirality in the Cholesteric Phase of Virus Suspensions ?, *Phys. Rev. Lett.* 90 (2003) 198302.
- [166] A. A. Kornyshev, S. Leikin, S. V. Malinin, Chiral electrostatic interaction and cholesteric liquid crystals of DNA, *Eur Phys J E* 7 (2002) 83–93.
- [167] F. Tombolato, A. Ferrarini, From the double-stranded helix to the chiral nematic phase of B-DNA: a molecular model, *J. Chem. Phys.* 122 (2005) 54908.
- [168] C. B. Stanley, H. Hong, H. H. Strey, DNA cholesteric pitch as a function of density and ionic strength, *Biophys J* 89 (2005) 2552–2557.
- [169] F. Tombolato, A. Ferrarini, E. Grelet, Chiral Nematic Phase of Suspensions of Rodlike Viruses: Left-Handed Phase Helicity from a Right-Handed Molecular Helix, *Phys. Rev. Lett.* 96 (2006) 258302.
- [170] S. Trigueros, J. Roca, Production of highly knotted DNA by means of cosmid circularization inside phage capsids, *BMC Biotechnol* 7 (2007) 94–94, doi:10.1186/1472-6750-7-94
- [171] R. R. Netz, D. Andelman, Neutral and charged polymers at interfaces, *Phys. Rep.* 380 (2003) 1–95.
- [172] E. J. Janse van Rensburg, *The Statistical Mechanics Of Interacting Walks, Polygons, Animals And Vesicles*, Oxford University Press, 2000.
- [173] E. Eisenriegler, K. Kremer, K. Binder, Adsorption of polymer chains at surfaces: Scaling and Monte Carlo analyses, *J. Chem. Phys.* 77 (1982) 6296–6320.
- [174] C. Vanderzande, On knots in a model for the adsorption of ring polymers, *J. Phys. A: Math. Gen.* 28 (1995) 3681–3700.
- [175] E. J. Janse van Rensburg, Knotting in adsorbing lattice polygons., *Contemp. Math.* 304 (2002) 137–151.
- [176] J. P. J. Michels, F. W. Wiegel, The distribution of the Alexander polynomials of knots confined to a thin layer, *J. Phys. A: Math. Gen.* 22 (1989) 2393–2398.
- [177] C. Rivetti, M. Guthold, C. Bustamante, Scanning force microscopy of DNA deposited onto Mica: equilibration versus kinetic trapping studied by statistical polymer chain analysis, *J. Mol. Biol.* 264 (1996) 919–932.
- [178] F. Valle, M. Favre, P. De Los Rios, A. Rosa, G. Dietler, Scaling exponents and probability distribution of DNA End-to-end distance, *Phys. Rev. Lett.* 95 (2005) 158105.
- [179] G. Witz, K. Rechendorff, J. Adamcik, G. Dietler, Conformation of circular DNA in two dimensions, *Phys. Rev. Lett.* 101 (2008) 148103.
- [180] E. Gutter, E. Orlandini, Monte Carlo results for projected self-avoiding polygons: A two-dimensional model for knotted polymers, *J. Phys. A: Math. Gen.* 32 (1999) 1359–1385.
- [181] O. B. Bakajin, T. A. J. Duke, C.-F. Chou, S. S. Chan, R. H. Austin, E. C. Cox, Electrohydrodynamic Stretching of DNA in Confined Environments, *Phys. Rev. Lett.* 80 (1998) 2737–2740.
- [182] A. Askin, Optical Trapping and Manipulation of Neutral Particles Using Lasers, *Proc. Natl. Acad. Sci. USA* 94 (1997) 4853–4860.
- [183] P. Pincus, Excluded Volume Effects and stretched Polymer Chains, *Macromol.* 9 (1976) 386–388.
- [184] Y. Sheng, M. Wang, Statics and dynamics of a single polymer chain confined in a tube, *J. Chem. Phys.* 114 (2001) (4724-4729).
- [185] S. Jun, D. Thirumalai, B.-Y. Ha, Compression and Stretching of a Self-avoiding chain in cylindrical Nanopores, *Phys. Rev. Lett.* 101 (2008) (138101).
- [186] E. J. Janse van Rensburg, E. Orlandini, M. C. Tesi, S. G. Whittington, Knotting in stretched polygons, *J. Phys. A: Math. Theor.* 41 (2008) arto no. 015003.
- [187] E. J. Janse van Rensburg, E. Orlandini, M. C. Tesi, S. G. Whittington, Knot probability of polygons subjected to a force: a Monte Carlo study, *J. Phys. A: Math. Theor.* 41 (2008) art. no 025003.
- [188] G. Morrison, C. Hyeon, N. Toan, b.Y. Ha, D. Thirumalai, Stretching homopolymers, *Macromolecules* 40 (7343-7353).
- [189] R.M. Neumann, Nonequivalence of the stress and strain ensembles in describing polymer-chain elasticity *Phys. Rev. A* 31 (1985) 3516-3517
- [190] R.M. Neumann, On the precise meaning of extension in the interpretation of polymer-chain stretching experiments *Biophys. J.* 85 (2003) 3418-3420
- [191] D. Ioffe, Y. Velenik, Ballistic phase of self-interacting random walks, *Analysis and Stochastics of Growth Processes and Interface Models*; ed P Morters, R Moser, M Penrose, H Schwetlick and J Zimmer (2008) 55–79.

- [192] E. J. Janse van Rensburg, E. Orlandini, M. C. Tesi, S. G. Whittington, Thermodynamics and entanglements of walks under stress, *J. Stat. Mech.* (2009) P07014.
- [193] M. Atapour, C. E. Soteros, S. G. Whittington, Stretched polygons in a lattice tube, *J. Phys. A: Math. Theor.* 42 (2009) art. no. 322002.
- [194] K. B. Marathe, History and Science of Knots, *Math. Intelligencer* 28 (2006) 54–57.
- [195] S. F. Edwards, Statistical mechanics with topological constraints: II, *J. Phys. A: Math. Gen.* 1 (1968) 15–28.
- [196] M. Kapnistos, M. Lang, D. Vlassopoulos, W. Pyckhout-Hintzen, D. Richter, D. Cho, T. Chang, M. Rubinstein, Unexpected power-law stress relaxation of entangled ring polymers, *Nature Materials* 7 (2008) 997–1002, ISSN 1476-1122, doi:10.1038/nmat2292.
- [197] C. O. Dietrich-Buchecker, J.-P. Savage, Templated synthesis of interlocked macrocyclic ligands: The catenands, *J. Am. Chem. Soc.* 106 (1984) 3043–3045.
- [198] E. Logemann, Real molecules as models for mathematical chemistry. I. Strategy for a synthesis of macromolecules with catenane subunits: A bifunctional catenane, *J. Math. Chem.* 13 (1993) 47–51.
- [199] D. E. Adams, E. M. Shekhtman, E. L. Zechiedrich, M. B. Schmid, N. R. Cozzarelli, The role of topoisomerase-IV in partitioning bacterial replicons and the structure of catenated intermediates in DNA-replication, *Cell* 71 (1992) 277–288.
- [200] J. Chen, C. A. Rauch, J. H. White, P. T. Englund, N. R. Cozzarelli, The topology of the kinetoplast DNA network, *Cell* 80 (1995) 61–69.
- [201] W. F. Pohl, The probability of linking of random closed curves, *Lect. Notes Math.*, (Springer-Verlag, Berlin) 894 (1981) 113–126.
- [202] J. des Cloizeaux, R. Ball, Rigid curves at Random Position and Linking Numbers, *Comm. Math. Phys.* 80 (1981) 543–553.
- [203] B. Duplantier, Linking numbers of closed manifolds at random in R^n , inductances and contacts, *Comm. Math. Phys.* 85 (1982) 221–264.
- [204] A. V. Vologodskii, A. V. Lukashin, M. D. Frank-Kamenetskii, Topological interaction between polymer chains, *Sov. Phys.-JETP* 40 (5) (1975) 932–936.
- [205] E. Orlandini, E. J. Janse Van Rensburg, M. C. Tesi, S. G. Whittington, Random Linking of Lattice Polygons, *J. Phys. A: Math. Gen.* 27 (1994) 335–345, ISSN 0305-4470.
- [206] N. Hirayama, K. Tsurusaki, T. Deguchi, Linking probabilities of off-lattice self-avoiding polygons and the effects of excluded volume, *J. Phys. A: Math. Theor.* (2009) 105001.
- [207] E. Orlandini, M. C. Tesi, S. G. Whittington, Polymer entanglement in melts, *J. Phys. A: Math. Gen.* 33 (2000) L181–L186, ISSN 0305-4470.
- [208] M. G. Brereton, T. A. Vilgis, The statistical mechanics of a melt of polymer rings, *J. Phys. A: Math. Gen.* 28 (1995) 1149–1167.
- [209] M. C. Tesi, E. J. Janse Van Rensburg, E. Orlandini, S. G. Whittington, Topological entanglement complexity of polymer chains in confined geometries, *Topology and geometry in polymer science*, edited by S. G. Whittington, D. W. Sumners and T. Lodge, *IMA Volumes in Mathematics and Its Application* 103 (1998) 135–157.
- [210] J. Arsuaga, T. Blackstone, Y. Diao, E. Karadayi, M. Saito, Linking of uniform random polygons in confined spaces, *J. Phys. A: Math. Theor.* 40 (2007) 1925–1936, ISSN 1751-8113, doi:10.1088/1751-8113/40/9/001.
- [211] M. Atapour, C. Soteros, C. Ernst, S. G. Whittington, The linking probability for 2-component links which span a lattice tube, *J. Knot Theo. Ramif.* 19 (2010) 27–54.
- [212] E. Panagiotou, K. C. Millett and S. Lambropoulou, The linking number and the writhe of uniform random walks and polygons in confined spaces., *J. Phys. A: Math. Theor.* 43 (2010) 045208.
- [213] E. Wassermann, The Preparation of Interlocking Rigs: a Catenane, *J. Am. Chem. Soc.* 82 (1960) 4433–4434.
- [214] C. Peinador, V. Blanco, J. M. Quintela, A New Doubly Interlocked [2]Catenane, *J. Math. Chem.* 131 (2009) 920–921.
- [215] W. R. Wikoff, L. Liljas, R. L. Duda, H. Tsuruta, R. W. Hendrix, J. E. Johnson, Topologically linked protein rings in the bacteriophage HK97 capsid, *Science* 289 (2000) 2129–2133, ISSN .
- [216] L. Z. Yan, P. E. Dawson, Design and synthesis of a protein catenane, *Angew. Chem. Int. Ed.* 40 (2001) 3625–3627.
- [217] J. W. Blankenship, P. E. Dawson, Thermodynamics of a designed protein catenane, *J. Mol. Biol.* 327 (2003) 537–548.
- [218] B. Hudson, J. Vinograd, Catenated circular DNA molecules in HeLa cells mitochondria, *Nature* 216 (1967) 647–652.
- [219] B. Alberts, A. Johnson, J. Lewis, M. Raff, K. Roberts, P. Walter, *Molecular Biology of the Cell: fifth edition*, New York (Garland Science (Taylor and Francis)), 2007.
- [220] F. B. Fuller, The writhing number of a space curve, *Proc. Natl. Acad. Sci. U S A* 68 (1971) 815–819.
- [221] J. H. White, J. H., Self-linking and the Gauss integral in higher dimensions, *Am. J. Math.* 91 (1969) 683–728.
- [222] G. Torres, On the Alexander polynomial, *Annals Mathematics* 57 (1953) 57–89.
- [223] C. Soteros, D. W. Sumners, S. G. Whittington, Linking of random p-spheres in Z^d , *J. Knot Theo. Ramif.* 8 (1999)

- 49–70.
- [224] K. Millett, Monte Carlo Exploration of Polygonal Knot Space, *Knots in Hellas'98 (Delphi)* (Series on Knots and Everything (Singapore: World Scientific) 24 (6735) (2000) 306–334.
- [225] Y. Diao, C. Ernst, The complexity of lattice knots, *Topology Appl.* 90 (1998) 1–9.
- [226] Y. Diao, C. Ernst, E. J. Janse van Rensburg, Upper bounds on linking numbers of thick links, *J. Knot Theo. Ramif.* 11 (2002) 199–210.
- [227] M. Doi, S. F. Edwards, *The theory of Polymer Dynamics*, Clarendon Press, 1986.
- [228] R. Everaers, S. K. Sukumaran, G. S. Grest, C. Svaneborg, A. Sivasubramanian, K. Kremer, Rheology and Microscopic Topology of Entangled Polymeric Liquids, *Science* 303 (5659) (2004) 823–826.
- [229] R. Dickman, C. K. Hall, High density Monte Carlo simulations of chain molecules: Bulk equation of state and density profile near walls, *J. Chem. Phys.* 89 (1988) 3168–3174.
- [230] S. W. Smith, C. K. Hall, B. D. Freeman, J. A. Mc Cormick, Self diffusion coefficients and atomic mean-squared displacements in entangled hard chain fluids, *Numerical Methods for Polymeric Systems*, edited by S. G. Whittington, *IMA Volumes in Mathematics and Its Application* 102 (1998) 203–215.
- [231] K. Kremer, S. K. Sukumaran, R. Everaers and G. S. Grest, Entangled polymer systems, *Comp. Phys. Comm.* 169 (2005) 75–81.
- [232] E. Orlandini, S. G. Whittington, Entangled polymers in condensed phases, *J. Chem. Phys.* 121 (2004) 12094–12099, ISSN 0021-9606, doi:10.1063/1.1814077.
- [233] V. Katritch, J. Bednar, D. Michoud, R. G. Scharein, J. Dubochet, A. Stasiak, Geometry and physics of knots, *Nature* 384 (1996) 142–145, ISSN 0028-0836.
- [234] J. J. Kasianowicz, E. Brandin, D. Branton, D. W. Deamer, Characterization of individual polynucleotide molecules using a membrane channel, *Proc. Natl. Acad. Sci. USA* 93 (1996) 13770–13773.
- [235] S. Jun, B. Mulder, Entropy-driven spatial organization of highly confined polymers: Lessons for the bacterial chromosome, *Proc. Natl. Acad. Sci. USA* 103 (2006) 12388–12393.
- [236] M. R. Branco, A. Pombo, Intermingling of Chromosome Territories in Interphase Suggests Role in Translocations and Transcription-Dependent Associations, *PLOS Biology* 4 (2006) 780–788.
- [237] M. E. Cates, J. M. Deutsch, Conjectures on the statistics of ring polymers, *J. Physique* 47 (1986) 2121–2128.
- [238] A. Y. Grosberg, A. Feigel, Y. Rabin, Flory-type theory of a knotted ring polymer, *Phys. Rev. E* 54 (1996) 6618–6622.
- [239] A. Y. Grosberg, Critical Exponents for Random Knots, *Phys. Rev. Lett.* 85 (2000) 3858–3862.
- [240] E. Orlandini, M. C. Tesi, E. J. Janse van Rensburg, S. G. Whittington, Entropic exponents of lattice polygons with specified knot type, *J. Phys. A: Math. Gen.* 29 (1996) L299–L303, ISSN 0305-4470.
- [241] E. Orlandini, M. C. Tesi, E. J. Janse van Rensburg, S. G. Whittington, Asymptotics of knotted lattice polygons, *J. Phys. A: Math. Gen.* 31 (1998) 5953–5967, ISSN 0305-4470.
- [242] N. T. Moore, R. C. Lua, A. Y. Grosberg, Topologically driven swelling of a polymer loop, *Proc. Natl. Acad. Sci. USA* 101 (2004) 13431–13435.
- [243] S. G. Whittington, *Topology of Polymers, New Scientific Applications of Geometry and Topology*, edited by D. W. Sumners et al 45 (1992) 73–95.
- [244] O. Farago, Y. Kantor, M. Kardar, Pulling knotted polymers, *Europhys. Lett.* 60 (2002) 53–59.
- [245] C. Soteros, S. G. Whittington, Critical exponents for lattice animals with fixed cyclomatic index, *J. Phys. A: Math. Gen.* 21 (1988) 2187–2193.
- [246] R. Guida, J. Zinn-Justin, Critical exponents of the N-vector model, *J. Phys. A: Math. and Gen.* 31 (1997) 8103–8121.
- [247] B. Li, N. Madras, A. D. Sokal, Critical exponents, hyperscaling and universal amplitude ratios for two- and three-dimensional self-avoiding walks, *J. Stat. Phys.* 80 (1995) 661–754.
- [248] E. J. Janse van Rensburg, S. G. Whittington, The dimensions of knotted polygons, *J. Phys. A: Math. Gen.* 24 (1991) 3935–3948.
- [249] S. R. Quake, Topological effects of knots in polymers, *Phys. Rev. Lett.* 73 (1994) 3317–3320.
- [250] H. Matsuda, A. Yao, H. Tsukahara, T. Deguchi, K. Furuta, T. Inami, Average size of random polygons with fixed knot topology, *Phys. Rev. E* 68 (2003) 011102.
- [251] S. Brown, T. Lenczycki, G. Szamel, Influence of topological constraints on the statics and dynamics of ring polymers, *Phys. Rev. E* 63 (5) (2001) 052801.
- [252] M. L. Mansfield, J. F. Douglas, Properties of knotted ring polymers. I. Equilibrium dimensions, *J. Chem. Phys.* 133 (2010) 044903.
- [253] G. B. McKenna, G. Hadziioannou, P. Lutz, G. Hild, C. Strazielle, C. Straupe, P. Rempp, A. J. Kovacs, Dilute solution characterization of cyclic polystyrene molecules and their zero-shear viscosity in the melt, *Macromol.* 20 (1987) 498–512.
- [254] J. Roovers, Melt Properties of Ring Polystyrenes, *Macromol.* 18 (1985) 1359–1361.
- [255] J. Roovers, P. M. Toporowski, Synthesis of high molecular weight ring polystyrenes, *Macromol.* 16 (1983) 843–

- [256] J. Roovers, Dilute-solution properties of ring polystyrenes, *Journal of Polymer Science: Polymer Physics Edition* 23 (1985) 1087–1097.
- [257] A. Takano, Y. Kushida, Y. Ohta, K. Masuoka, Y. Matsushita, The second virial coefficients of highly-purified ring polystyrenes in cyclohexane, *Polymer* 50 (2009) 1300–1303.
- [258] J. des Cloizeaux, Ring polymers in solution : topological effects, *Journal de Physique Letters* 42 (1981) L433–L436.
- [259] N. T. Moore, A. Y. Grosberg, Limits of analogy between self-avoidance and topology-driven swelling of polymer loops, *Phys Rev E Stat Nonlin Soft Matter Phys* 72 (6 Pt 1) (2005) 061803.
- [260] M. K. Shimamura, T. Deguchi, Finite-size and asymptotic behaviors of the gyration radius of knotted cylindrical self-avoiding polygons, *Phys. Rev. E* 65 (2002) 051802.
- [261] A. Dobay, J. Dubochet, K. Millett, P.-E. Sottas, A. Stasiak, Scaling behavior of random knots, *Proc. Natl. Acad. Sci. USA* 100 (2003) 5611–5615.
- [262] J. M. Deutsch, Equilibrium size of large ring molecules, *Phys. Rev. E* 59 (3) (1999) R2539–R2541, doi: 10.1103/PhysRevE.59.R2539.
- [263] M. K. Shimamura, T. Deguchi, Gyration radius of a circular polymer under a topological constraint with excluded volume., *Phys. Rev. E* 64 (2001) 020801.
- [264] D. Marenduzzo, E. Orlandini, Entropic approach curves of a polymer of fixed topology, *Europhys. Lett.* 76 (2006) 519–525, ISSN 0295-5075, doi:10.1209/epl/i2006-10278-2.
- [265] E. Eisenriegler, *Polymer Near Surfaces*, World Scientific, Singapore, 1993.
- [266] K. Iwata, Evidence of topological interaction among polymers: A_2 of ring polymers in the θ -state, *Macromolecules* 18 (1) (1985) 115–116.
- [267] F. Tanaka, Osmotic pressure of ring-polymer solutions, *The Journal of Chemical Physics* 87 (1997) (4201).
- [268] T. Deguchi, K. Tsurusaki, Random knots and links and applications to polymer physics, *Lectures at Knots 96* (Singapore:World Scientific) (1997) 95–122.
- [269] D. Marenduzzo, E. Orlandini, Topological and entropic repulsion in biopolymers, *J. Stat. Mech.* (2009) L09002.
- [270] B. Duplantier, Polymer Network of fixed topology: renormalization, exact critical exponent in two dimensions, and $d=4$ -, *Phys. Rev. Lett.* 57 (1986) 941–944.
- [271] B. Duplantier, Statistical mechanics of polymer networks of any topology, *J. Stat. Phys.* 54 (1989) 581.
- [272] A. Y. Grosberg, P. G. Khalatur, A. R. Khokhlov, Polymeric coils with excluded volume in dilute solution: The invalidity of the model of impenetrable spheres and the influence of excluded volume on the rates of diffusion-controlled intermacromolecular reactions, *Makromol. Chem., Rapid Commun.* 3 (1982) 709–713.
- [273] J. Chuang and A. Y. Grosberg and T. Tanaka, Topological repulsion between polymer globules, *J. Chem. Phys.* 112 (2000) 6434–6442.
- [274] T. Blackstone, R. Scharein, B. Borgo, R. Varela, Y. Diao, J. Arsuaga, Modeling of chromosome intermingling by partially overlapping uniform random polygons, *J Math Biol* (2) (2010) (371-389) doi:10.1007/s00285-010-0338-8.
- [275] D. Marenduzzo, C. Micheletti, P. R. Cook, Entropy-driven genome organization, *Biophys J* 90 (10) (2006) 3712–3721, doi:10.1529/biophysj.105.077685.
- [276] N. M. Toan, D. Marenduzzo, P. R. Cook, C. Micheletti, Depletion effects and loop formation in self-avoiding polymers, *Phys Rev Lett* 97 (17) (2006) 178302.
- [277] M. Müller, J. P. Wittmer, M. E. Cates, Topological effects in ring polymers: A computer simulation study, *Phys Rev E Stat Phys Plasmas Fluids Relat Interdiscip Topics* 53 (5) (1996) 5063–5074.
- [278] S. Brown, G. Szamel, Structure and dynamics of ring polymers, *J. Chem. Phys.* 108 (1998) 4705–4708.
- [279] S. Gagliardi, V. Arrighi, A. Dagger, A. J. Semlyen, Conformation of cyclic and linear polydimethylsiloxane in the melt: a small-angle neutron-scattering study, *Appl. Phys. A* 74 (2002) S469–S471.
- [280] M. Muller, J. P. Wittmer, M. E. Cates, Topological effects in ring polymers. II. Influence of persistence length, *Phys. Rev. E* 61 (2000) 4078–4089.
- [281] T. Vettorel, A. Y. Grosberg, K. Kremer, Statistics of polymer rings in the melt: a numerical simulation study, *Phys. Biol.* 6, ISSN 1478-3967, doi:10.1088/1478-3975/6/2/025013.
- [282] S. P. Obukhov, M. Rubinstein, T. Duke, Dynamics of a Ring Polymer in a Gel, *Phys. Rev. Lett.* 73 (1994) 1263–1266.
- [283] A. R. Khokhlov, S. K. Nechaev, Polymer chain in an array of obstacles, *Phys. Lett. A* 112 (1985) 156–160.
- [284] A. Rosa, R. Everaers, Structure and dynamics of interphase chromosomes, *PLOS Comp. Biol.* 4 (2008) e1000153.
- [285] P. R. Cook, D. Marenduzzo, Entropic organization of interphase chromosomes, *J. Cell. Biol.* 186 (2009) 825–834.
- [286] A. Y. Grosberg, Crumpled globule model of DNA packing in chromosomes: from predictions to open questions, *Biomat 2010: International Symposium on Mathematical and Computational Biology* (2011) Rubem P. Mondaini (Editor), World Scientific, Singapore.
- [287] L. A. Mirny, The fractal globule as a model of chromatin architecture in the cell, *Chromosome Res* (2011) in

- press.
- [288] E. Lieberman-Aiden *et al.*, Comprehensive mapping of long-range interactions reveal folding principles of the human genome, *Science* (2009) 289-293.
 - [289] J. Dorier, A. Stasiak, Topological origin of chromosome territories, *Nucl. Acid Res.* 37 (2009) 6316–6322.
 - [290] S. de Nooijer, J. Wollink, B. Mulder, T. Bisseling, Non-specific interactions are sufficient to explain the position of heterochromatic chromocenters and nucleoli in interphase nuclei, *Nucl. Acid Res.* 37 (2009) 3558–3568.
 - [291] M. Nicodemi, A. Prisco, Thermodynamic pathways to genome spatial organization in the cell nucleus, *Biophys J* 96 (6) (2009) 2168–2177, doi:10.1016/j.bpj.2008.12.3919.
 - [292] D. Marenduzzo, I. Faro-Trindade, P. R. Cook, What are the molecular ties that maintain genomic loops?, *Trends in Gen.* 23 (2007) 126–133.
 - [293] A. Arnold, S. Jun, Time scale of entropic segregation of flexible polymers in confinement: Implications for chromosome segregation in filamentous bacteria, *Phys. Rev. E* 76 (3) (2007) 031901, doi: 10.1103/PhysRevE.76.031901.
 - [294] M. A. White, J. K. Eykelboom, M. A. Lopez-Vernaza, E. Wilson, D. R. Leach, Non-random segregation of sister chromosomes in *Escherichia coli*, *Nature* 455 (2008) 1248–1250.
 - [295] G. Toussaint, A new class of stuck unknots in Pol6, *Beitr age Algebra Geom.* 42 (2001) 301–306.
 - [296] D. W. Sumners, S. G. Whittington, Detecting knots in self-avoiding walks, *J. Phys. A: Math. Gen.* 23 (1990) 1471–1472.
 - [297] E. J. Janse van Rensburg, D. W. Sumners, E. Wasserman, S. G. Whittington, Entanglement complexity of self-avoiding walks, *J. Phys. A: Math. Gen.* 25 (1992) 6557–6566.
 - [298] J. M. Hammersley, D. J. A. Welsh, Further results on the rate of convergence to the connective constant of the hypercubical lattice, *Quat. J. Math. Oxford* 53 (1962) 108–110.
 - [299] R. Metzler, A. Hanke, P. G. Dommersnes, Y. Kantor, M. Kardar, Equilibrium shapes of flat knots, *Phys. Rev. Lett.* 88 (2002) 188101.
 - [300] E. Orlandini, A. L. Stella, C. Vanderzande, Polymer θ -point as a knot delocalization transition, *Phys. Rev. E* 68 (2003) 031804.
 - [301] A. Hanke, R. Metzler, P. G. Dommersnes, Y. Kantor, M. Kardar, Tight and loose shapes in flat entangled dense polymers, *Europ. Phys. J. E* 12 (2003) 347–354.
 - [302] E. Orlandini, A. L. Stella, C. Vanderzande, Loose, flat knots in collapsed polymers, *J. Stat. Phys.* 115 (2004) 681–700.
 - [303] E. Ben-Naim, Z. A. Daya, P. Vorobieff, R. E. Ecke, Knots and random walks in vibrated granular chains, *Phys. Rev. Lett.* 86 (2001) 1414–1417.
 - [304] A. Y. Grosberg and S. Nechaev, Algebraic invariants of knots and disordered Potts model, *J. Phys. A: Math. Gen.* 25 (1992) 4659–4672.
 - [305] K. Ohno, K. Binder, Scaling theory of star polymers and general polymer networks in bulk and semi-infinite good solvents, *J. Physique* 49 (1988) 1329–1352.
 - [306] L. Schäfer, C. von Ferber, U. Lehr, B. Duplantier, Renormalization of Polymer Networks and Stars, *Nucl. Phys. B* 374 (1992) 473–495.
 - [307] B. Duplantier, H. Saleur, Exact tricritical exponents for polymers at the Θ -point in two dimensions, *Phys. Rev. Lett.* 59 (1987) 539–542.
 - [308] V. Katritch, W. K. Olson, A. Vologodskii, J. Dubochet, A. Stasiak, Tightness of random knotting, *Phys. Rev. E* 61 (2000) 5545–5549.
 - [309] B. Marcone, E. Orlandini, A. L. Stella, F. Zonta, What is the length of a knot in a polymer?, *J. Phys. A: Math. Gen.* 38 (2005) L15–L21.
 - [310] B. Marcone, E. Orlandini, A. L. Stella, F. Zonta, Size of knots in ring polymers, *Phys. Rev. E* 75 (2007) 041105–11.
 - [311] M. L. Mansfield, Tight knots in polymers, *Macromol.* 31 (1998) 4030–4032.
 - [312] R. Metzler, A. Hanke, P. G. Dommersnes, Y. Kantor, M. Kardar, Tightness of slip-linked polymer chains, *Phys. Rev. E* 65 (2002) 061103.
 - [313] P. Virnau, Y. Kantor, M. Kardar, Knots in globule and coil phases of a model polyethylene, *Phys. Rev. E* 127 (2005) 15102–15106.
 - [314] B. Marcone, E. Orlandini, A. L. Stella, Knot localization in adsorbing polymer rings, *Phys. Rev. E* 76 (2007) 051804–10.
 - [315] E. J. Janse van Rensburg, Squeezing knots, *J. Stat. Mech.* (2007) art. no. P03001.
 - [316] Y.-J. Sheng, P.-Y. Lai, H.-K. Tsao, Deformation of a stretched polymer knot, *Phys. Rev. E* 61 (2000) 2895–2901.
 - [317] Y.-j. Sheng, K.-L. Cheng, Polymer knot confined in a tube: Statics and relaxation dynamics, *Phys. Rev. E* 65 (2001) art. no. 011801.

19. Acknowledgements

We are indebted to Tetsuo Deguchi, Claus Enrst, Alexander Grosberg, Ken Millett, Eric Rawdon, De Witt Sumners, Luca Tubiana, Peter Virnau, Stu Whittington and Guillaume Witz for the critical reading of the manuscript and for suggesting several corrections. We acknowledge support from the Italian Ministry of Education.

Appendix A. Distance between two segments

We recall here the procedure necessary to calculate the distance of minimum approach of two segments with endpoints respectively equal to \vec{P}_1, \vec{P}_2 and \vec{Q}_1, \vec{Q}_2 . It is convenient to parametrize the points on the segments as follows:

$$\vec{P}(s) = \vec{P}_1 + s \vec{v} \quad \vec{Q}(t) = \vec{Q}_1 + t \vec{w} \quad (\text{A.1})$$

where $\vec{v} = \vec{P}_2 - \vec{P}_1$ and $\vec{w} = \vec{Q}_2 - \vec{Q}_1$ and the parameters s and t are limited to the $[0,1]$ range. The required distance is clearly given by minimizing $d(s, t) \equiv |\vec{P}(s) - \vec{Q}(t)|$ over the unit square in the s, t plane. First it is necessary to calculate the values of s and t which yield the global minimum of d :

$$s^* = \frac{(\vec{v} \cdot \vec{w})(\vec{w} \cdot \vec{\Delta}_1) - (\vec{w} \cdot \vec{w})(\vec{v} \cdot \vec{\Delta}_1)}{(\vec{v} \cdot \vec{v})(\vec{w} \cdot \vec{w}) - |(\vec{v} \cdot \vec{w})|^2} \quad (\text{A.2})$$

$$t^* = \frac{(\vec{v} \cdot \vec{v})(\vec{w} \cdot \vec{\Delta}_1) - (\vec{v} \cdot \vec{w})(\vec{v} \cdot \vec{\Delta}_1)}{(\vec{v} \cdot \vec{v})(\vec{w} \cdot \vec{w}) - |(\vec{v} \cdot \vec{w})|^2} \quad (\text{A.3})$$

$$(\text{A.4})$$

where $\Delta_1 \equiv \vec{P}_1 - \vec{Q}_1$. The points associated to s^* and t^* are the points of minimum approach of the infinite lines which contain the two segments. If s^* and t^* are both in the $[0,1]$ range then the points of closest approach of the lines fall inside the segments and $d(s^*, t^*)$ is clearly the sought inter-segment distance. On the contrary, if (s^*, t^*) falls outside the unit square then the minimum value of d must be searched on the perimeter of the unit square. This requires setting in turn s and t equal to 0 or 1 and minimizing $d^2(s^*, t^*)$ over the “free” parameter restricted to the $[0,1]$ range.

Appendix B. Local chain moves that preserve topology

Knot simplification algorithms usually rely on various geometrical manipulations of a ring that do not alter the ring topology. A ubiquitous simplification operation consists of picking a chain node, i , at random and displacing it from the current position, \vec{r}_i , to a new one, \vec{r}'_i , that is more collinear with the flanking nodes:

$$\vec{r}'_i = \alpha \vec{r}_i + \frac{1 - \alpha}{2} (\vec{r}_{i+1} + \vec{r}_{i-1}) \quad (\text{B.1})$$

with $\alpha \in [0, 1]$. It must be checked that during a continuously parametrised movement of the bond from \vec{r}_i to \vec{r}'_i no chain segment is crossed, as this might alter the topology.

To check the preservation of topology it is necessary to check [37, 106] that the two triangular faces with vertices $\{i - 1, i, i'\}$ and $\{i + 1, i, i'\}$ do not intersect any of the chain segments that do

not include $i - 1, i$ or $i + 1$ as endpoints. For the sake of self-containedness we recall here the procedure for checking whether a segment with endpoints \vec{P}_1, \vec{P}_2 intersects a triangular face with vertices $\{\vec{Q}_1, \vec{Q}_2, \vec{Q}_3\}$. First it is calculated the point of intersection of the face and the infinite line containing the P_1P_2 segment and the infinite plane containing the triangular face.

It is convenient to indicate with \vec{q} the normal to the plane containing the triangular face and with $\vec{P}(s) = \vec{P}_1 + s(\vec{P}_2 - \vec{P}_1)$ the parametrization of the line containing the segment. The point on the line at the intersection with the plane is identified as $P(s^*)$ where,

$$s^* = \frac{\vec{q} \cdot (\vec{Q}_1 - \vec{P}_1)}{\vec{q} \cdot (\vec{P}_2 - \vec{P}_1)} \quad (\text{B.2})$$

if the value of s^* falls outside the $[0,1]$ range (which parametrizes the P_1P_2 segment) then it means that the segment does not intersect the plane, and hence the face. However, if s^* is in the $[0,1]$ range, it is necessary to check if the point of intersection, $\vec{P}(s^*)$ falls within the face. To do so it is sufficient to write the vector $\vec{P}(s^*) - \vec{Q}_1$ as a linear combination of the two oriented face edges departing from Q_1 :

$$\vec{P}(s^*) - \vec{Q}_1 = \alpha(\vec{Q}_3 - \vec{Q}_1) + \beta(\vec{Q}_2 - \vec{Q}_1) \quad (\text{B.3})$$

The coefficients α and β are conveniently obtained by solving the two linear equations obtained multiplying both sides of eq. (B.3) by $(\vec{Q}_3 - \vec{Q}_1)$ and $(\vec{Q}_2 - \vec{Q}_1)$. if both α and β are in the $[0,1]$ range it means that the point falls inside the triangular face. In this case the displacement of the bead cannot be accomplished without causing the crossing of two chain segments. As the topology would not be necessarily preserved the bead move must be rejected.

We remark that the above mentioned procedure is used not only in knot simplification contexts, but also in topology-preserving Monte Carlo evolutions of a given conformation. In this case, the i^{th} bead is displaced randomly or with a crankshaft (local) move and the above criteria are applied. Notice that this requires that only a single bead is moved at a time, as the check of topology preservation is not easily generalizable to the case of simultaneous displacement of two beads. Also, this method does not preserve the bond lengths.